# Lateral Performance of Helical Piles Augmented with Collar Vane Technology

## Final Report
## December 2025

**Principal Investigator:** Aaron Gallant

Civil and Environmental Engineering
University of Maine

**Authors**
Aaron Gallant; Juan Sebastian Carvajal-Munoz; Camilo Ferdandez-Escobar; Keith Berube; Aaron Bradshaw

**Sponsored By**
Transportation Infrastructure Durability Center


**A report from**
University of Maine
Department of Civil and Environmental Engineering
5711 Boardman Hall
Orono, Maine 04469

## About the Transportation Infrastructure Durability Center

The Transportation Infrastructure Durability Center (TIDC) is the 2018 US DOT Region 1 (New England) University Transportation Center (UTC) located at the University of Maine Advanced Structures and Composites Center. TIDC's research focuses on efforts to improve the durability and extend the life of transportation infrastructure in New England and beyond through an integrated collaboration of universities, state DOTs, and industry. The TIDC is comprised of six New England universities, the University of Maine (lead), the University of Connecticut, the University of Massachusetts Lowell, the University of Rhode Island, the University of Vermont, and Western New England University.

## U.S. Department of Transportation (US DOT) Disclaimer



## Acknowledgements

Funding for this research is provided by the Transportation Infrastructure Durability Center at the University of Maine under grant 69A3551847101 from the U.S. Department of Transportation's University Transportation Centers Program and Hubbell Power Systems, Inc. This project would not have been possible without the technical support and resources provided by Gary Seider, Shawn Downey, and Ben Jennings from Hubbell Power Systems.

## Technical Report Documentation Page

| | | |
|---|---|---|
| **1. Report No.** | **2. Government Accession No.** | **3. Recipient Catalog No.** |
| **4 Title and Subtitle**<br>Lateral Capacity of Helical Piles Augmented with Collar Vane Technology | | **5 Report Date**<br>**6 Performing Organization Code** |
| **7. Author(s)**<br>Aaron Gallant; Juan Sebastian Carvajal Munoz; Camilo Ferdandez-Escobar; Keith Berube; Aaron Bradshaw | | **8 Performing Organization Report No.** |
| **9 Performing Organization Name and Address** | | **10 Work Unit No. (TRAIS)**<br>**11 Contract or Grant No.** |
| **12 Sponsoring Agency Name and Address** | | **13 Type of Report and Period Covered**<br>**14 Sponsoring Agency Code** |

**15 Supplementary Notes**

**16 Abstract**

This report presents the results of a full-scale experimental investigation of helical pile (HP) foundations augmented with collar vane (CV) technology. The collar vane is a finned element installed near the pile head to mobilize soil resistance at shallow depths and reduce bending demands in slender helical pile shafts. Testing was conducted in cohesive soil and a constructed sand pit and included monotonic and cyclic lateral and torsional loading, as well as overturning tests representative of wind loading on roadside sign structures. Results show that collar vanes significantly increase lateral and torsional geotechnical resistance and reduce shaft bending moments relative to helical piles without vanes. Overturning tests demonstrate that selected HP–CV systems can perform comparably to conventional drilled shaft foundations used for sign support. Overall, the findings indicate that collar vane technology can expand the applicability of helical piles for transportation infrastructure, offering an efficient foundation alternative for infrastructure subjected to lateral loads.

| | | | |
|---|---|---|---|
| **17 Key Words** | | **18 Distribution Statement**<br>No restrictions. This document is available to the public through | |
| **19 Security Classification (of this report)**<br>Unclassified | **20 Security Classification (of this page)**<br>Unclassified | **21 No. of pages** | **22 Price** |

Form DOT F 1700.7 (8-72)

# Contents

## Abstract

*This report presents the results of a full-scale experimental investigation of helical pile (HP) foundations augmented with collar vane (CV) technology. The collar vane is a finned element installed near the pile head to mobilize soil resistance at shallow depths and reduce bending demands in slender helical pile shafts. Testing was conducted in cohesive soil and a constructed sand pit and included monotonic and cyclic lateral and torsional loading, as well as overturning tests representative of wind loading on roadside sign structures. Results show that collar vanes significantly increase lateral and torsional geotechnical resistance and reduce shaft bending moments relative to helical piles without vanes. Overturning tests demonstrate that selected HP–CV systems can perform comparably to conventional drilled shaft foundations used for sign support. Overall, the findings indicate that collar vane technology can expand the applicability of helical piles for transportation infrastructure, offering an efficient foundation alternative for infrastructure subjected to lateral loads.*

# Chapter 1: Introduction and Background

## 1.1 Project Motivation

Helical piles (HPs) are widely used in transportation and civil infrastructure due to their rapid installation, minimal site disturbance, and adaptability to a wide range of subsurface conditions. These advantages make helical piles particularly attractive for applications requiring expedited construction, limited excavation, or installation in constrained rights-of-way. Despite these benefits, the use of helical piles has historically been limited in applications governed by lateral, torsional, or overturning loading, such as roadside sign, lighting, and signal structures. In such cases, the slender pile shaft and installation-induced soil disturbance often result in relatively low lateral stiffness and resistance at shallow depths, where lateral deformations and bending demands are greatest.

State Departments of Transportation (DOTs) therefore continue to rely heavily on conventional reinforced concrete drilled shafts for roadside sign foundations, even in situations where axial demands are modest. While effective, drilled shafts are comparatively time- and labor-intensive, generate spoils, require curing time, and can be difficult to construct in restricted or environmentally sensitive locations. As a result, there is a strong motivation to develop alternative foundation systems that retain the constructability advantages of helical piles while providing lateral, torsional, and overturning performance comparable to conventional sign foundation types.

The collar vane (CV) concept was developed to address this need. By introducing a shallow, finned element near the pile head, the collar vane is intended to mobilize lateral soil resistance where it is most effective and transfer these forces directly to the pile head connection. In doing so, the CV has the potential to substantially reduce bending demands in the helical pile shaft and enable the use of helical piles in applications traditionally reserved for larger foundation systems. This project was motivated by the need to evaluate the feasibility, performance, and load-transfer mechanisms of HP–CV systems and to assess their applicability to DOT sign structure foundations subjected to wind-induced loading.

## 1.2 Background

Helical piles derive their axial capacity primarily from the bearing resistance of one or more helices welded to a central shaft, with shaft resistance typically playing a secondary role. Extensive laboratory, field, and numerical studies have been conducted to characterize axial capacity, failure mechanisms, and design methods for HPs in both cohesive and granular soils (e.g., Adams and Klym 1972; Mitsch and Clemence 1985; Ghaly et al. 1991; Merifield et al. 2001, 2003, 2006; Perko 2009). In contrast, the lateral and torsional behavior of HPs has received comparatively less attention and remains a limiting factor for many applications.

Previous research has shown that the lateral resistance of vertically oriented HPs is primarily controlled by shaft diameter and soil conditions, and that the presence of helices has only a modest influence on lateral performance (Prasad and Rao 1996; Perko 2003; Sakr 2009; Elkasabgy et al. 2019). Increasing shaft diameter can improve lateral and torsional resistance, but doing so undermines the material efficiency that makes HPs attractive in the first place.

To address similar limitations in other foundation systems, several researchers have investigated the use of *fin piles*, in which steel fins are attached near the pile head to increase the effective foundation width and mobilize greater passive soil resistance at shallow depths. Fin piles have been studied through laboratory-scale testing, numerical simulations, and limited field testing, and have generally demonstrated increased lateral capacity relative to conventional piles (Reinert and Newman 2002; Peng 2006; Nasr 2014; Sakr et al. 2020; Hubler et al. 2023). However, most fin pile systems must be driven or pushed into the ground to avoid excessive soil disturbance, making them incompatible with helical pile installation, which requires rotation.

Several concepts have been proposed to adapt fin systems for HPs by decoupling the fins from pile rotation during installation. These include collar-based or shell-based systems that allow fins to remain stationary while the pile shaft rotates (Maier and Oskoorouchi 2010; Stone et al. 2020; Qin et al. 2024). While these systems have demonstrated increased lateral resistance, the mobilized soil resistance is typically transferred to the pile shaft at depth, similar to conventional piles, resulting in elevated bending demands in the shaft.

The collar vane (CV) system evaluated in this study builds on these concepts but introduces a fundamentally different load-transfer mechanism. By structurally connecting the collar vane to the helical pile at the pile head through a bolted flange connection, the system is designed to mobilize lateral and torsional soil resistance at shallow depths while transferring the majority of that resistance to the pile head rather than along the embedded shaft. This approach is intended to substantially reduce bending and shear demands in the slender pile shaft while simultaneously increasing overall lateral, torsional, and overturning resistance—distinguishing the CV system from previously reported fin pile concepts.

## 1.3 Research Objectives and Report Overview

The primary objective of this study is to evaluate the effectiveness of collar vane (CV) technology for enhancing the lateral, torsional, cyclic, and overturning performance of helical pile (HP) foundations, with particular emphasis on applications relevant to transportation infrastructure and roadside sign support systems. The research focuses on quantifying load–displacement behavior, load transfer mechanisms, and bending demand reduction in slender helical pile shafts when augmented with collar vanes installed near the ground surface. Particular attention is given to comparing HP–CV systems with conventional foundation types commonly specified by state departments of transportation.

To meet these objectives, a comprehensive full-scale experimental program was conducted in both cohesive and granular soils. The program included monotonic lateral and torsional load tests, cyclic loading to simulate long-term wind effects, and overturning load tests representative of wind-induced demands on single-post roadside sign structures. The experimental results are used to assess performance trends across collar vane geometries, soil conditions, and loading modes, and to identify practical implications for foundation design.

This report is organized as follows. **Chapter 2** introduces the collar vane concept, describes the CV configurations evaluated in this study, and summarizes installation procedures and intended

load-transfer mechanisms. **Chapter 3** describes the test sites and subsurface conditions at the cohesive soil field site and the constructed sand test pit. **Chapter 4** presents the full-scale monotonic and cyclic lateral and torsional load testing program, including test configurations, instrumentation, loading protocols, and detailed interpretation of measured responses. **Chapter 5** presents the full-scale overturning tests performed to simulate wind loading on roadside sign foundations. **Chapter 6** summarizes the key findings of the study and discusses their implications for helical pile foundation design, including relevance to transportation infrastructure applications such as roadside sign foundations.

# Chapter 2: Collar Vane Concept and Design

## 2.1 Collar Vane Design

The Collar Vane consists of a finned steel collar installed near the ground surface and is connected to the head of a helical pile (HP). The collar vane (CV) is implemented as either a one-piece (CV1) or two-piece (CV2) attachment and consists of four steel fins welded to a steel collar that surrounds the central shaft of the helical pile (HP). In both configurations, the CV is structurally connected to the HP through bolted flanges located at the pile head. The CV1 configuration comprises a continuous cylindrical collar that is pre-installed around the upper portion of the HP central shaft (Figure 1a). In contrast, the CV2 configuration consists of two half-cylindrical collar sections that are assembled in the field using longitudinal bolts and can be installed around the central shaft of either a new or existing HP (Figure 1b). For the CV2 configuration, three fins are welded to one half of the cylindrical collar, while the fourth fin is welded to the opposing half. A more detailed drawing of the CV2 design is shown in Figure 2.

For both CV1 and CV2, the upper portion of the collar vane consists of a prismatic section with height $H_p$ and diameter $D$. Beneath the prismatic section, a tapered conical section of height $H_c$, inclined at 45°, is provided to facilitate installation. In all cases, the HP flange is welded to the HP central shaft, and the CV flange is welded to the upper ends of the CV fins.

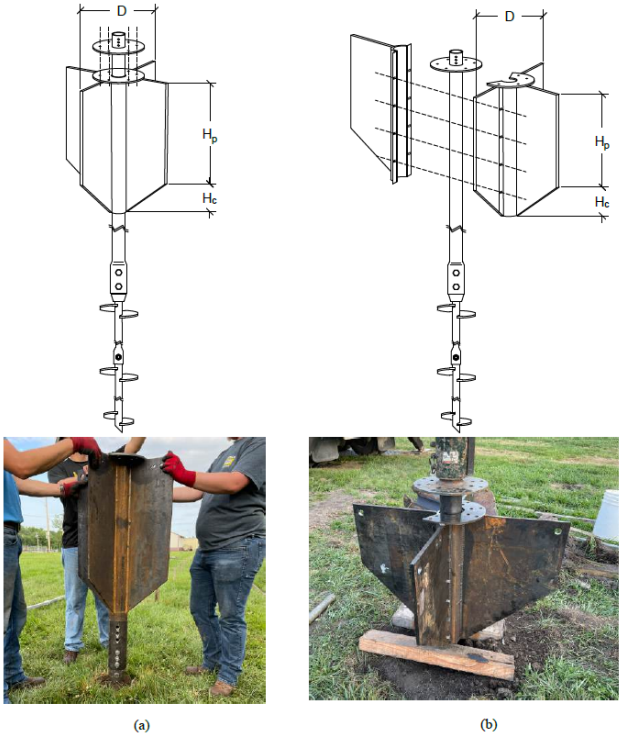


*Figure 1. Collar vane system illustrating the collar vane dimensions, configuration, and flanges welded at the head of the helical pile shaft and top of the collar vane a.) One-piece collar vane with a continuous steel collar pre-installed and wrapped around the top central shaft of a helical pile. b.) Two-piece collar vane with two half-cylindrical collar sections that are fastened together with bolts along depth of the collar around the central shaft of a helical pile. Photos show the collar vane prior to installation in the ground.*

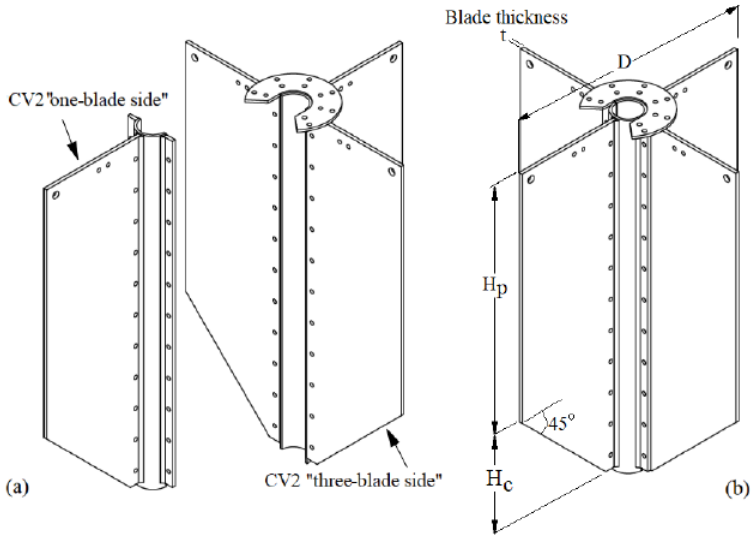


*Figure 2. Two-piece Collar Vane (CV2) sides: (a) exploded view of the two pieces and (b) final position (Hubbell Power Systems Inc.)*

The pile head connection designs shown in Figure 1and Figure 2 were used during the initial phases of field testing, where both lateral and torsional resistance were investigated. For the second phase of testing where overturning resistance was investigated, the CV flange was replaced with a "base plate", as illustrated in Figure 3. The base plate connection allows attachment of the vane to the pile head flange in the same manner (see Figure 1), but also allows attachment of a post (e.g. for a sign or light pole structure) to the foundation. A base plate was only used for the CV1-type vanes.

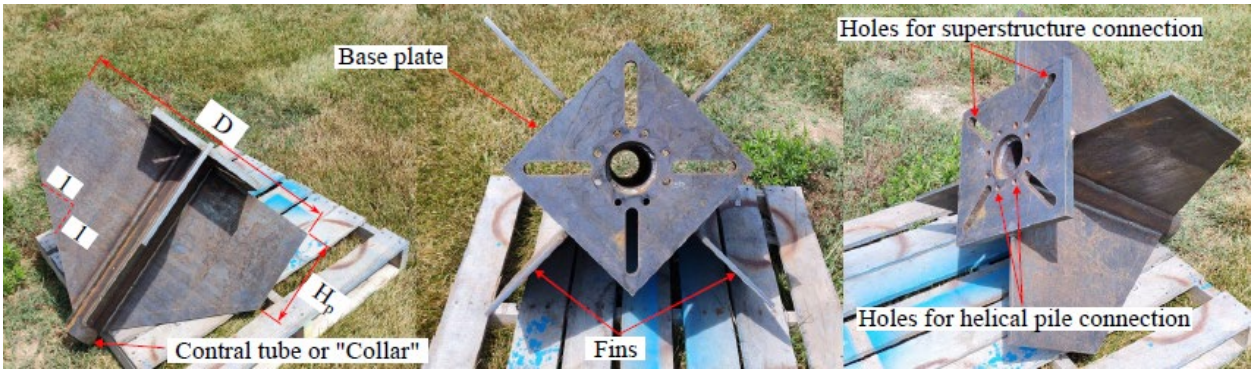


*Figure 3. Photographs illustrating collar vane dimensions and a base plate connection.*

## 2.2 Collar Vane Installation

Figure 4 illustrates the installation procedure for the collar vane (CV). In general, CV installation is efficient and can be readily incorporated into standard helical pile (HP) installation practices. Installation begins by rotating the HP lead section and associated shaft extensions with helices into the ground (Figure 4a). When a two-piece collar vane (CV2) is used, the collar is assembled and bolted around the HP central shaft as the final installation depth of the pile is approached (Figure

4b). The CV is not structurally connected to the HP via the flanges during this stage of installation, permitting the HP shaft to rotate freely within the collar. As installation progresses, contact between the HP and CV flanges produces a vertical downward force that pulls the CV into the ground (Figure 4c). Although the HP flange rotates during installation, the CV remains stationary because the flanges are not yet bolted together. In this study, a *Molykote* lubricant was applied between the HP and CV flanges to reduce friction and further limit unintended rotation of the CV during penetration. Once the HP and CV are installed to the target depth, the CV is structurally connected to the HP through the bolted flange connection at the pile head (Figure 4d). Following attachment, the HP-CV system can resist lateral and torsional loads.

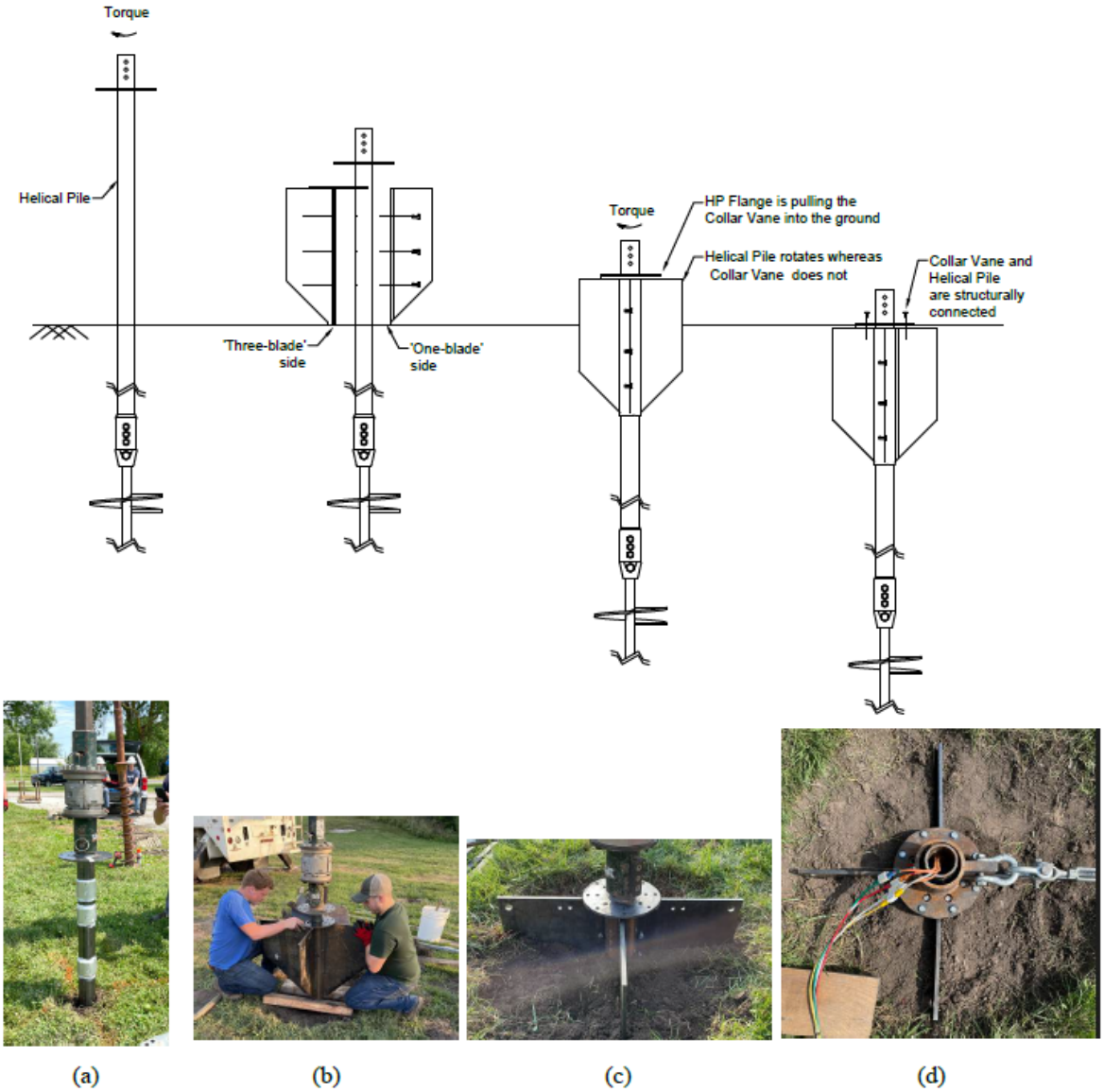


*Figure 4. Collar Vane installation sequence for CV2-type vanes. a.) Helical pile and lead sections are installed by a conventional torque motor. b.) Two collar vane sections are connected via bolts around the central shaft, but are not yet connected via flanges. c.) Helical pile installation continues and contact between the flanges pulls the collar vane into the ground without rotating. d.) The Collar Vane and helical pile are structurally connected via bolts through the flanges.*

A CV1-type vane is installed in a nearly identical manner a CV2. The primary difference is that the HP central shaft is slotted through the collar and attached to the lead sections, as illustrated in Figure 5a-b for CV1-type vane with a base plate. The remainder of installation (Figure 5c-d) progresses in the same manner as the CV2-type vanes. If a base plate is used instead of a flange for the CV, the installation remains identical to the one-piece systems, as illustrated in Figure 6. The only difference is that the flange attached to the central shaft pile head pulls down on the base plate to drag the CV into the ground (Figure 6c-d).

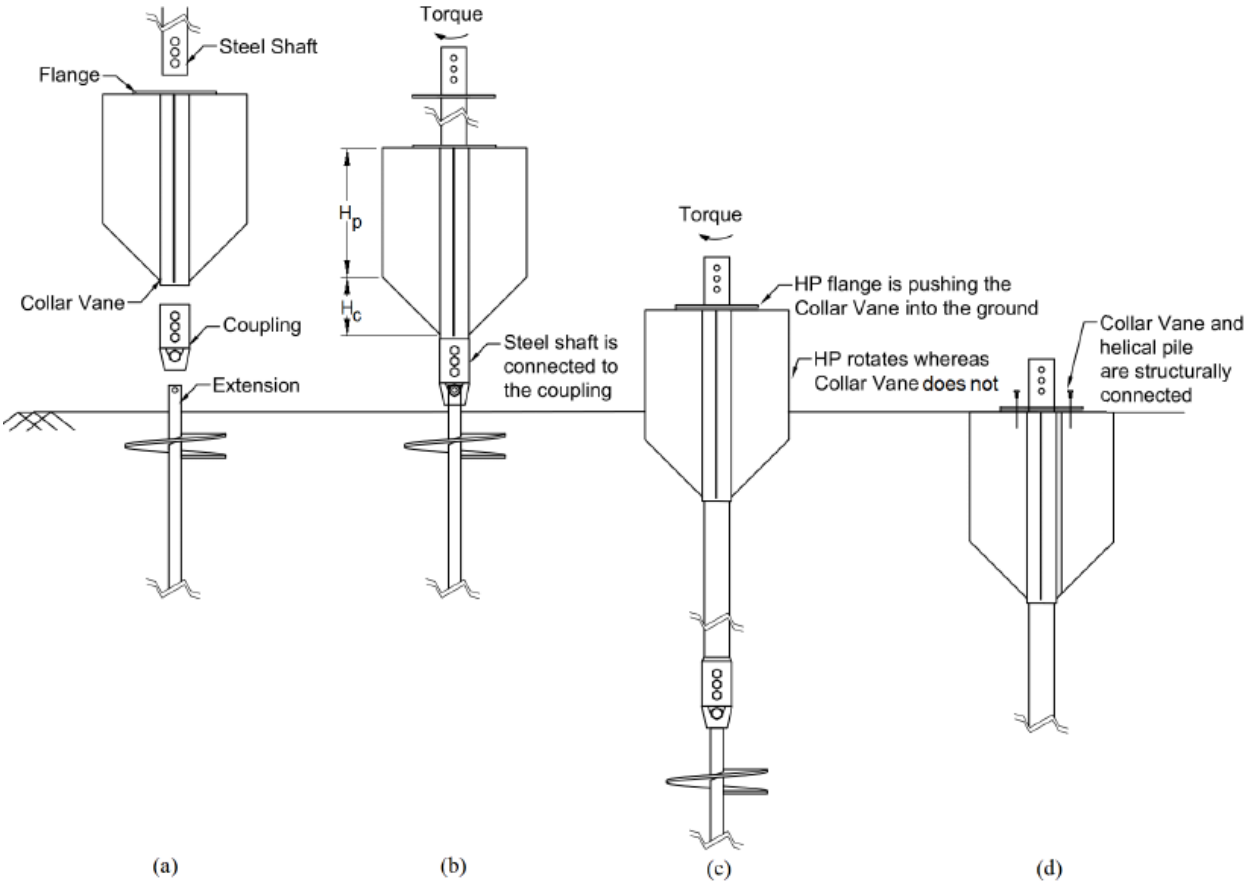


*Figure 5. One-piece Collar Vane installation sequence: (a) Collar Vane is placed after installing the extension; (b) steel shaft is connected to the extension after being passed through the CV; (c) Collar Vane does not rotate while being pushed into the ground and;(d) the Collar Vane is pushed into its final position and then locked off.*

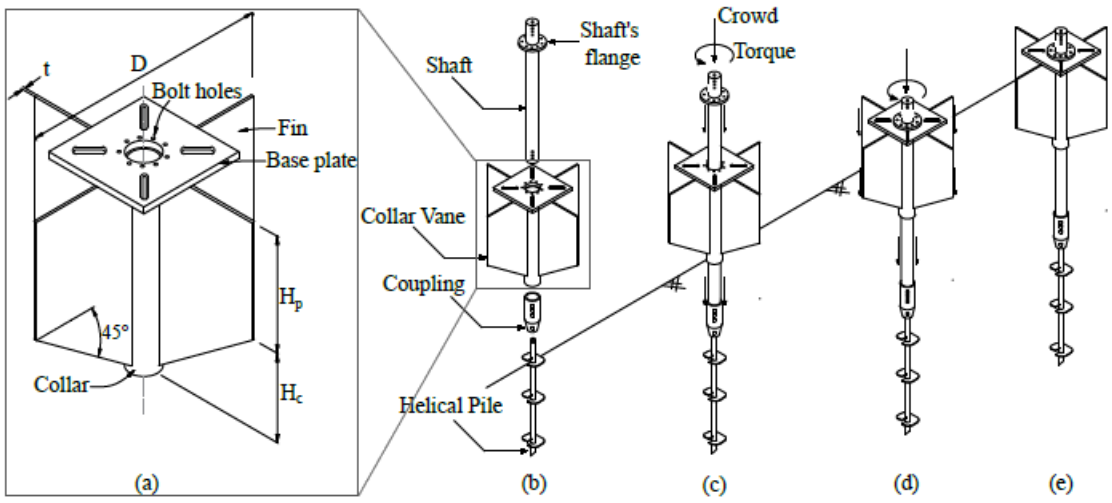


*Figure 6. Components and installation of a CV1-type vane with a base plate: (a) Schematic of a collar vane device; (b) Coupling of the collar vane to the helical pile; (c)-(e) Installation of the helical pile with a collar vane into the ground.*

## 2.3 Lateral and Torsional Resistance

Under lateral loading, the CV is intended to serve two primary functions: (a) to increase the effective diameter contributing to geotechnical resistance through the mobilization of soil resistance on the fins at shallow depths, where lateral deformations are greatest and the majority of passive resistance develops; and (b) to transfer the resistance mobilized by the CV to the pile head such that shear forces and bending moments in the slender helical pile (HP) shaft remain low. Figure 3a conceptually illustrates the application of a lateral load, $P$, and the corresponding transfer of mobilized lateral resistance from the CV to the HP.

A small annulus exists between the CV collar and the HP shaft, and the CV is not intended to transfer load directly to the HP shaft along the depth of the vane. That is, resistance mobilized by the surrounding soil is not transmitted to the shaft at depth. Instead, the passive soil resistance mobilized by the CV, $V_R$, is carried upward and transferred near the pile head through the bolted flange connection (Figure 7a). Concentrating the mobilized passive resistance at the pile head is expected to reduce shear forces and the associated bending moments in the slender HP shaft.

As illustrated in Figure 7b, torsional resistance is expected to be mobilized in a manner analogous to a field vane shear test (FVST), wherein rotation of the CV induces the development of a shear surface around the perimeter of the fins. Accordingly, cylindrical and conical shear surfaces are anticipated to form along the prismatic and tapered portions of the CV, respectively. The ultimate torsional resistance is governed by the shear resistance mobilized over the resulting failure surface area. Similar to lateral loading, torsional resistance is transferred to the HP through the bolted flange connection at the pile head.

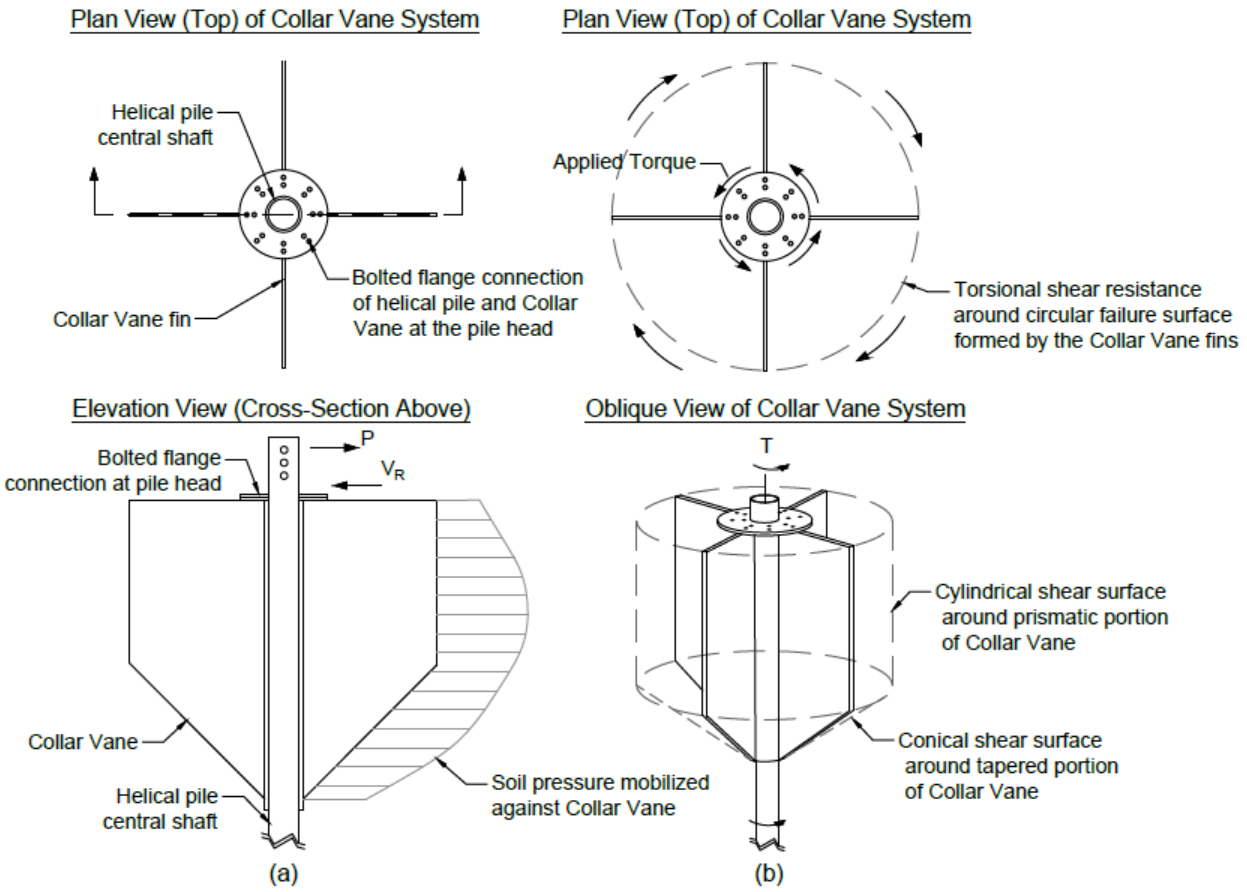


*Figure 7. a.) Plan view of collar vane system with helical pile (top) showing the cross-section of the elevation view (bottom) illustrating a lateral load, P, and the passive soil pressure mobilized along depth of the vane and the resulting lateral resisting force from the vane, VR, that is ultimately transferred through bolted flange connection near the pile head. b.) Plan (top) and perspective (bottom) views illustrating the torsional resistance and cylindrical and conical shear surfaces along the prismatic and tapered portions of the collar vane fins.*

## 2.4 Collar Vane Systems Tested

All collar vanes (CVs) were manufactured in Centralia, Missouri by Hubbell Power Systems. The CV geometries evaluated in this study included diameters of $D = 0.30$, 0.61, and 0.91 m and prismatic heights of $H_p = 0.30$, 0.61, and 0.91 m. In all cases, the tapered section was inclined at 45°, and the tapered height, $H_c$, varied as a function of the CV diameter. The fin thickness, $t$, ranged from 6.35 to 12.7 mm. The collar shaft had an internal diameter of 95.0 mm and a wall thickness of 8.0 mm. The nine CV geometries tested in this study are summarized in Table 1. The "Collar Vane ID" presented in Table 1 denotes the collar vane type (i.e., CV1 or CV2) and the corresponding diameter and prismatic height expressed in feet. For example, CV1 3-2 refers to a one-piece collar vane with $D = 3$ft (0.91 m) and $H_p = 2$ft (0.61 m).

*Table 1. Summary of collar vane types and dimensions tested in this study.*

| Collar Vane ID | Fin Thickness, $t$ (mm) | Diameter, $D$ (m) | Prismatic Height, $H_p$ (m) | Total Height, $H_t = H_p + H_c$ (m) |
|---|---|---|---|---|
| CV2 1-1 | 6.35 | 0.30 (1 ft.) | 0.30 (1 ft.) | 0.36 |
| CV2 1-2 | 6.35 | 0.30 (1 ft.) | 0.61 (2 ft.) | 0.66 |
| CV2 1-3 | 6.35 | 0.30 (1 ft.) | 0.91 (3 ft.) | 0.97 |
| CV2 2-1 | 6.35 | 0.61 (2 ft.) | 0.30 (1 ft.) | 0.51 |
| CV2 2-2 | 6.35 | 0.61 (2 ft.) | 0.61 (2 ft.) | 0.81 |
| CV2 2-3 | 6.35 | 0.61 (2 ft.) | 0.91 (3 ft.) | 1.12 |
| CV2 3-1 | 12.7 | 0.91 (3 ft.) | 0.30 (1 ft.) | 0.66 |
| CV2 3-2 | 12.7 | 0.91 (3 ft.) | 0.61 (2 ft.) | 0.97 |
| CV2 3-3 | 12.7 | 0.91 (3 ft.) | 0.91 (3 ft.) | 1.27 |
| CV1 2-2 | 9.52 | 0.61 (2 ft.) | 0.61 (2 ft.) | 0.81 |
| CV1 2-3 | 9.52 | 0.61 (2 ft.) | 0.91 (3 ft.) | 1.12 |
| CV1 3-1 | 12.7 | 0.91 (3 ft.) | 0.30 (1 ft.) | 0.66 |
| CV1 3-2 | 12.7 | 0.91 (3 ft.) | 0.61 (2 ft.) | 0.97 |
| CV1 3-3 | 12.7 | 0.91 (3 ft.) | 0.91 (3 ft.) | 1.27 |

**Note**: CV1 signifies a single-piece collar vane and CV2 signifies a two-piece collar vane. Collar vane ID refers to the collar vane type (i.e. CV1 or CV2) and the diameter and prismatic height of the CV in feet. For example, CV1 3-2 refers to a one-piece collar vane with $D$ = 3 ft. = 0.91 m and $H_p$ = 2 ft. = 0.61 m.

All CV1 vanes were fabricated using grade-80 steel with a minimum yield strength of 550 MPa. CV2 vanes with a diameter of 0.91 m were also manufactured using grade-80 steel, whereas CV2 vanes with diameters of 0.30 and 0.61 m were fabricated from grade-36 steel (minimum yield strength of 250 MPa) due to material availability at the time of manufacturing and testing. Higher-strength steel and increased fin thickness were prioritized for the larger CV geometries, and all vanes performed satisfactorily throughout the testing program, with no structural damage observed.

Each CV was attached to a helical pile consisting of a round pipe shaft (Hubbell catalog ID: RS3500.300) with a length of 3.05 m, fabricated from grade-50 steel (minimum yield strength $\sigma_y = 350$MPa). The shaft had a section modulus of $S_x = 34.5\ cm^3$, an outer diameter of $d =$ 88.9mm, and a wall thickness of $t = 7.15$mm. Two 1.2 m long square shaft extensions (catalog ID: SS 175), each fitted with a single 355 mm diameter helix, and a 2.1 m long square shaft lead section (SS 175) equipped with 254, 304, and 355 mm diameter helices were used to install all CVs. The same HP configuration was employed for all CV systems to isolate the influence of the CV geometry on performance during testing, although the CV concept may be applied to other HP sizes as well.

Two lateral and torsional load tests were conducted with collar vanes attached to extremely slender SS175 square shaft helical piles. These tests were performed to demonstrate that the collar vanes were responsible for the substantial majority of all lateral and torsional resistance mobilized when they were used—and thus applicable to a broad range of helical pile types. This is discussed in greater detail in the test results section.

# Chapter 3: Test Site and Subsurface Conditions

All load tests were conducted at the Hubbell Power Systems headquarters in Centralia, Missouri. Collar vanes (CVs) were tested at two locations: a natural clay site and an artificially constructed sand test area, as shown in Figure 4. Subsurface conditions at both sites were characterized using cone penetration tests (CPTs), borings, and field vane shear tests (FVSTs), with test locations also indicated in Figure 8. A summary of the subsurface conditions at the clay and artificial sand sites is presented in Figure 9.

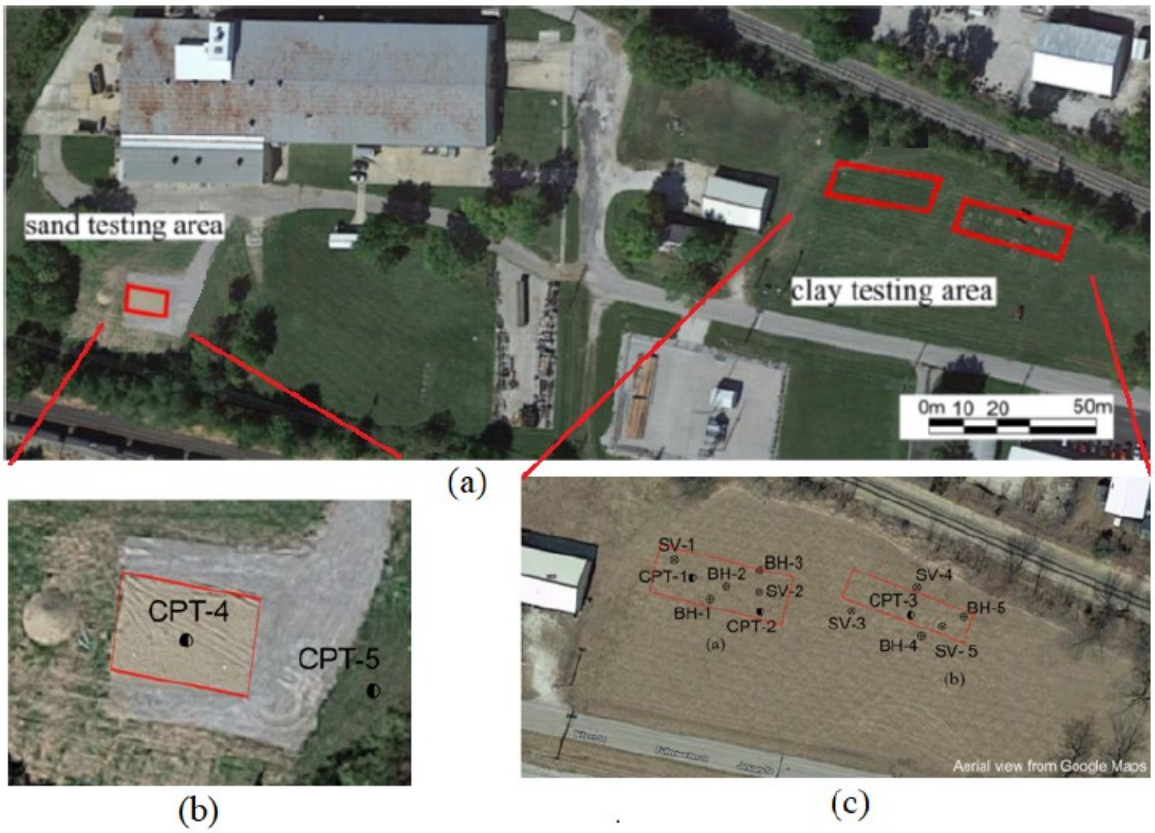


*Figure 8. (a) Aerial image of testing site locations (b) sand testing area and (c) clay testing area. Test site location: Hubbell Inc., Centralia, MO. Geographical coordinates of test site: 39◦ 12' 52.6104" N, 92◦ 08' 32.1504" W.*

According to Whitfield (1992), the surficial geologic unit at the site consists of Glacial Drift, composed primarily of sandy clay, clayey sand, and clayey silt with thicknesses ranging from 3 to 61 m and colors varying from tan to dark gray (Figure 9a,c). Water content and undrained shear strength profiles indicate the presence of an approximately 0.5 m thick crust underlain by overconsolidated cohesive materials (Figure 9d,e). Differences between the undrained shear strength ($S_u$) and residual undrained shear strength ($S_{ur}$) profiles estimated from CPT soundings, FVSTs, and unconfined compressive strength (UCS) tests are shown for reference in Figure 9e. Within the upper 4.5 m, FVST measurements of $S_u$ranged from 111 to 249 kPa, while $S_{ur}$ranged from 24 to 162 kPa, and these values showed reasonable agreement with CPT-based estimates (Figure 9e).

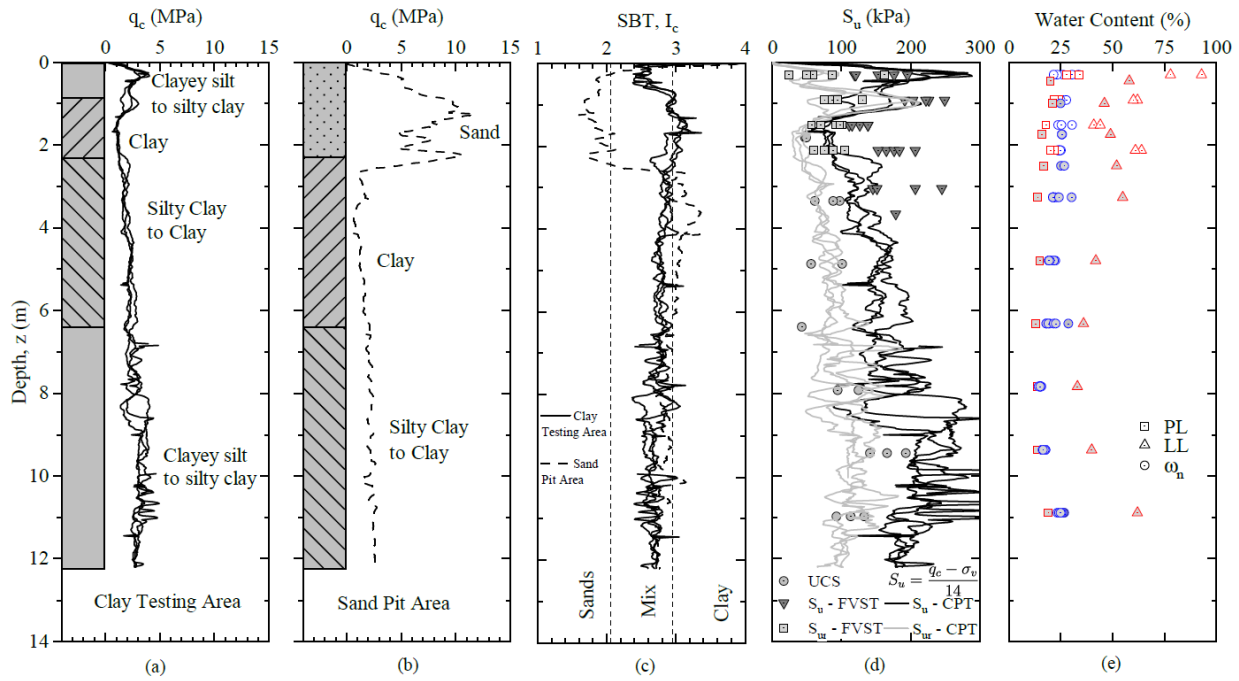


*Figure 9. Subsurface profile at the test site: a.) CPT tip resistance in the clay area; b.) CPT tip resistance in the constructed sand pit (depth ≈ 2.4 m; c.) CPT soil behavior type index in the clay and sand areas; d.) undrained shear strength profile in the clay; e.) natural water contents and Atterberg limits in the clay.*

The artificial sand test site was constructed within the same clay profile by excavating a pit and backfilling it with sand, as illustrated in Figure 10. An area measuring approximately 9.1 m in length and 6.4 m in width was excavated to a depth of about 2.4 m and subsequently backfilled with clean, poorly graded medium sand (Figure 9b). The pit was constructed using nine 0.27 m thick lifts, with each lift compacted using a vibratory compactor to achieve a relatively uniform density. CPT correlations with relative density and friction angle indicate a relative density ($D_r$) ranging from 55 to 80% and an effective friction angle between 39° and 42° (Jamiolkowski et al. 2003; Kulhawy and Mayne 1990). The grain size distribution of the sand is shown in Figure 11 and the index properties are summarized in Table 2.


*Figure 10. Artificial sand test site under construction for testing in summer 2022.*

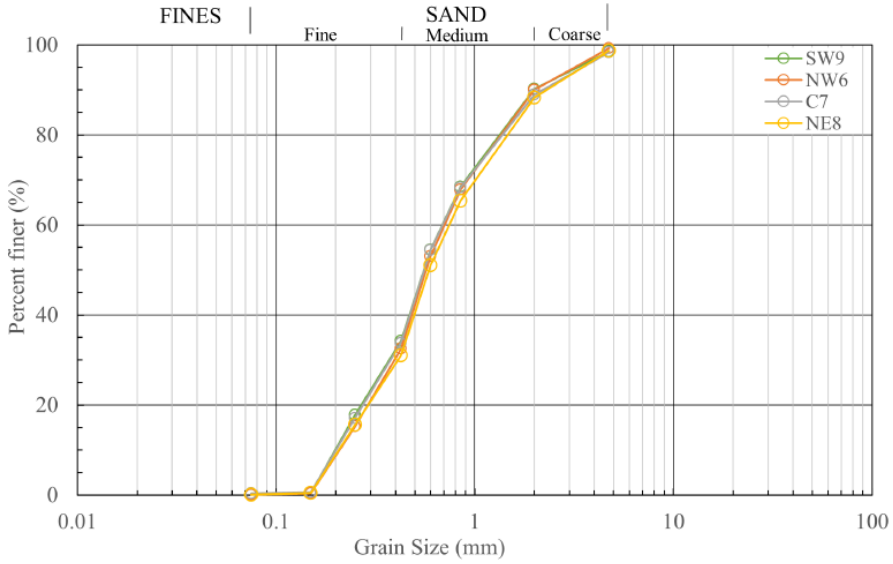


*Figure 11. Grain size distribution from several test pit sand samples.*

*Table 2. Index properties of sand used to backfill an artificial sand pit for collar vane testing.*

| Physical properties of sand used in the tests | |
|---|---|
| Effective grain size, $D_{10}$ (mm) | 0.21 |
| Average grain size, $D_{50}$ (mm) | 0.57 |
| Uniformity coefficient, $C_u$ | 3.27 |
| Coefficient of curvature, $C_c$ | 1.11 |
| Maximum dry unit weight, $\gamma_{d_{max}}$ (kN/m$^3$) | 18.53 |
| Minimum dry unit weight, $\gamma_{d_{min}}$ (kN/m$^3$) | 16.54 |
| Maximum void ratio, $e_{max}$ | 0.58 |
| Minimum void ratio, $e_{min}$ | 0.41 |
| Specific gravity, $G_s$ | 2.66 |
| Coarse to medium sand (%) | 66 |
| Fine sand (%) | 34 |
| Classification (USCS, ASTM D2487-17 (2020)) | SP |
| Water content, $\omega_c$ (%) | 3 |

# Chapter 4: Full-Scale Testing: Lateral and Torsional Resistance

## 4.1 Load Test Details

### Lateral Load Tests

Figure 12 presents plan and elevation views of the experimental field setup used for the lateral load tests. In cohesive soils, lateral loads were applied using two tie-rod hydraulic cylinders, each with a stroke of 0.41 m and a capacity of 29 kN, arranged in a parallel configuration between a reaction helical pile and the HP–CV test system. At the sand test site, lateral loads were applied using a 600 kN hollow-plunger hydraulic cylinder. The hydraulic cylinders were connected to a loading steel cap bolted to the HP pile head using a turnbuckle. The load application point was located between 0.22 and 0.33 m above the ground surface for all tests. The hydraulic cylinders were connected to a manifold equipped with a calibrated 69 MPa pressure transducer to monitor the applied pressure, and an air-hydraulic pump was used to regulate the pressure supply.

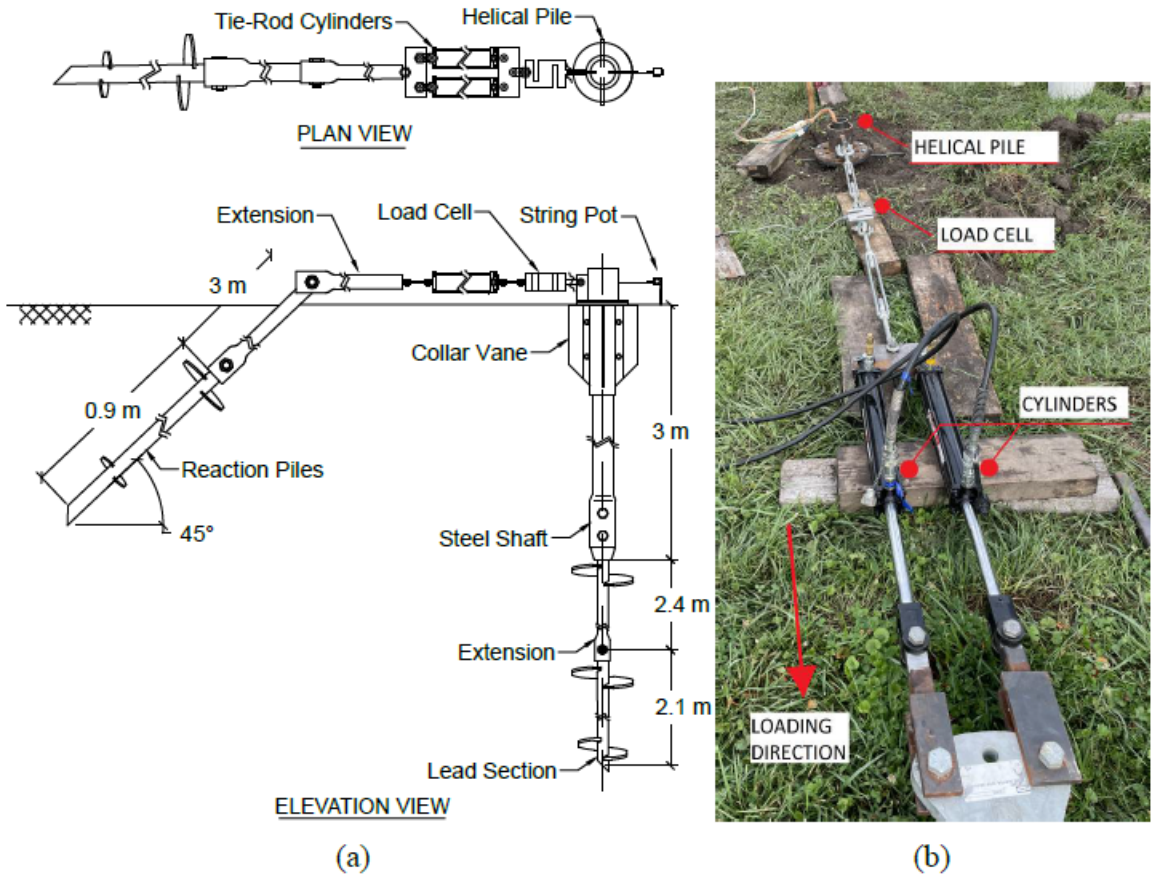


*Figure 12. Lateral load test setup and associated instrumentation: a) plan and elevation views illustrating the reaction pile, hydraulic cylinders, load cells, string pots, HP-CV system; b) photograph of experimental setup in the field.*

A calibrated S-type load cell with a capacity of 49 kN was used to measure lateral loads in cohesive soils, while a 178 kN S-type load cell was used at the sand site. Pile head displacements were measured using a calibrated string potentiometer (SP) with a maximum stroke of 254 mm. The SPs were mounted on an independently supported reference beam positioned 2 m from the pile head.

The HP shaft was instrumented with electrical resistance strain gauges installed at eight locations along the outer surface of the shaft and aligned with the direction of loading, as illustrated in Figure 13. At each location, two strain gauges were bonded on opposite sides of the shaft and configured in a half-Wheatstone bridge arrangement to compensate for temperature effects and axial strain, thereby enabling accurate determination of bending moments in the shaft. The depths of the strain gauge locations (SG-1 through SG-8), shown in Figure 13a, began 0.15 m below the top flange near the pile head. The strain gauge locations were selected to capture bending response to depths at or near the anticipated depth of fixity under lateral loading conditions.

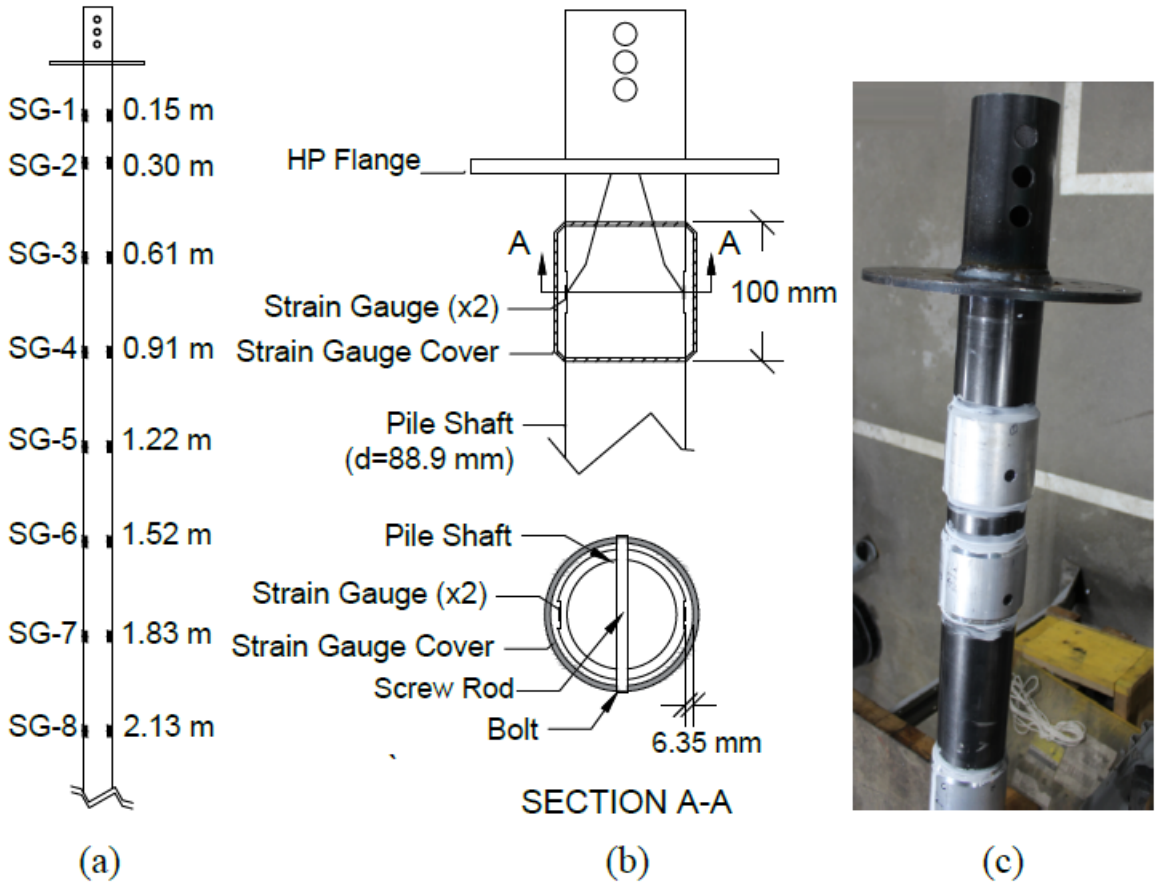


*Figure 13. Strain gauge configuration and details: a.) depth of strain gauges along the HP shaft measured from the HP flange; b.) schematic of strain gauge covers; c.) photograph of strain gauge covers.*

To protect strain gauges and wiring from environmental exposure and installation damage, a water-resistant protective coating was applied, and mechanical strain gauge covers were installed. Figure 13b-c illustrate the protective covers, which consisted of two half-cylindrical aluminum shells assembled to form a continuous barrier around the shaft circumference at each gauge location. The

covers were 100 mm in length and 5 mm in thickness and were designed to avoid contact with both the strain gauges and the CV collar. Each cover was secured to the shaft using flat socket screw rods inserted through holes drilled through both the covers and the shaft and bolted at each end. This attachment method minimized any influence of the covers on the bending stiffness of the shaft, which was verified through controlled out-of-ground bending tests involving applied moments and measured strains. Although the protection system generally performed well, strain gauge failures occurred intermittently, and damaged gauges were replaced at the conclusion of each day of testing.

All measurements, including strain, displacement, applied load, and hydraulic cylinder pressure, were recorded continuously using a data acquisition system (DAQ). The DAQ system consisted of a National Instruments cDAQ-9184 four-slot chassis equipped with one NI-9205 module and three NI-9219 modules. The NI-9205 module is a 16-channel differential voltage input module used to record string potentiometer signals, while the NI-9219 modules are four-channel universal analog input modules used to acquire data from the strain gauges, load cells, and pressure transducer monitoring the hydraulic system.

Lateral load tests were performed in general accordance with ASTM D3966. Loads were applied monotonically such that each load increment corresponded to approximately 20% of the flexural yield capacity of the HP shaft. This loading protocol was selected for efficiency, as lateral capacity varied substantially among the different CV geometries. Each load increment was maintained for a minimum duration of 10 minutes or until pile head displacements stabilized and strain gauge readings exhibited no further change. Loading continued until a pile head displacement of approximately 25 mm was reached or until the hydraulic system approached its maximum capacity. Following completion of loading, the pile was unloaded in four equal decrements, with each decrement held constant for 5 minutes. Test durations were consistent across all cases, ranging from approximately 1 h 20 min to 1 h 40 min.

### Torsion Load Tests

A dedicated torsional load frame was developed to conduct torsional load tests on helical pile–collar vane (HP–CV) systems. Figure 14 illustrates the torsional load test configuration, in which a steel torsional load frame was attached to the pile head using a bolted flange connection. Torsional loads were applied by two 29 kN hydraulic cylinders, each with a stroke of 0.76 m, mounted at opposite ends of a 3.0 m long loading arm and actuated in opposing directions. The forces applied by the hydraulic cylinders were measured using two 49 kN load cells. Similar to the lateral load testing configuration, a single manifold was used to supply uniform pressure to both tie-rod hydraulic cylinders.

Forces were applied at lever arm distances of either 0.75 or 1.5 m from the center of rotation at the pile head, with the 1.5 m configuration used for most tests and shown in Figure 14. Torsional loading was increased to target small rotations early on and then progressively increased to target larger rotation increments as testing advanced to capture the nonlinear mobilization of torsional resistance. Between 16 and 20 loading increments targeting 0.2°, 0.5°, or 4° of rotation were imposed, with each increment maintained for a minimum of 5 minutes or until no further creep

deformation was observed. Loading continued until the maximum torque was reached, defined as $dT/d\theta \leq 0$, or until the hydraulic cylinders reached their stroke limits.

String potentiometers were mounted to fixtures located at the tops of two CV fins and at each end of the torsional load frame to measure displacements and to evaluate both pile head rotation and CV rotation (Figure 14). All measurements were recorded using the same data acquisition system employed for the lateral load tests, as described in the preceding section.

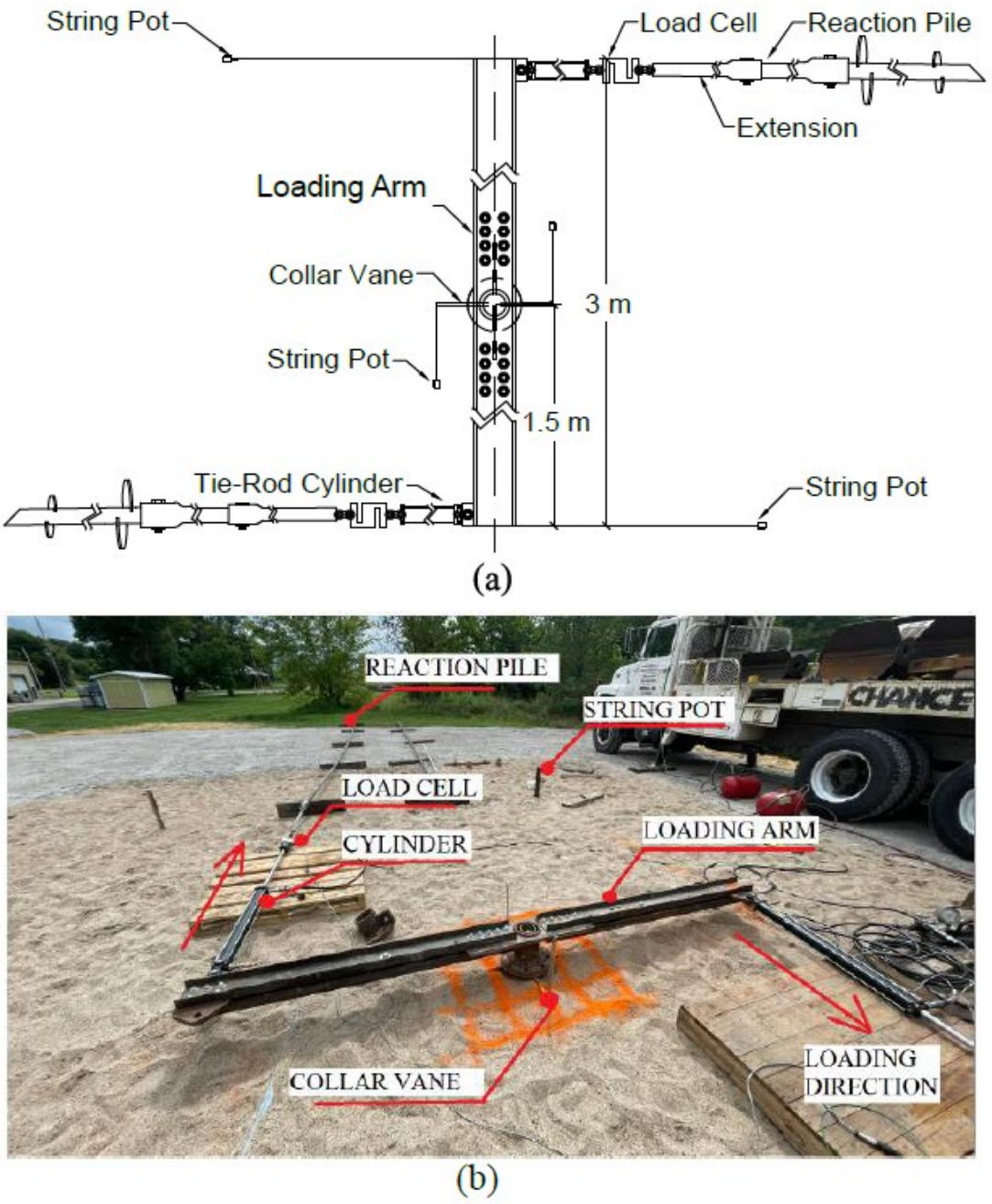


*Figure 14. Torsion load test setup: a.) plan view; b.) photograph of setup in sand pit*

## Cyclic Testing

Cyclic loading was applied to simulate repetitive (e.g. wind) loading on the HP-CV system. A total of 1,000 load cycles were imposed using the hydraulic controller, with each cycle having a period of 8 s (0.125 Hz). Cyclic load ratios, $\zeta_b$, of approximately 30, 50, and 70% of the predefined ultimate capacity were used. These cyclic load ratios were defined based on the ultimate torsional capacity and the lateral load required to produce a pile head displacement of 12.5 mm (from monotonic testing). Following completion of each cyclic loading sequence, a monotonic lateral load test was conducted to evaluate the post-cyclic lateral capacity of the pile.

For each helical pile (HP), approximately 1,000 load cycles were applied during both lateral and torsional cyclic tests at the same installation location. As a result, the measured torsional response is expected to reflect the influence of prior cyclic lateral loading. This loading sequence was intentionally selected to investigate the combined effects of cyclic lateral and torsional loading on a single foundation element, consistent with conditions that may be experienced by piles subjected to long-term wind loading in practice.

Cyclic loads for both lateral and torsional tests were applied using a PG1204S hydraulic pump coupled with a Tescom ER5K electro-pneumatic pressure control system manufactured by Emerson Process Management. The ER5K regulator, rated for a maximum hydraulic pressure of 69,000 kPa, was used to control the hydraulic pressure supplied to the double-acting cylinders during cyclic testing. The hydraulic pump and regulator assembly are shown in Figure 15.

The ER5K system operates as a closed-loop pressure regulation unit and includes an internal pressure transducer that continuously monitors hydraulic pressure within the flow line. During pressurization, the regulator exhaust vent remains closed to allow pressure to build, and once the target pressure is reached, excess fluid is diverted through a return line back to the pump reservoir. Regulation is achieved through a pneumatically actuated diaphragm that controls the opening and closing of the hydraulic vent valve (Keefe, 2020).

Pressure histories were implemented using *ERTune* software developed by TESCOM, which enables user-defined pressure profiles to be applied as a function of time. The software was used to generate repeatable cyclic pressure commands compatible with the pump capacity and regulator response. Manufacturer-supplied default tuning parameters were used for all tests, as they provided stable and consistent pressure regulation without excessive overshoot or oscillation under the cyclic loading conditions employed in this study.

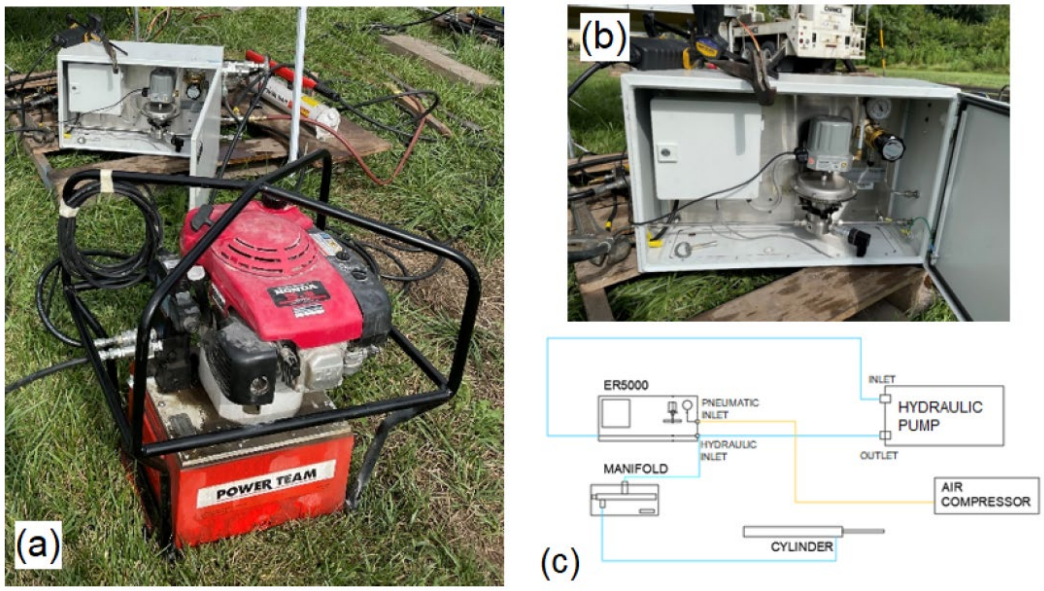


*Figure 15. (a) PG1204S hydraulic pump; (b) Tescom ER5K hydraulic pressure controller and; (c) flow schematic for the cyclic test.*

## Load Test Sequence, Layout, and Summary

The minimum center-to-center spacing between tested piles was 3 m, and reaction piles were located at least 4.5 m from the tested helical pile–collar vane (HP–CV) systems. In general, both lateral and torsional load tests were conducted at each location where an HP–CV system was installed. For tests performed in cohesive soils using CV2-type vanes, lateral and torsional load tests were conducted using two different loading sequences. In one sequence, a lateral load test was performed within approximately one hour of HP installation, followed by a torsional load test; this sequence is herein referred to as the lateral–torsional (LT) sequence. In the second sequence, a torsional load test was conducted prior to a lateral load test; this sequence is referred to as the torsional–lateral (TL) sequence.

The two loading sequences were adopted to maximize the number of lateral and torsional tests conducted within practical time constraints, as they did not require installation of additional piles. The LT sequence provided measurements of lateral response without prior disturbance, as well as torsional resistance following the application of relatively large lateral loads. Conversely, the TL sequence allowed assessment of torsional resistance prior to any disturbance associated with lateral loading. The CV1-type vanes were developed later in the testing program, and only the LT loading sequence was performed due to time constraints and because the LT sequence was not observed to have a significant influence on the torsional response for CV2-type vanes (Carvajal-Munoz 2023).

Only CV1-type vanes were tested in granular soil; therefore, only the LT sequence was applied. This decision was driven by space limitations within the sand test pit and by observations from cohesive soil testing indicating that lateral loading did not significantly influence subsequent torsional response.

During the first testing phase in summer 2021, load tests were only conducted in cohesive soil. Load tests were performed sequentially at locations T1-1 through T1-11 along the top row, followed by locations T2-11 through T2-1 in the middle row, and T3-10 through T3-5 in the bottom row, as shown in Figure 16a. In the second testing phase conducted in summer 2022, the same layout was used and testing was carried out at locations T4-1 through T4-11, as well as locations T5-3 and T5-1, as shown in Figure 16b. This systematic progression across rows and phases allowed efficient use of the test area while providing multiple spatially distinct locations.

Figure 17 illustrates the layout of test pile locations and reaction piles at the granular soil test site in summer 2022. Reaction piles were positioned approximately 15 m apart, resulting in a minimum center-to-center spacing of 3 m between adjacent test pile locations and at least 4.5 m between test piles and reaction piles to limit interaction effects. Test piles were installed and removed after completion of each test, with testing conducted sequentially at locations TS1-1 through TS3-2 within the sand test pit.

All reaction piles were installed outside the test pit perimeter. Separate reaction pile groupings were used to support lateral and torsional loading, with reaction piles for torsional testing arranged to provide an effective lever arm of approximately 1.5 m at each end of the loading system. This layout enabled multiple lateral and torsional tests to be conducted efficiently while maintaining consistent pile spacing and minimizing boundary effects within the granular test area, as shown in Figure 17.

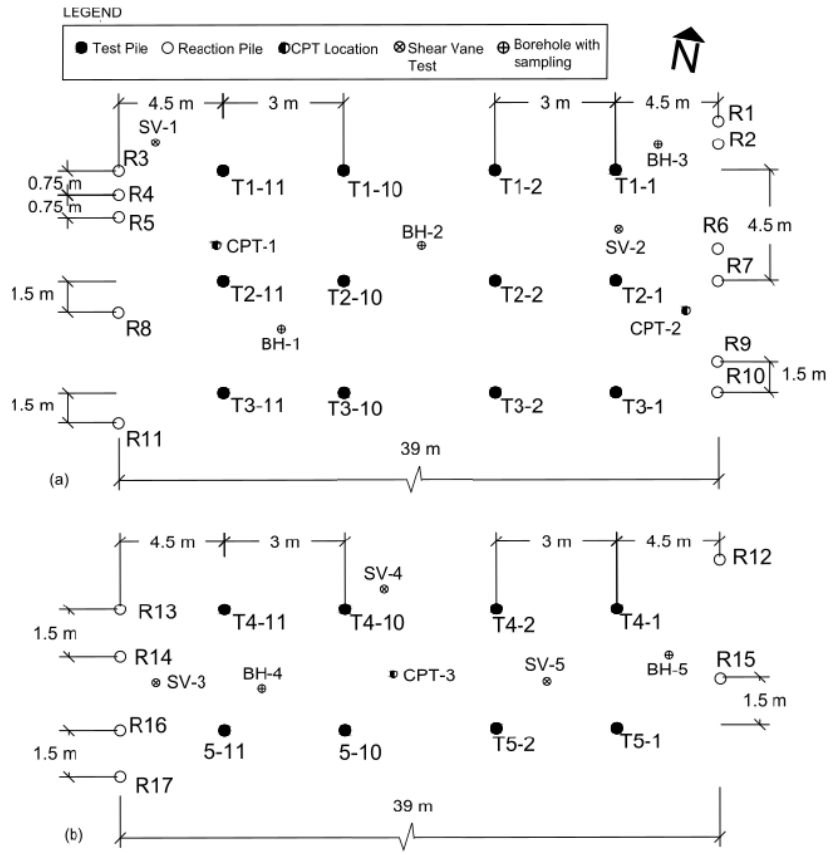


*Figure 16. Cohesive soil test site layout for test piles and reaction piles during a.) summer 2021 and b.) summer 2022.*

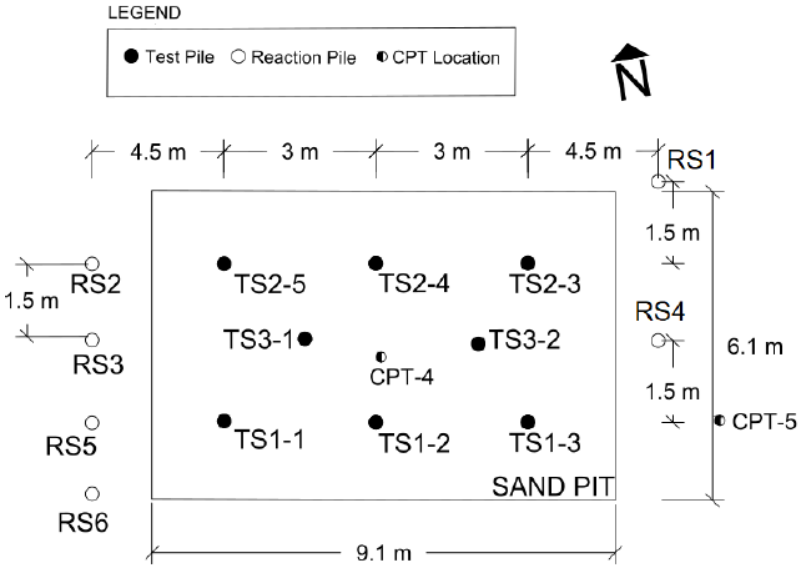


*Figure 17. Granular soil site test pile and reaction pile layout in summer 2022.*

The experimental program summarized in Table 3 and Table 4 was designed to evaluate the lateral and torsional performance of helical piles augmented with Collar Vanes across multiple vane geometries, soil conditions, loading types, and test sequences. Phase 1 testing, conducted in 2021

(Table 3), focused on two-piece Collar Vanes (CV2) installed in cohesive soil and included monotonic lateral and torsional load tests performed using both lateral–torsional (LT) and torsional–lateral (TL) sequences, as well as cyclic loading conducted using the LT sequence; a cyclic baseline test on a helical pile without a Collar Vane was also performed for comparison.

Phase 2 testing conducted in 2022 (Table 4) primarily consisted of additional torsional testing of selected CV2 configurations that weren't failed in summer 2021 and testing of a newly developed single-piece Collar Vane (CV1) in both cohesive soil and a backfilled sand test pit (only available in summer 2022). Cyclic loading was performed in both soil conditions for selected configurations, with repeated cyclic tests conducted at different cyclic load-to-ultimate load ratios, $\zeta_b = P_c/P_u$.

*Table 3. Summary lateral and torsion load tests performed during summer 2021 with a two-piece collar vane.*

| Date | Collar Vane | Location | Load Sequence | Type of Test | Test Name |
|---|---|---|---|---|---|
| 2021-07-12 | Helical Pile no CV | T 1-1 | Lateral | Monotonic in cohesive soil | HP LT |
| 2021-07-13 | Helical Pile no CV | T 1-1 | Torsion | Monotonic in cohesive soil | |
| 2021-07-15 | Helical Pile no CV | T 1-2 | Torsion-Lateral | Monotonic in cohesive soil | HP TL |
| 2021-07-16 | CV2 1-1 | T 1-3 | Lateral-Torsion | Monotonic in cohesive soil | CV2 1-1 LT |
| 2021-07-19 | CV2 2-1 | T 1-4 | Lateral-Torsion | Monotonic in cohesive soil | CV2 2-1 LT |
| 2021-07-20 | CV2 2-1 | T 1-5 | Torsion-Lateral | Monotonic in cohesive soil | CV2 2-1 TL |
| 2021-07-21 | CV2 1-2 | T 1-6 | Lateral-Torsion | Monotonic in cohesive soil | CV2 1-2 LT |
| 2021-07-22 | CV2 1-2 | T 1-7 | Torsion-Lateral | Monotonic in cohesive soil | CV2 1-2 TL |
| 2021-07-23 | CV2 1-1 | T 1-8 | Torsion-Lateral | Monotonic in cohesive soil | CV2 1-1 TL |
| 2021-07-26 | CV2 1-3 | T 1-9 | Lateral-Torsion | Monotonic in cohesive soil | CV2 1-3 LT |
| 2021-07-27 | CV2 1-3 | T 1-10 | Torsion-Lateral | Monotonic in cohesive soil | CV2 1-3 TL |
| 2021-07-28 | CV2 2-2 | T 1-11 | Lateral-Torsion | Monotonic in cohesive soil | CV2 2-2 LT |
| 2021-07-30 | CV2 2-2 | T 2-11 | Torsion-Lateral | Monotonic in cohesive soill | CV2 2-2 TL |
| 2021-08-02 | CV2 2-3 | T 2-10 | Lateral-Torsion | Monotonic in cohesive soil | CV2 2-3 LT |
| 2021-08-10 | CV2 3-1 | T 2-9 | Torsion-Lateral | Monotonic in cohesive soil | CV2 3-1 TL |
| 2021-08-11 | CV2 3-1 | T 2-8 | Lateral-Torsion | Monotonic in cohesive soil | CV2 3-1 LT |
| 2021-08-12 | CV2 3-2 | T 2-7 | Lateral-Torsion | Monotonic in cohesive soil | CV2 3-2 LT |
| 2021-08-13 | CV2 3-3 | T 2-6 | Lateral-Torsion | Monotonic in cohesive soil | CV2 3-3 LT |
| 2021-08-16 | CV2 3-3 | T 2-5 | Torsion-Lateral | Monotonic in cohesive soil | CV2 3-3 TL |
| 2021-08-17 | CV2 3-2 | T 2-4 | Torsion-Lateral | Monotonic in cohesive soil | CV2 3-2 TL |
| 2021-08-18 | CV2 2-3 | T 2-3 | Torsion-Lateral | Monotonic in cohesive soil | CV2 2-3 TL |
| 2021-08-19 | CV2 3-2 | T 2-2 | Lateral-Torsion | Cyclic in cohesive soil | CV2 3-2 LT Cyc |
| 2021-08-20 | CV2 3-3 | T 3-10 | Lateral-Torsion | Cyclic in cohesive soil | CV2 3-3 LT Cyc |
| 2021-08-23 | CV2 3-1 | T 3-9 | Lateral-Torsion | Cyclic in cohesive soil | CV2 3-1 LT Cyc |
| 2021-08-24 | CV2 2-1 | T 3-8 | Lateral-Torsion | Cyclic in cohesive soil | CV2 2-1 LT Cyc |
| 2021-08-25 | CV2 3-3 | T 3-7 | Lateral-Torsion | Cyclic in cohesive soil | CV2 3-3 LT Cyc R |
| 2021-08-26 | CV2 3-2 | T 3-6 | Lateral-Torsion | Cyclic in cohesive soil | CV2 3-2 LT Cyc R |
| 2021-08-27 | Helical Pile no CV | T 3-5 | Lateral | Cyclic in cohesive soil | HP L Cyc |

**Note**: LT, Lateral-Torsion sequence; TL, Torsion-Lateral sequence; Cyc, cyclic loading test; R, repeated test with a different $\zeta_b$; L, only lateral test performed.

*Table 4. Summary lateral and torsion load tests performed during summer 2022 with one- and two-piece collar vanes.*

| Date | Collar Vane | Location | Load Sequence | Type of Test | Test Name |
|---|---|---|---|---|---|
| 2022-07-22 | CV2 3-1 | T 3-2 | Lateral-Torsion | Long term monotonic test in cohesive soil | CV2 3-1 LT* |
| 2022-07-25/26 | CV2 3-1 | T 3-1 | Torsion | Monotonic in cohesive soil | CV2 3-1 T |
| 2022-07-27 | CV2 3-2 | T 4-1 | Torsion | Monotonic in cohesive soil | CV2 3-2 T |
| 2022-07-28 | CV2 2-2 | T 4-2 | Torsion | Monotonic in cohesive soil | CV2 2-2 T |
| | CV2 2-3 | T 4-3 | Torsion | Monotonic in cohesive soil | CV2 2-3 T |
| 2022-07-29 | CV2 3-3 | T 4-4 | Torsion | Monotonic in cohesive soil | CV2 3-3 T |
| 2022-08-01 | CV1 2-2 | T 4-5 | Lateral-Torsion | Monotonic in cohesive soil | CV1 2-2 LT |
| 2022-08-02 | CV1 3-2 | T 4-6 | Lateral-Torsion | Monotonic in cohesive soil | CV1 3-2 LT |
| 2022-08-03 | CV1 2-3 | T 4-7 | Lateral-Torsion | Monotonic in cohesive soil | CV1 2-3 LT |
| 2022-08-04 | CV1 3-3 | T 4-8 | Lateral-Torsion | Monotonic in cohesive soil | CV1 3-3 LT |
| 2022-08-08 | Helical Pile no CV | TS 1-1 | Lateral-Torsion | Monotonic in granular soil | HP LT S |
| 2022-08-09 | CV1 2-2 | TS 1-2 | Lateral-Torsion | Monotonic in granular soil | CV1 2-2 LT S |
| 2022-08-10 | CV1 2-3 | TS 1-3 | Lateral-Torsion | Monotonic in granular soil | CV1 2-3 LT S |
| 2022-08-11 | CV1 3-2 | TS 2-3 | Lateral-Torsion | Monotonic in granular soil | CV1 3-2 LT S |
| 2022-08-15 | CV1 3-3 | TS 2-2 | Lateral-Torsion | Monotonic in granular soil | CV1 3-3 LT S |
| 2022-08-17 | CV1 3-2 | TS 2-1 | Lateral | Monotonic in granular soil | CV1 3-2 L S |
| 2022-08-19 | CV1 3-2 | TS 3-2 | Lateral-Torsion | Cyclic in granular soil | CV1 3-2 LT Cyc S |
| 2022-08-22 | CV1 3-2 | TS 3-1 | Lateral-Torsion | Cyclic in granular soil | CV1 3-2 LT Cyc S R |
| 2022-08-23 | CV1 2-2 | T 4-9 | Lateral | Cyclic in cohesive soil | CV1 2-2 L Cyc |
| | CV1 2-2 | T 4-10 | Torsion | Cyclic in cohesive soil | CV1 2-2 T Cyc |
| 2022-08-24 | CV1 3-2 | T 4-11 | Lateral-Torsion | Cyclic in cohesive soil | CV1 3-2 LT Cyc |
| 2022-08-25 | CV1 2-2 | T 5-1 | Lateral-Torsion | Monotonic in cohesive soil using square shaft | CV1 2-2 LT SS175 |
| 2022-08-26 | CV1 3-2 | T 5-3 | Lateral-Torsion | Monotonic in cohesive soil using square shaft | CV1 3-2 LT SS175 |

**Note**: LT, Lateral-Torsion sequence; TL, Torsion-Lateral sequence; Cyc, cyclic loading test; R, repeated test with different $\zeta_b$; *, Long Term test; S, test performed in granular soil; SS175, square shaft; L, only lateral test performed; T, only torsion test performed

## 4.2 Monotonic Load Test Results

### Lateral Load Tests

The load–displacement responses for all collar vane (CV) configurations tested in cohesive soil are presented in Figure 18 for the lateral–torsional (LT) loading sequence. Because helical pile–collar vane (HP–CV) systems are not expected to experience torsional failure prior to lateral loading in practice, the LT sequence provides a more realistic assessment of lateral performance associated with the CV. The influence of CV diameter on lateral resistance is illustrated for prismatic heights of $H_p = 0.30$, 0.61, and 0.91 m in Figure 18a, Figure 18b, and Figure 18c, respectively. Recall, only CV configurations 2-2, 2-3, 3-2, and 3-3 were tested for CV1-type vanes. For reference, the dashed curve in each figure represents the load–displacement response of a helical pile without a collar vane ("No CV").

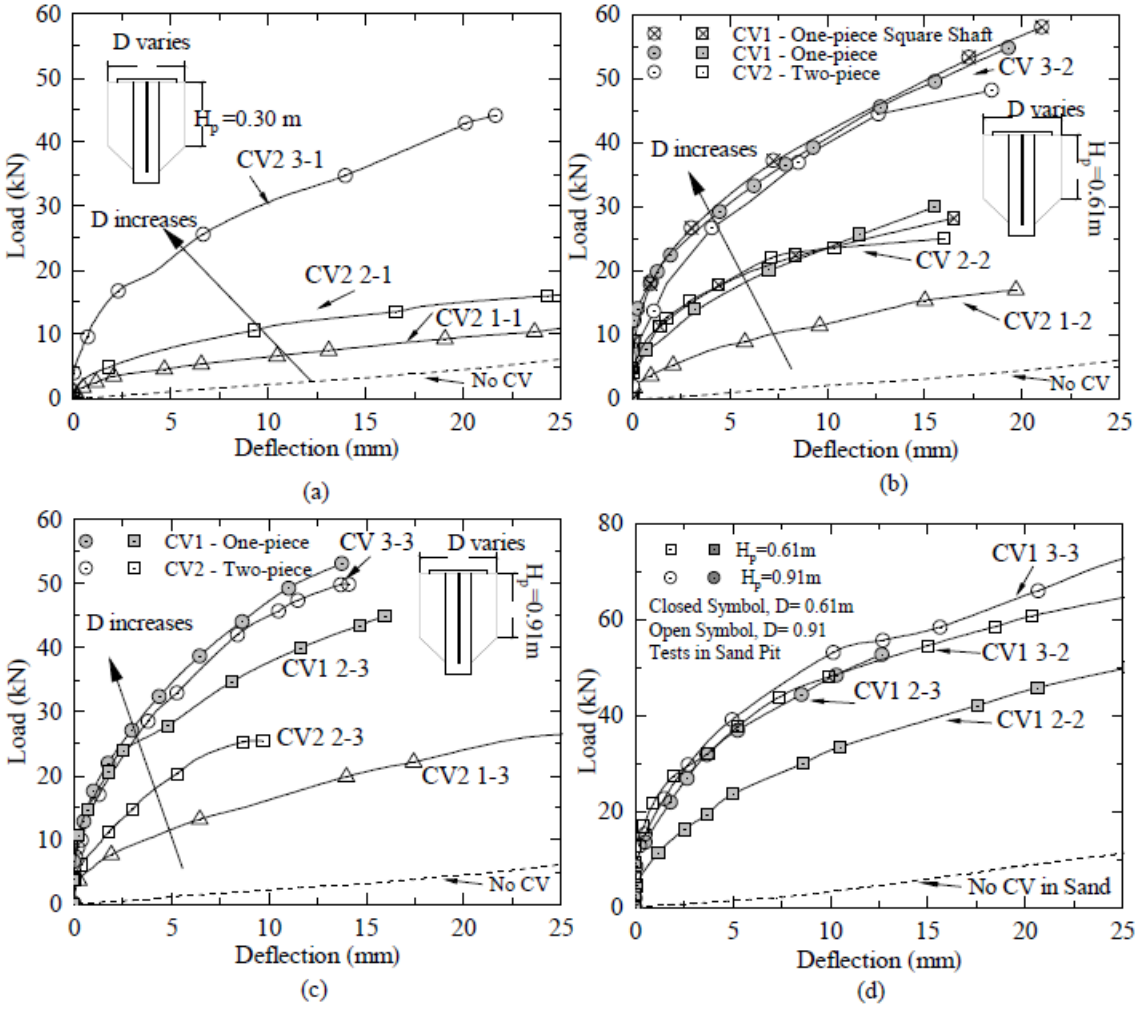


*Figure 18. Load-pile head deflection curves for lateral load tests performed on HP-CV systems in clay soil for CV1- and CV2-type vanes and D = 0.3, 0.61, or 0.91 m (a-c) and in sand for CV1-type vanes (d): a.) $H_p$=0.30 m in clay; b.) $H_p$=0.61 m in clay; c.) $H_p$=0.91 m in clay; d.) CV configurations tested in sand. All results are shown for test sequence where lateral load tests were performed prior to torsion (i.e. LT load sequence). The CV $D - H_p$ nomenclature indicates the CV-type and dimensions of D and $H_p$ in feet.*

In addition to increasing the effective width (i.e., diameter) of the foundation system, the placement of the CV at shallow depths near the pile head—where the largest lateral deformations occur—contributes to the observed increase in lateral resistance. Helical piles without a CV exhibited substantially lower resistance compared to HP–CV systems in all cases. The minimal resistance observed for the "No CV" case, particularly at small displacements, is attributed to the relatively small diameter of the HP shaft and to the presence of a soil–shaft gap that commonly develops following installation of conventional helical piles in cohesive soils. Beyond providing higher ultimate resistance, HP–CV systems also exhibited significantly stiffer responses at small displacements. Recall that as the HP is rotated into the ground during installation, the CV is pulled vertically into place without rotation. Consequently, the CV behaves similarly to a small-displacement foundation element and remains in firm contact with the surrounding soil immediately after installation, contributing to the observed stiffness in the load–displacement response.

For CV1- and CV2-type vanes with identical configurations, the lateral load–displacement responses and ultimate lateral resistances in cohesive soil were generally similar (Figure 18a–c). The only notable deviation occurred for the CV2 configuration 2-3, which exhibited a different load–displacement response compared to the corresponding CV1 configuration (Figure 18c). Given that other CV1–CV2 comparisons with identical diameters and embedment depths showed nearly identical behavior, this difference is likely attributable to localized variability in soil conditions surrounding that particular test pile. Nonetheless, the ultimate lateral resistance for the CV1- and CV2-type vanes with the 2-3 configuration was the same. Overall, the method of assembling the CV around the HP shaft—either as a one-piece element or as a two-piece assembly bolted around the shaft—did not significantly influence the lateral resistance or load–displacement response in cohesive soil. Moreover, when the CV was used to support a slender square shaft HP, an identical load-deflection response was observed (see Figure 18c). Thus, this demonstrates any geotechnical lateral resistance being mobilized by the shaft helical pile shafts (i.e. not the CV) negligible or very limited in comparison.

Due to time constraints associated with the experimental program, tests conducted in sand were limited to CV1-type vanes, as no substantial performance differences between CV1- and CV2-type vanes were observed in cohesive soil. The load–displacement responses for CV1-type vanes tested in sand are shown in Figure 18d. Like the results observed in clay, HPs augmented with CVs exhibited substantially stiffer responses at small displacements compared to HPs without a CV. In addition, the lateral capacities achieved in sand were comparable to those measured in stiff clay for the same CV geometries.

Despite having a torsional load test performed first during a TL load sequence, the lateral load-deflection response was comparable to the LT load sequence. Figure 19 shows the load-deflection response for CVs tested with the TL load sequence in cohesive materials.

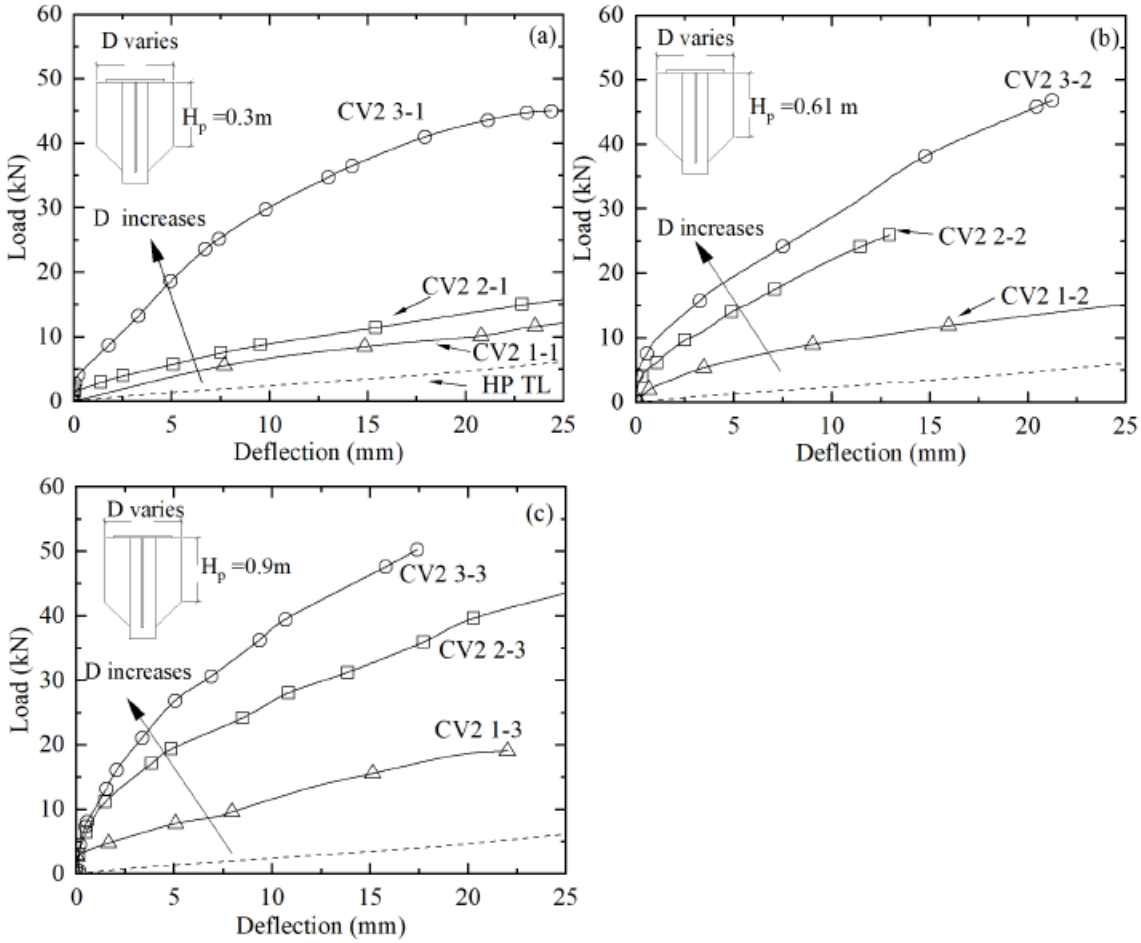


*Figure 19. Lateral load-deflection response for collar vanes tested in cohesive soil with the TL load sequence for $H_p$ values of: a.) 0.3 m; b.) 0.61 m; c.) 0.91 m.*

To further highlight the relative performance of the tested collar vane (CV) geometries, the normalized lateral resistance of helical piles (HPs) with and without a CV, expressed as $P/P_{wo}$, at pile head displacements of 5 and 10 mm is presented in Figure 20. Given the limited differences observed between CV1- and CV2-type vanes in cohesive soil, only CV2-type vanes are shown in Figure 20, as more geometries were tested for this CV type. Figure 20 highlights the influence of CV diameter, $D$, and prismatic height, $H_p$, on lateral resistance and the additional capacity provided relative to HPs without a CV. Overall, CV diameter exerted the greatest influence on lateral capacity, with CVs having $D = 0.91$m consistently generating the highest resistance regardless of $H_p$. For CVs with $D = 0.91$m and $H_p = 0.91$m, lateral resistance increased by approximately 25 to 30 times relative to HPs without a CV at pile head displacements of 5 and 10 mm.

Increasing $H_p$ generally resulted in measurable gains in lateral resistance across all CV geometries; however, the most significant marginal increase typically occurred when $H_p$ increased from 0.30 to 0.61 m. In contrast, further increases in $H_p$from 0.61 to 0.91 m often produced limited or negligible gains in resistance for CVs with diameters of 0.30 and 0.61 m (Figure 20). This behavior is likely attributable, at least in part, to reduced lateral deformations and diminished mobilization

of passive geotechnical resistance at depths greater than 0.61 m. A notable exception occurred for CVs with $D = 0.91$ m, for which a pronounced increase in resistance was observed as $H_p$ increased from 0.61 to 0.91 m (Figure 20). It is noted that on the day the CV2 3-2 configuration ($D = 0.91$ m, $H_p = 0.61$m) was tested, approximately 30 mm of rainfall occurred, which may have softened the upper portion of the clay crust (Carvajal-Munoz 2023). This localized softening may have reduced system stiffness and contributed to the comparatively larger increase in mobilized resistance observed for the largest CVs when $H_p$ increased from 0.61 to 0.91 m.

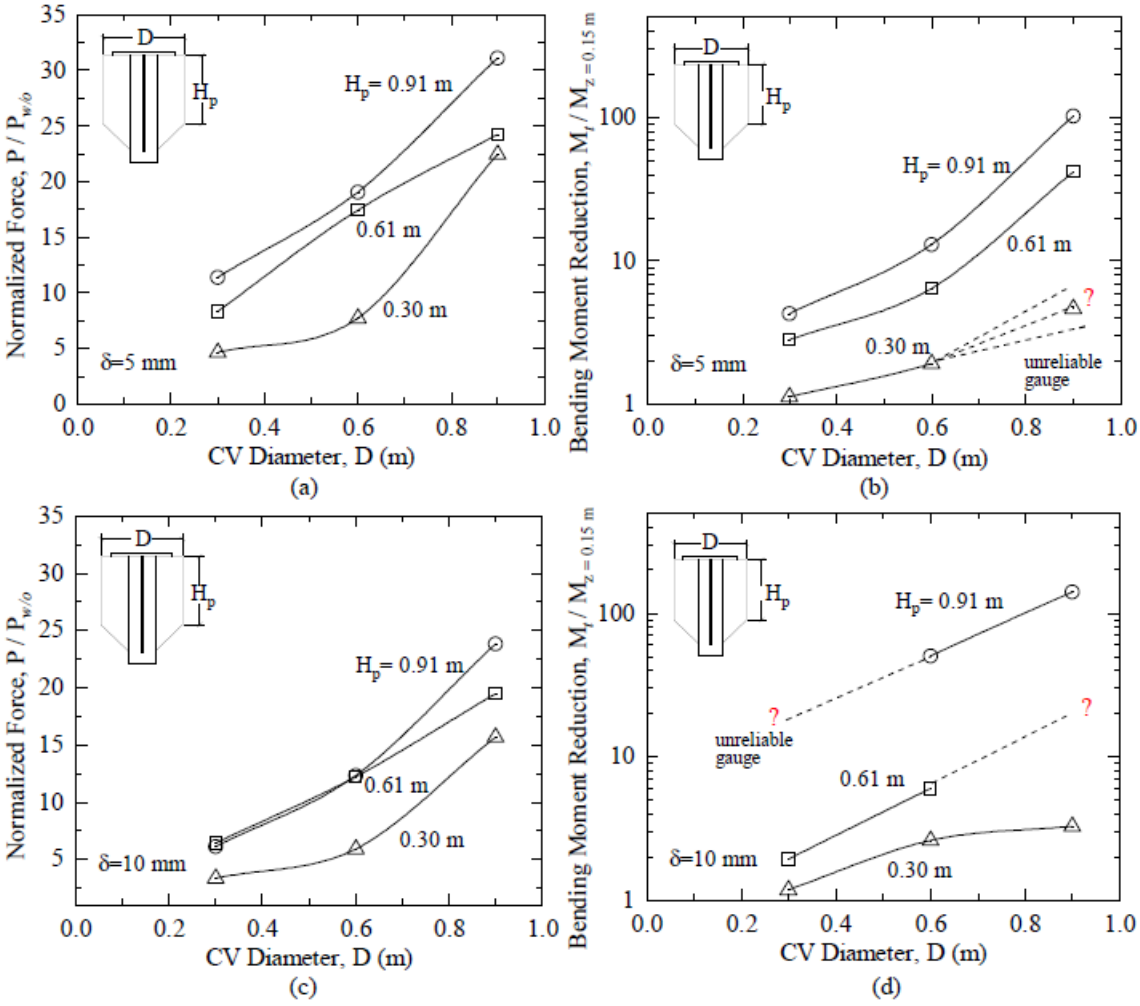


*Figure 20. Normalized lateral resistance with and without a collar vane ($P/P_{w/o}$) mobilized at pile head displacements of: a.) 5 mm and c.) 10 mm for CV2-type vanes in cohesive soil, where a broader range of CV geometries were tested. Bending moment reduction at the top of the pile shaft (z = 0.15 m) relative to the theoretical moment expected with no CV at displacements of b.) 5 mm and d.) 10 mm.*

In addition to increasing lateral geotechnical resistance, the CV is intended to reduce bending moments induced in the HP central shaft. In the absence of a CV, HPs provide negligible lateral resistance at shallow depths due to the slender geometry of the central shaft and installation-induced disturbance that commonly results in highly disturbed soil and/or a gap adjacent to the shaft. Under this "No CV" condition, the bending moment at the top strain gauge was observed to be governed primarily by the applied pile head load and its eccentricity relative to the strain gauge

location, such that $M_1 = P \times e_1$, where $M_1$ is the moment at the top strain gauge, $e_1$ is the distance between the pile head load application point and the top strain gauge, and $P$ is the applied lateral load.

Although equivalent lateral loads could not be directly applied to HPs without a CV due to the risk of yielding the HP shaft, the corresponding bending moment at the top strain gauge for those loads could be reasonably estimated using this relationship for comparison with tests conducted on HP–CV systems. Figure 21 presents representative bending moment distributions measured for HPs with a CV, along with the estimated bending moment at the top strain gauge for an HP without a CV subjected to the same lateral load (shown by closed symbols). As illustrated, the presence of the CV results in a substantial reduction in bending moment at the top strain gauge. This also summarized for a broad range of CV geometries shown in Figure 20b and Figure 20d.

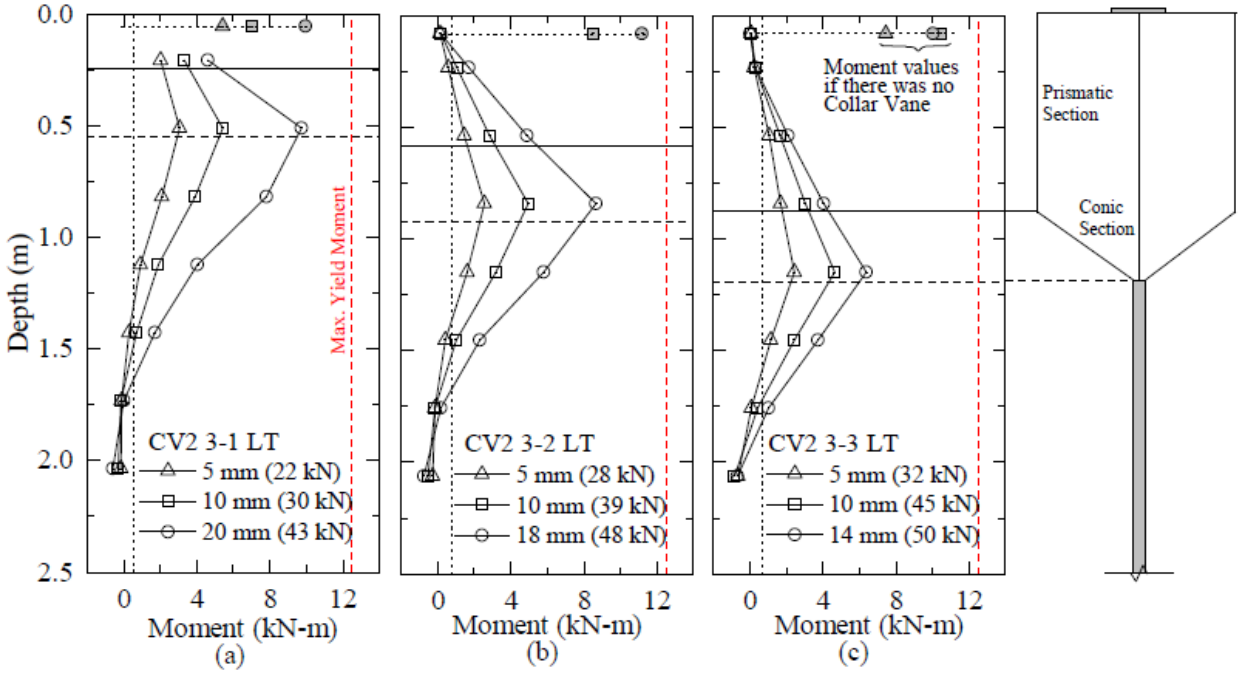


*Figure 21. Representative bending moment distributions for D = 0.91 m diameter collar vanes in clay soil for: a.) $H_p$ = 0.3 m; b.) $H_p$ = 0.61 m; c.) $H_p$ = 0.91 m. As illustrated in the schematic to the right, horizontal solid and dashed lines indicate the end of the prismatic and tapered sections, respectively. Moment distribution curves are shown for various displacements imposed by pile hide loads indicated in parentheses. The vertical dashed line indicates the yielding moment.*

This reduction is attributed to the CV's load-transfer mechanism, whereby passive soil resistance mobilized by the CV is concentrated near the pile head and transferred through the bolted flange connection, thereby counteracting the eccentric lateral load applied at the pile head. Additionally, the CV collar encapsulates the HP shaft with a slightly larger diameter and effectively isolates the shaft from direct soil interaction along the depth of the collar. This isolation results in a constant shear force and a linear increase in bending moment within the HP shaft through the depth of the collar. As shown by the bending moment distributions in Figure 21 for different CV configurations and displacement levels, the moment varies linearly throughout the depth of the CV, confirming that the collar shields the HP shaft from soil interaction along the vane depth, as intended.

Interpreting shear forces within the portion of the helical pile (HP) central shaft encapsulated by the collar vane (CV) provides additional insight into the magnitude of lateral resistance mobilized by the vane. Because the CV collar is not intended to interact directly with the HP shaft, the shear force within the encapsulated portion of the shaft is expected to remain constant, consistent with the observations shown in Figure 11. Under this assumption, the mobilized lateral resistance contributed by the CV, $V_R$, can be expressed as,

$$V_R = P - V \tag{1}$$

where $P$is the applied lateral load and $V$is the shear force in the HP shaft.
The shear force in the HP shaft was interpreted from the measured bending moments, $M$, within the portion of the shaft encapsulated by the CV using,

$$V = \frac{dM}{dz} = \frac{M_j - M_i}{z_j - z_i} \tag{2}$$

where $dM = M_j - M_i$represents the change in bending moment between two strain gauge locations separated by a distance $dz = z_j - z_i$, and subscripts $i$and $j$correspond to measurements at the respective depths.

Figure 22 compares the interpreted mobilized vane shear resistance with the applied lateral load (left column) and the normalized vane resistance, $V_R/P$, with pile head displacement (right column) for all CV2-type vanes tested in cohesive soil. These results are presented for CV2-type vanes because strain gauge survival rates were highest for this configuration, enabling more consistent comparisons across the range of tested CV geometries. Shear was interpreted between all surviving strain gauge pairs within the collar, resulting in a range of calculated $V_R$ and $V_R/P$values shown in Figure 22.

In general, both the absolute mobilized vane resistance, $V_R$, and the normalized resistance, $V_R/P$, increased with increasing CV diameter, $D$, and/or prismatic height, $H_p$ (Figure 22). At small pile head displacements, strain gauge measurements indicate that most lateral resistance was mobilized by the CV, as reflected by high values of $V_R/P$. As loading increased, the relative contribution of the CV to the total lateral resistance generally decreased, resulting in lower $V_R/P$ values at larger loads and displacements. For a given CV diameter, the lowest $V_R/P$ values were observed for the shortest vanes ($H_p = 0.30$ m = 1 ft) and increased with increasing $H_p$, as expected. Similarly, for a given $H_p$, CVs with larger diameters exhibited greater mobilized resistance. Nevertheless, for most CV geometries tested, the CV contributed the substantial majority of the geotechnical lateral resistance. For cases where both $D$and $H_p \geq 0.61$m, more than 80% of the lateral resistance was derived from the CV, even at relatively large pile head displacements.

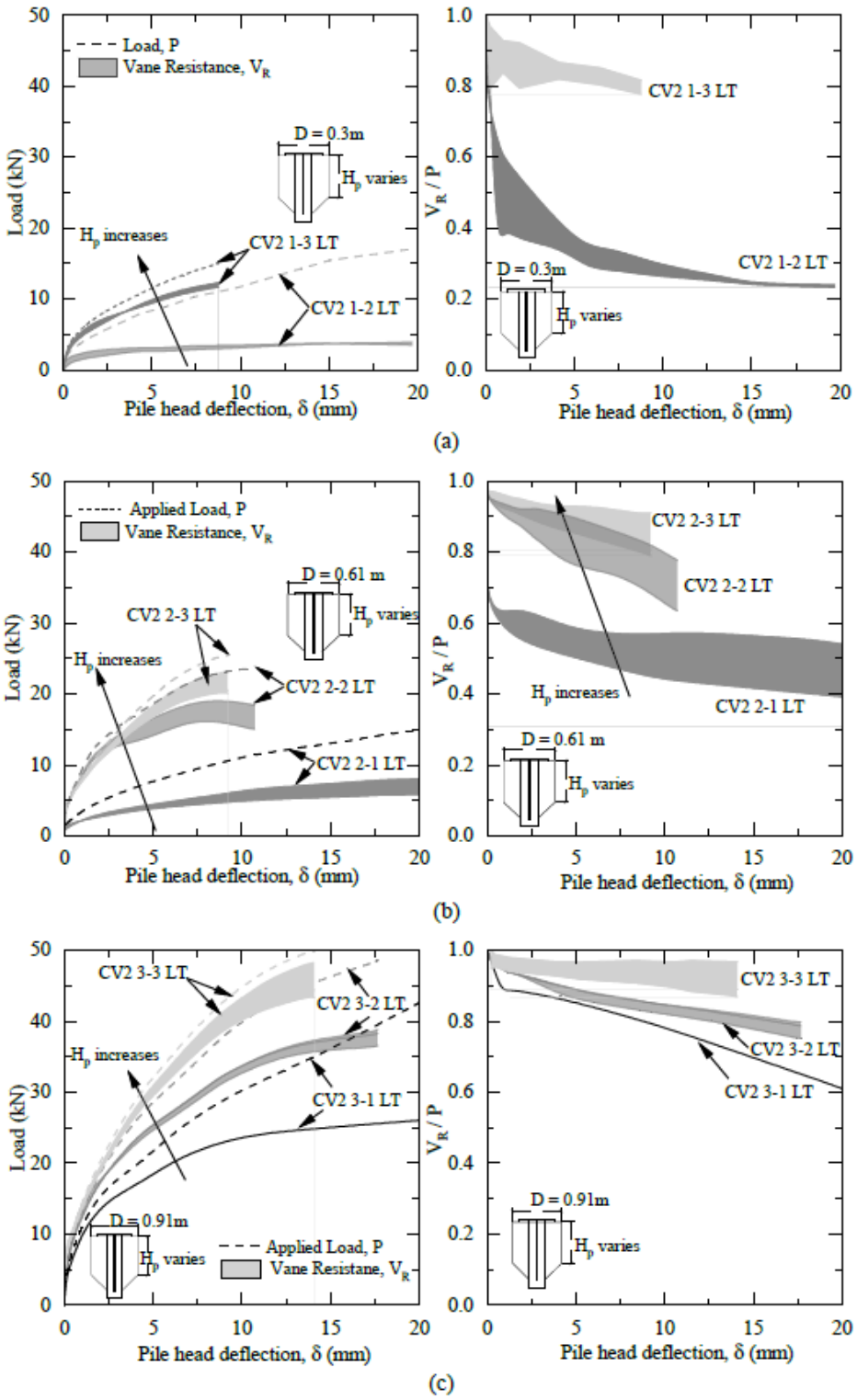


*Figure 22. Applied lateral load, P, and interpreted vane resistance, $V_R$, from strain gauges (left) and normalized vane resistance, $V_R/P$, (right) for different CV diameters with varying $H_p$: a.) D = 0.30 m; b.) D = 0.61 m; and c.) D = 0.91 m. Shear was interpreted between all strain gauges within the collar that survived, so a range of interpreted $V_R$ and associated $V_R/P$ is displayed. The CV# D − $H_p$ nomenclature indicates the CV-type and dimensions of D and $H_p$ in feet.*

## Torsion Load Tests

Figure 23 presents the torque–rotation responses for the various CV types and geometries tested in cohesive soils (Figure 23 13a–c) and granular soil (Figure 23d). A HP without a CV was also tested in torsion; however, it exhibited negligible torsional resistance and is therefore not shown. To isolate the torsional resistance contributed by the CV, the results shown in Figure 23 were processed by subtracting the limited torsional resistance measured for an HP without a CV at the same rotation level (Carvajal-Munoz 2023). This approach was adopted to provide a clear appraisal of the torsional resistance attributable to the CV itself, independent of the specific HP configuration, as CVs may be coupled with HPs having different shaft diameters and helix arrangements. As shown in Figure 23, the available torsional resistance increased systematically with both the diameter and embedment depth of the CV.

For CV geometries in which both one-piece and two-piece collar vanes were tested in cohesive soil, the CV1-type vane generally exhibited a stiffer torque–rotation ($T$–$\theta$) response and a higher ultimate torsional resistance (Figure 23b and Figure 23c). As previously described, the two-piece CV2-type vane consists of collar sections that are bolted together around the HP shaft along the depth of the collar, with three fins welded to one collar section and a single fin welded to the opposing section. In addition, the top flange connecting the CV to the pile head is welded only to the collar section with three fins (Figure 2). This configuration introduces greater flexibility into the CV–HP system relative to the CV1-type vane.

During testing, two string potentiometers were used to measure deflections of fins attached to each collar section. Although both collar sections rotated during torsional loading, the section with a single fin did not rotate in perfect unison with the three-fin section and exhibited a lag in rotation (not shown in Figure 23), as reported by Carvajal-Munoz (2023). This behavior is attributed to the more rigid connection between the pile head flange and the three-fin collar section, whereas the single-fin section is connected only through the bolted collar and lacks a direct rigid connection to the pile head flange. In contrast, for CV1-type vanes, the pile head flange can be welded to all fins, resulting in rotation of the fins in unison.

Consequently, the greater $T$–$\theta$ stiffness and higher torsional resistance observed for CV1-type vanes are likely due to more effective mobilization of shear strength along the cylindrical shear surface that develops around the perimeter of the CV. For CV2-type vanes, partial lag in rotation of the single-fin collar section limits full mobilization of shear resistance along this shear surface. This behavior partially motivated the subsequent development of the CV1-type vane. Nevertheless, despite these differences, both CV1- and CV2-type vanes were capable of mobilizing substantial torsional resistance.

For the largest collar vane (CV) configurations tested in cohesive soil, specifically the CV 3-3 shown in Figure 23c, an abrupt reduction in measured torque was observed and attributed to shear failure of bolts at the HP–CV flange connection. During the first summer of testing, when CV2-type vanes were evaluated, the CV-to-HP and loading arm connections were made using Grade-5 1/2-13 × 1-1/2 bolts. For the CV2 3-3 configuration, bolt rupture occurred when the mobilized torsional resistance reached approximately $T = 50\text{kN}\cdot\text{m}$.

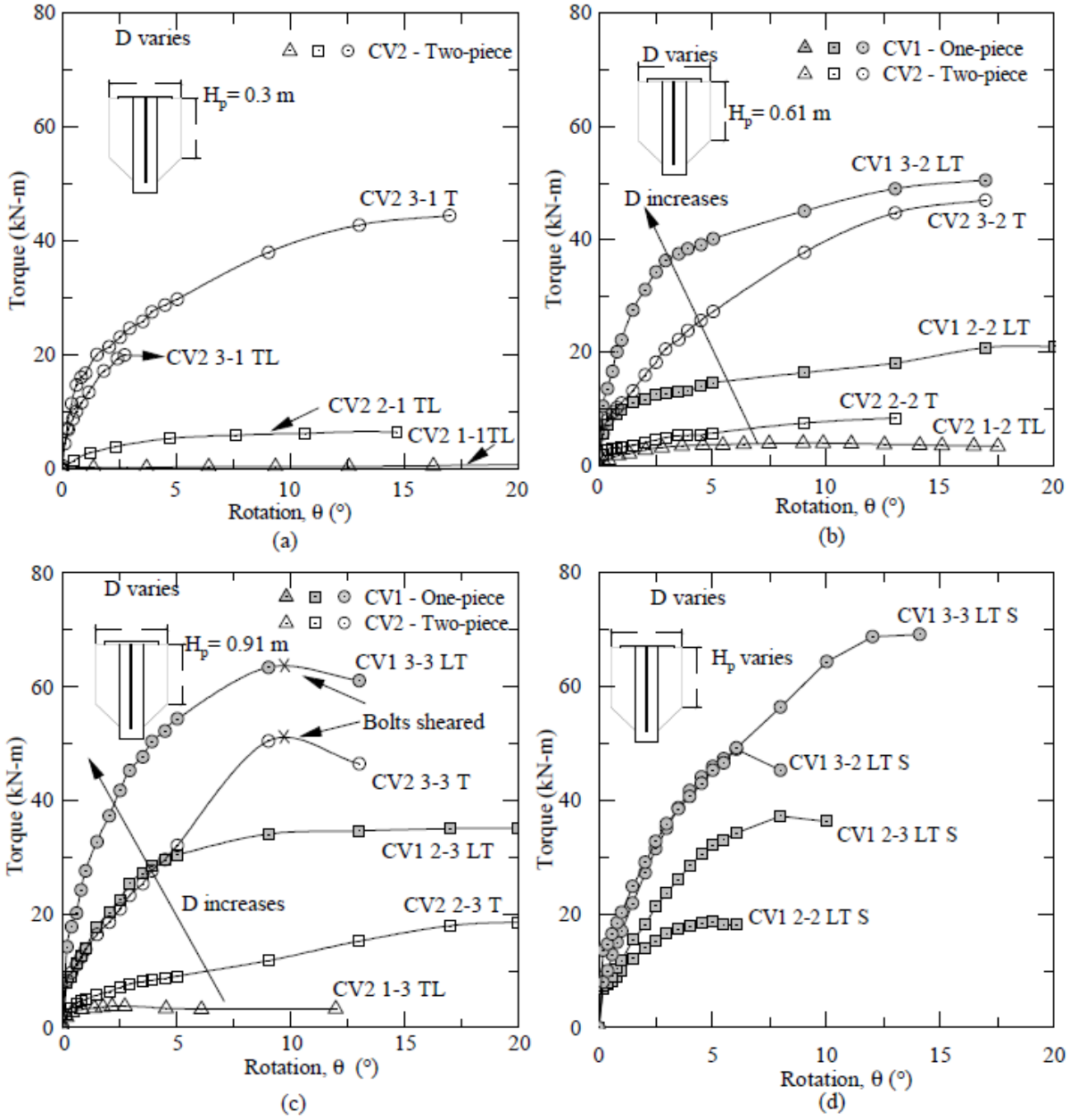


*Figure 23. Torque-rotation response for CV1- and CV2-type collar vanes in cohesive soil with: a.) $H_p$ = 0.3 m, b.) $H_p$ = 0.6 m, c.) $H_p$ = 0.91 m in cohesive soil. d.) All CV1-type collar vanes installed in granular soil.*

In the second summer of testing, a CV1 3-3 configuration was evaluated using larger Grade-8 1/2-13 × 2-1/2 bolts at the flange connection. In this case, bolt shear failure occurred at a higher mobilized torsional resistance of approximately $T = 63$ kN·m. Based on these observations, it was concluded that larger collar vane geometries require a stronger rotational connection at the HP–CV flange to fully sustain the torsional loads that can be mobilized. Nonetheless, it is believed that the CV1 3-3 configuration had nearly reached its maximum geotechnical torsional resistance at the time of bolt failure (Figure 23c). This interpretation is supported by results from granular soil

testing, where the same CV size mobilized a torsional resistance of approximately $T = 70$ kN·m without any observed bolt failures (Figure 23d).

The torsional resistance mobilized by the collar vane (CV), along with the associated shear resistance developed along the prismatic and tapered sections of the vane, can be derived within both total stress and effective stress analytical frameworks. These formulations may be used to interpret apparent soil strength parameters based on measured torsional resistances obtained from field testing. The total torsional resistance is expressed as,

$$T = T_p + T_c \tag{3}$$

where $T_p$and $T_c$ represent the torsional resistances attributed to the prismatic and conical failure surfaces, respectively, that develop along the perimeter of the vane (Figure 7b).

The torsional resistance associated with the prismatic portion of the vane is given by,

$$T_p = \int_0^{H_p} \tau(\pi D)\, r\, dz \tag{4}$$

where $\tau$ is the mobilized shear resistance integrated over the depth of the prismatic section ($z = H_p$; see Figure 7), $\pi D$ is the CV perimeter, and $r = D/2$ is the effective torque arm corresponding to the CV radius.

For total stress analyses (TSA) assuming a constant undrained shear strength, $S_u$, the torsional resistance contributed by the prismatic section may be expressed as,

$$T_p = \int_0^{H_p} S_u(\pi D)\, r\, dz \tag{5a}$$

which simplifies to,

$$T_p = S_u(\pi D H_p)\, r = \frac{S_u \pi D^2 H_p}{2} \tag{5b}$$

For effective stress analyses (ESA), assuming that the top of the prismatic section is located at the ground surface, the torsional resistance mobilized along the prismatic portion of the collar vane (CV) is expressed as,

$$T_p = \int_0^{H_p} (\gamma z \beta)(\pi D)\, r\, dz \tag{6a}$$

which simplifies to,

$$T_p = \beta(\gamma H_p^2)\, \frac{\pi D^2}{4} \tag{6b}$$

where $\gamma$ is the effective unit weight of the soil, $\beta = K\tan\phi$, $K$ is the lateral earth pressure coefficient, and $\tan\phi$ is the effective friction angle.

The torsional resistance attributed to the conical failure surface is evaluated by integrating shear resistance along the slant length of the tapered vane section over the vertical interval $z = H_c$, such that,

$$T_c = \int_0^{H_c} \tau[2\pi r(1 - z \cdot \tan\theta_c)]\,(r - z \cdot \tan\theta_c)\,\frac{1}{\cos\theta_c}\,dz \tag{7}$$

where $\theta_c$ is the taper angle of the CV, and the terms in the integrand account for the variation in perimeter, torque arm, and slant length with depth below the prismatic section. In this formulation, $z$ represents the vertical distance below the prismatic section rather than absolute depth.

For total stress analyses (TSA), assuming a constant undrained shear strength $S_u$, the torsional resistance contributed by the conical section is given by,

$$T_c = \int_0^{H_c} S_u\,[2\pi r(1 - z \cdot \tan\theta_c)]\,(r - z \cdot \tan\theta_{Hc})\,\frac{1}{\cos\theta_c}\,dz \tag{8a}$$

which simplifies to,

$$T_c = \frac{S_u\,2\pi H_c}{\cos\theta_c}\left[r^2 + H_c \cdot \tan\theta_c\left(\frac{H_c \cdot \tan\theta_c}{3} - r\right)\right] \tag{8b}$$

For ESA, variations in effective stress over the vertical interval $H_c$ must be explicitly considered, resulting in,

$$T_c = \int_0^{H_c} \beta(\sigma_v' + \gamma z)\,[2\pi r(1 - z \cdot \tan\theta_c)]\,(r - z\tan\theta_c)\,\frac{1}{\cos\theta_c}\,dz \tag{9a}$$

which becomes,

$$T_c = \beta\,\frac{2\pi H_c}{\cos\theta_c}\left[r^2\left(\sigma_v' + \frac{\gamma H_c}{2}\right) + H_c \cdot \tan\theta_c\left(-r\left(\sigma_v' + \frac{2\gamma H_c}{3}\right) + H_c \cdot \tan\theta_c\left(\frac{\sigma_v'}{3} + \frac{\gamma H_c^2}{4}\right)\right)\right] \tag{9b}$$

where $\sigma_v'$ is the vertical effective stress at the top of the tapered section, corresponding to the bottom of the prismatic section.

By combining Equations (5b) and (8b), the undrained shear strength $S_u$ may be isolated and compared directly with measured torsional resistance to interpret the apparent undrained shear strength mobilized along the assumed failure surface in cohesive soils, such that,

$$S_u = \frac{T}{(\pi D H_p)\,r + \frac{2\pi H_c}{\cos\theta_c}\left[r^2 + H_c \cdot \tan\theta_c\left(\frac{H_c \cdot \tan\theta_c}{3} - r\right)\right]} \tag{10}$$

Similarly, for granular soils, the parameter $\beta$ can be isolated by combining Equations (6b) and (9b), allowing interpretation of the apparent effective stress strength parameters mobilized along the assumed failure surface. The resulting expression for $\beta$ is given by,

$$\beta = \frac{T}{(\gamma H_p^2)\,(\pi D^2)/4 + \frac{2\pi H_c}{\cos\theta_c}\left[r^2\left(\sigma_v' + \frac{\gamma H_c}{2}\right) + H_c \tan\theta_c\left(-r\left(\sigma_v' + \frac{2\gamma H_c}{3}\right) + H_c \tan\theta_c\left(\frac{\sigma_v'}{3} + \frac{\gamma H_c^2}{4}\right)\right)\right]} \quad (11)$$

This formulation enables direct back-calculation of $\beta$ from measured torsional resistance, $T$, facilitating interpretation of the effective stress response of granular soils mobilized by the collar vane.

The effective undrained shear strength inferred from torsional collar vane (CV) resistances measured in the field using Equation (10) is compared with interpreted peak and residual undrained shear strengths in Figure 24a. In general, the effective shear strength mobilized by the CV aligns more closely with the residual undrained shear strength than with the peak strength. This behavior is not unexpected, as the upper clay profile at the test site is relatively stiff and brittle. Under such conditions, it is unlikely that peak shear strength would be mobilized simultaneously along the extensive cylindrical and conical failure surfaces generated by the CV, particularly when compared to the much smaller failure surface associated with a field vane shear test (FVST).

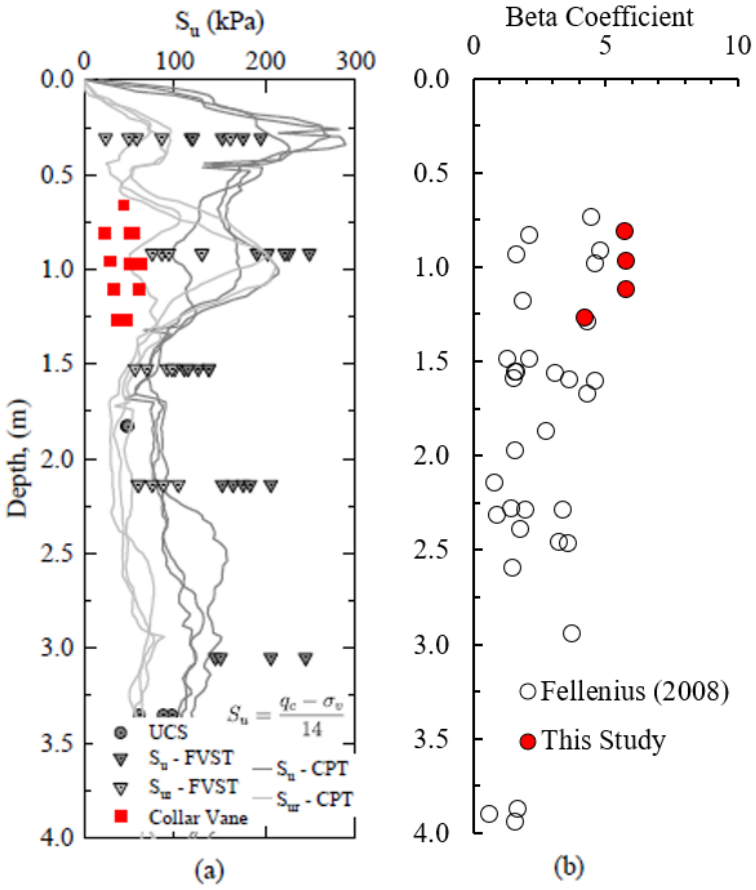


*Figure 24. a.) Comparison of effective undrained shear strength associated with collar vane torsional resistance with interpreted residual and peak shear strength; b.) comparison of effective beta coefficients associated with collar vane torsional resistance compared with interpreted measurements for drilled shafts at shallow depths.*

This observation is also consistent with well-established trends in deep foundation behavior in stiff clays, where lower adhesion factors ($\alpha$) are commonly inferred from load tests. Such lower $\alpha$values reflect effective interface shear strengths that are below peak values and more representative of residual conditions, which are typically mobilized in stiff soils.

For tests conducted in sand, $\beta$ values ranging from approximately 4 to 6 were back-calculated from torsional load tests using Equation (11), as shown in Figure 24b. While these values may be considered high for many foundation applications, they are not unexpected at shallow embedment depths. As illustrated in Figure 24b, the inferred $\beta$ values are generally consistent—though toward the upper end—of reported values for other deep foundation systems with relatively low embedment depths (Fellenius, 2008).

## 4.3 Cyclic Load Tests

### Lateral Load Tests

Following LeBlanc et al. (2010), the parameters $\zeta_b$ and $\zeta_c$ are used to characterize cyclic loading conditions. The parameter $\zeta_b$ is defined as the ratio of the maximum cyclic load to the maximum static load capacity, $P_{c,\max}/P_u$. The parameter $\zeta_c$ is defined as the ratio of the minimum to maximum cyclic loads, $P_{c,\min}/P_{c,\max}$, and characterizes the symmetry of the applied loading. Specifically, $\zeta_c = 0$ corresponds to one-way loading, $\zeta_c = -1$ to fully reversed (symmetric) two-way loading, and $\zeta_c = 1$ to constant loading (i.e. no cycling).

Together, $\zeta_b$ and $\zeta_c$ describe the cyclic load amplitude relative to a reference load $P_u$, which in this study is defined at a reference pile head displacement of $\delta = 12.5$ mm at the load application point. Table 5 summarizes the characteristics of the one-way lateral cyclic loading applied in this study. It is noted that a strictly one-way loading condition ($\zeta_c = 0$) could not be achieved experimentally because the hydraulic controller required a minimum continuous flow pressure to operate.

*Table 5. Summary of lateral forces applied in the cyclic tests.*

| Collar Vane | $P_u$ (kN) | $P_{c,\max}$ (kN) | $\Delta P$ (kN) | $\zeta_b$ | $\zeta_c$ | $N$ |
|---|---|---|---|---|---|---|
| | Cohesive Soil | | | | | |
| HP L Cyc | 2.6 | 8 | 4 | 3.1 | 0.50 | 1000 |
| CV2 2-1 LT Cyc | 12 | 13 | 8 | 1.0 | 0.38 | 1000 |
| CV1 2-2 L Cyc | 27 | 15 | 12 | 0.5 | 0.17 | 850 |
| CV2 3-1 LT Cyc | 34 | 31 | 24 | 0.9 | 0.23 | 1000 |
| CV2 3-2 LT Cyc | 45 | 18 | 11 | 0.4 | 0.39 | 1100 |
| CV2 3-2 LT Cyc R | 45 | 31 | 26 | 0.7 | 0.16 | 1000 |
| CV1 3-2 LT Cyc | 46 | 32 | 27 | 0.7 | 0.16 | 1000 |
| CV2 3-3 LT Cyc | 49 | 31 | 21 | 0.6 | 0.32 | 850 |
| CV2 3-3 LT Cyc R | 49 | 34 | 29 | 0.7 | 0.15 | 1000 |
| | Cohesionless Soil | | | | | |
| CV1 3-2 LT Cyc S | 50 | 49 | 40 | 1.0 | 0.18 | 700 |
| CV1 3-2 LT Cyc S R | 50 | 25 | 19 | 0.5 | 0.24 | 1000 |

**Note:** R stands for 'repeated' test for the same CV with a different $\zeta_b$ or $\zeta_c$.

Figure 25 presents representative cyclic lateral load–displacement responses for helical pile (HP) systems with and without collar vanes. Figure 25a illustrates the behavior of an HP without a collar vane, for which the cyclic load ratio $\zeta_b$ was set to 3 due to the relatively low lateral capacity of the pile and the minimum load deliverable by the hydraulic controller. Under these conditions, the HP exhibited progressive accumulation of lateral displacement, indicative of limited lateral resistance and sustained ratcheting under cyclic loading.

Figure 25b and Figure 25c present representative cyclic responses for HP–CV systems. The CV2 2-1 configuration shown in Figure 25b exhibits a gradual accumulation of displacement with increasing cycle number, with the majority of displacement occurring during the early stages of cyclic loading. In contrast, the CV1 2-2 configuration shown in Figure 25c demonstrates a more stable cyclic response, characterized by limited displacement accumulation following an initial adjustment during the early cycles. A sudden increase in load was recorded after approximately 100 cycles; this event was unplanned and is attributed to the hydraulic controller. However, no additional progressive displacement was observed thereafter, indicating a predominantly hysteretic response under continued cyclic loading.

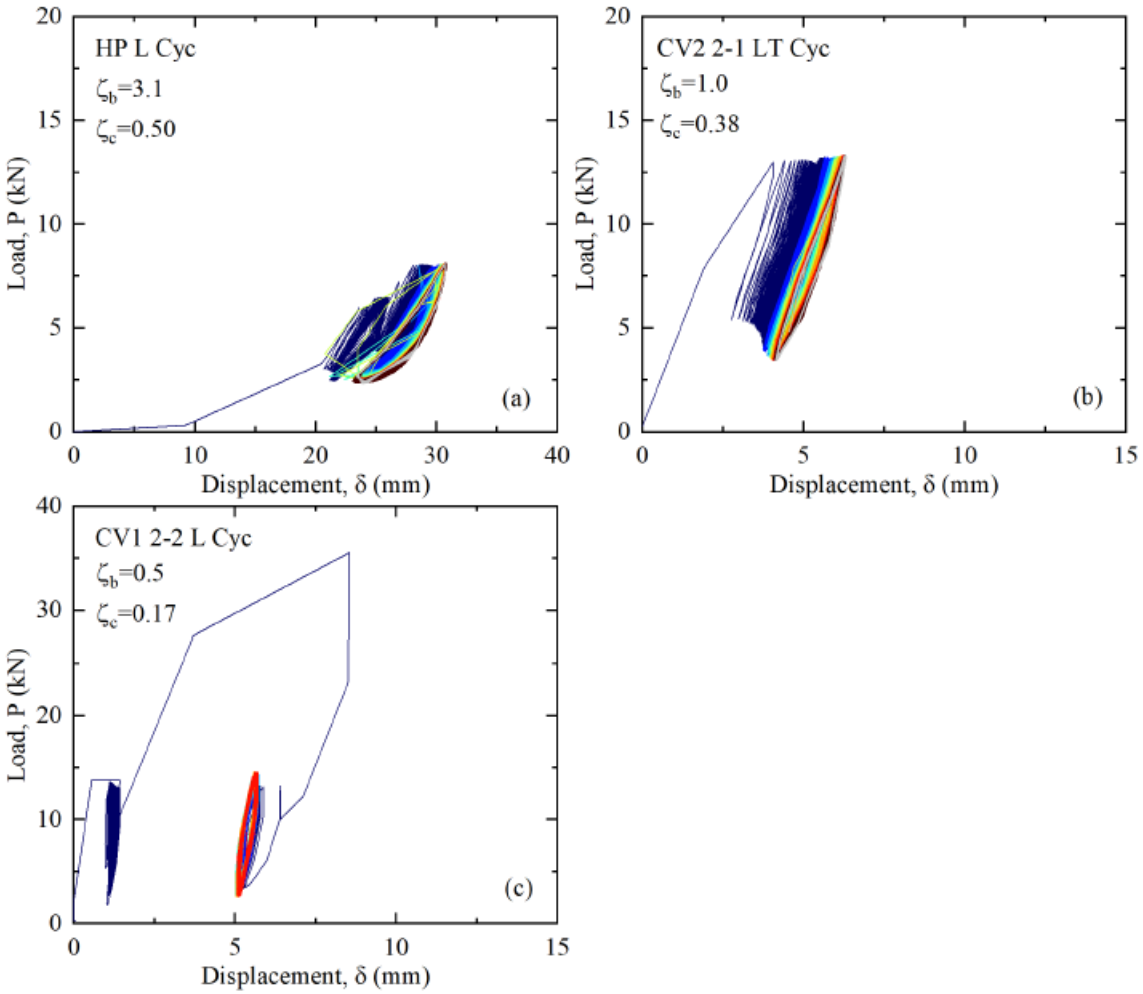


*Figure 25. Displacement accumulation from cyclic lateral loading in cohesive soil for: a.) HP without CV; b.) CV2 2-1; and; c.) CV1 2-2.*

Cyclic lateral loading responses for collar vane (CV) configurations with a diameter of $D = 0.91$ m in cohesive soil are presented in Figure 26. The CV2 3-1 configuration, tested at a cyclic load ratio of $\zeta_b = 1$, exhibited appreciable accumulation of lateral displacement during the first 100 load cycles, followed by pronounced ratcheting over the remaining 900 cycles (Figure 26a). Approximately 80% of the total displacement occurred after the first 100 cycles. In contrast, the CV 3-2 configuration tested at a lower cyclic load ratio of $\zeta_b = 0.4$ did not exhibit progressive displacement accumulation, with the exception of an excessive force applied during the first load cycle (Figure 26b).

Figure 26c and Figure 26d present results for the same CV geometry subjected to identical cyclic loading conditions but differing in prototype configuration and testing year (CV2 tested in 2021 and CV1 tested in 2022). For the CV1-type vane, the maximum cyclic load was exceeded during the first load cycle. Both CV configurations accumulated comparable total displacements; however, ratcheting behavior was not observed for the CV2 configuration until after approximately 100 cycles, when the cyclic load level was exceeded. The more rapid onset of ratcheting observed for the CV1 configuration is therefore attributed to the initial overshoot of lateral load during the first cycle. Overall, both CV1- and CV2-type vanes exhibited similar cyclic performance, consistent with trends observed under monotonic loading.

Figure 26e and Figure 26f compare CV2 3-3 configurations tested at cyclic load ratios of $\zeta_b = 0.6$ and 0.7. Both configurations exhibited similar total displacements after 1,000 cycles (approximately 7.5 mm and 10 mm, respectively). In the case of $\zeta_b = 0.6$, ratcheting initiated almost immediately following the first load cycle. It is unclear whether the observed differences in displacement accumulation are primarily attributable to the modest difference in applied load level, localized site variability, or a combination of both. Nevertheless, the overall cyclic response was similar, with both configurations exhibiting ratcheting behavior while maintaining stable performance, even at relatively high values of $\zeta_b$.

Notably, the total displacements observed for the 3-2 configurations (Figure 26c and Figure 26d) and the 3-3 configurations (Figure 26e and Figure 26f) were comparable. Consistent with monotonic test results, this suggests that extending $H_p$ beyond 0.61 m (2 ft) did not substantially influence cyclic performance. This behavior is expected, as the greatest lateral deformation—and thus mobilization of lateral resistance—occurs at shallow depths.

Figure 27 presents the accumulated lateral displacement response for the CV1 3-2 configuration tested in sand under two cyclic load ratios, $\zeta_b = 1$ and 0.5. The test shown in Figure 27a for $\zeta_b = 1$ was terminated after 800 loading cycles as lateral displacements of approximately 80 mm had already accumulated. While some ratcheting was beginning to occur (i.e. decreasing accumulation of displacement with each load cycle), this response is characteristic of unstable cyclic loading behavior. Figure 28 illustrates the observed subsidence of soil adjacent to the CV that's characteristic of unstable cyclic loading, which occurred as a result of the imposed cyclic loading and associated yielding of the surrounding sand.

Under cyclic loading conditions, continued structural movement promotes particle migration and progressive bed subsidence in granular soils (Lu & Zhang, 2019; Nanda et al., 2017; Li et al., 2021). Similar observations have been reported in earlier studies by Cheang and Matlock (1983)

and Brown et al. (1988). Cuéllar et al. (2009) noted that when sand is sufficiently dense, the particle rearrangement phase begins immediately following the first loading cycle, leading to observable soil subsidence.

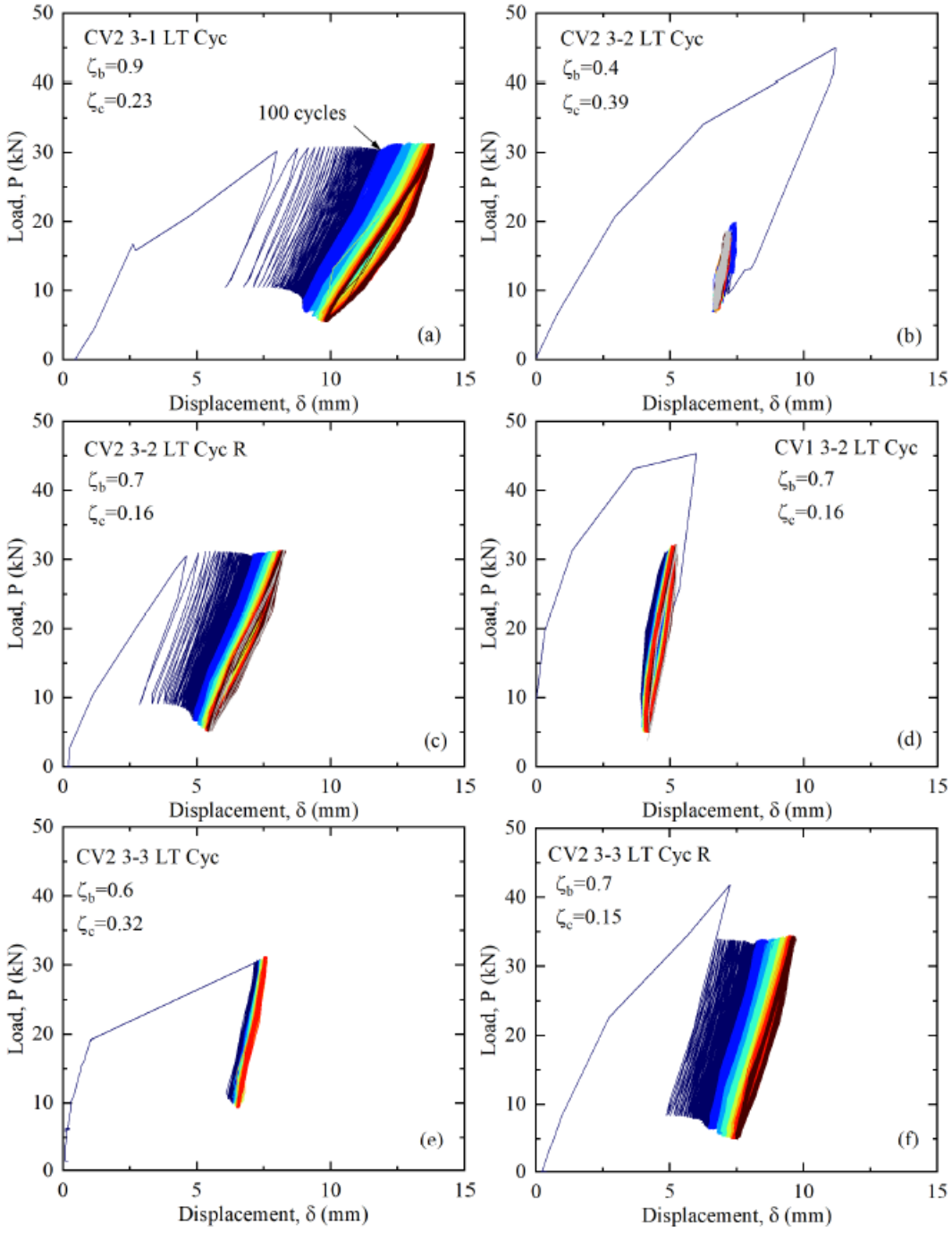


*Figure 26. Displacement accumulation from cyclic lateral loading in cohesive soil for Collar Vanes with D = 0.91 m for different CV types/configurations at various $\zeta_b$.*

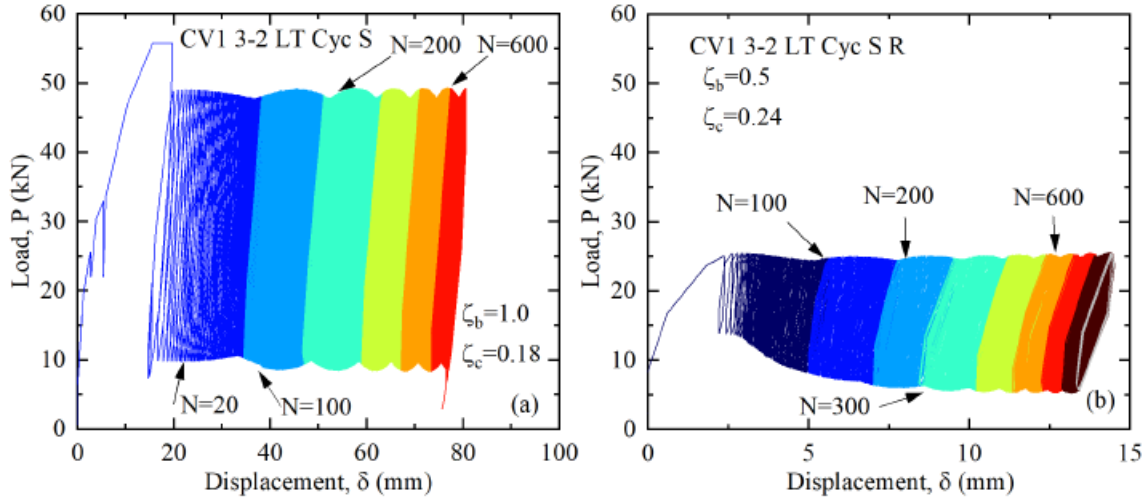


*Figure 27. Accumulated lateral displacements in sand under cyclic loading for CV1 3-2 for: a.)* $\zeta_b = 1.0$ *and b)* $\zeta_b = 0.5$.

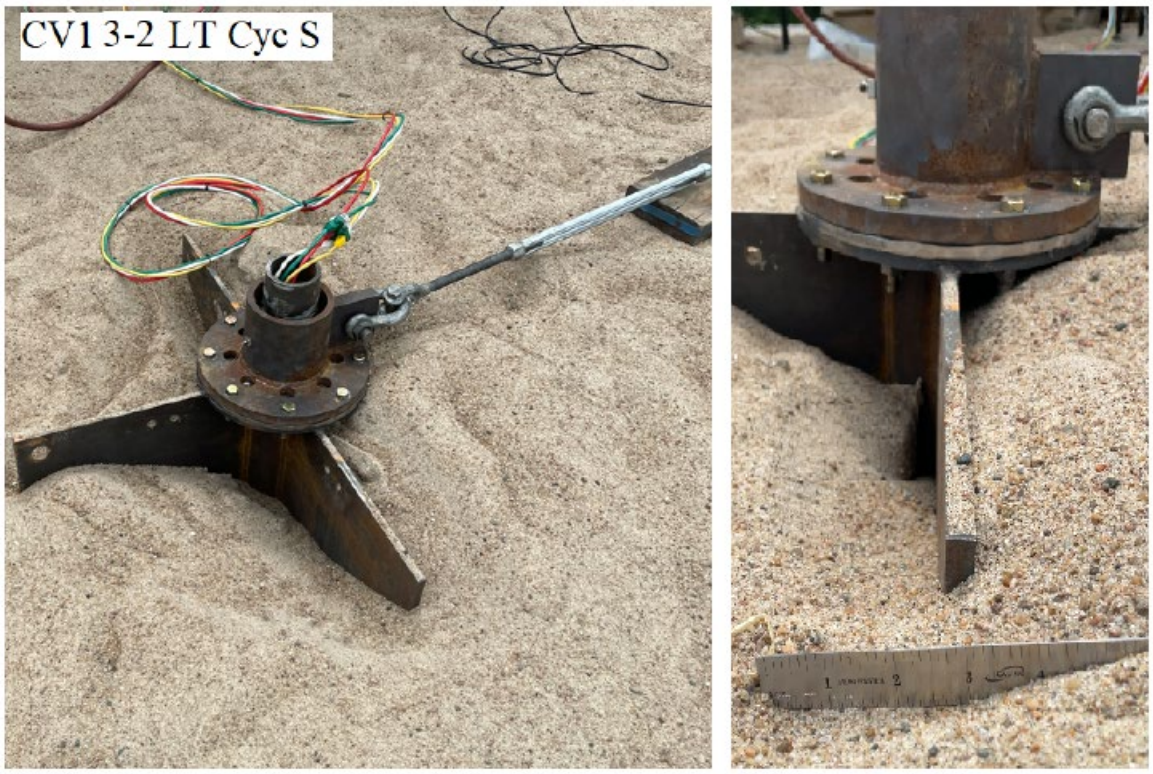


*Figure 28. Soil subsidence around the laterally loaded Collar Vane CV1 3-2 in sand with* $\zeta_b = 1.0$ *load level that's characteristic of unstable cyclic loading in sand.*

To evaluate the degradation of HP–CV system stiffness under cyclic loading, two stiffness measures are defined. The first is an equivalent stiffness, defined as the slope of the line connecting the origin to the peak load point of a given cycle. This stiffness metric is used to assess cumulative displacement behavior as cyclic loading progresses.

The second measure is the secant stiffness, which characterizes changes in pile head stiffness with increasing cycle number. The secant stiffness is defined as the slope between the minimum and maximum load points within a given loading cycle, expressed as (Chiou et al., 2018),

$$K = \frac{P_{\max} - P_{\min}}{y_{\max} - y_{\min}} \tag{12}$$

where $K$ is the HP-CV stiffness defined by pile head displacements, $P_{\max}$ and $P_{\min}$ are the maximum and minimum applied loads within a load cycle, and $y_{\max}$ and $y_{\min}$ are the corresponding pile head displacements.

Figure 29 illustrates the evolution of pile head HP-CV system stiffness for the CV2 3-2 configuration. The initial secant stiffness, $K_1$, is less steep than the stiffness values observed in subsequent cycles, $K_N$. As cyclic loading progresses, cumulative strain accumulation and localized remolding of the surrounding soil result in a reduction in lateral resistance, consistent with observations reported by others (e.g. Zhang et al., 2011).

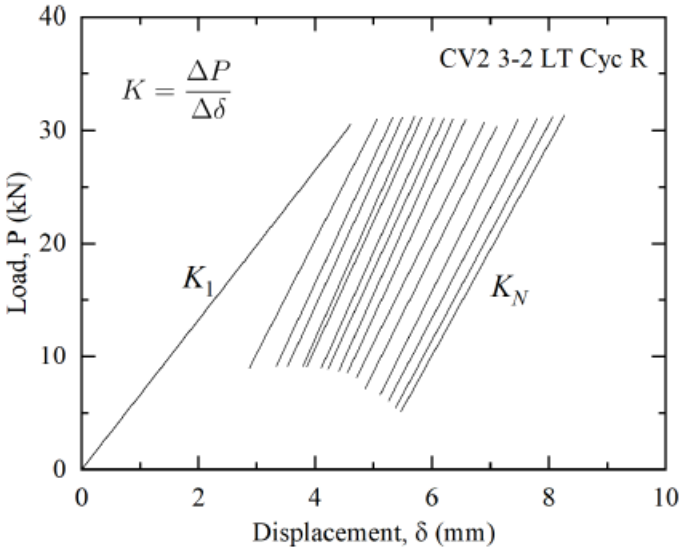


*Figure 29. Representative cyclic load-deflection response illustrating K, $K_1$, and $K_N$.*

Figure 30 illustrates the evolution of equivalent stiffness and secant stiffness as functions of the number of loading cycles. The observed reduction in equivalent stiffness is directly associated with the progressive accumulation of lateral displacement under cyclic loading.

The secant stiffness exhibits an initial increase following the first loading cycle, after which it decreases as the number of cycles increases. This trend has also been reported in previous studies (e.g. Abd Elaziz & El Naggar, 2015; Mondal & Disfani, 2022). The pronounced influence of the first loading cycle on pile–soil system stiffness is well documented, with subsequent cycles contributing to progressive stiffness degradation (Long & Vanneste, 1994), as reflected by the load–deflection slopes (e.g. Figure 29). Overall, the evolution of both equivalent and secant stiffness is governed by several factors, including the magnitude of the applied load, the characteristics of the cyclic loading protocol (i.e., $\zeta_b$ and $\zeta_c$), and the initial stiffness of the pile and surrounding soil.

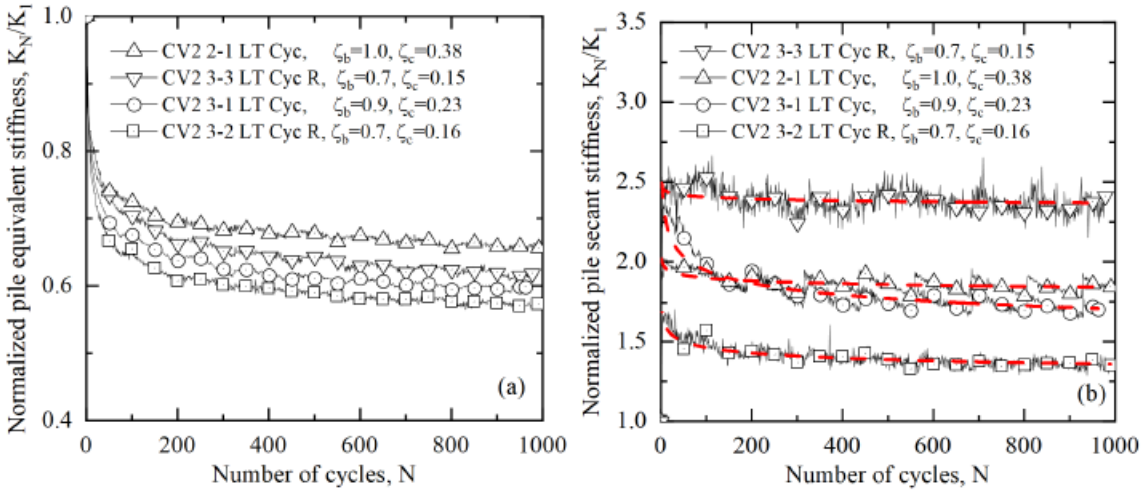


*Figure 30.HP-CV system stiffness evaluated based on pile head displacements: a.) Equivalent Stiffness; b.) Secant Stiffness*

The design of laterally loaded piles under cyclic loading is commonly performed using a global analysis approach, in which initial pile displacements and rotations are first computed from static analyses and then modified to account for cyclic loading effects (Garnier, 2013). One widely used methodology for predicting lateral cyclic response expresses displacement accumulation as a function of the number of loading cycles using either a logarithmic relationship,

$$\frac{y_N}{y_1} = 1 + b\ln(N) \tag{13}$$

or a power-law relationship,

$$\frac{y_N}{y_1} = N^{\alpha} \tag{14}$$

where $y_N$ is the pile head displacement after $N$ cycles, $y_1$ is the displacement after the first cycle, and $b$ and $\alpha$ are degradation parameters that characterize cyclic response.

Figure 31 presents the evolution of normalized pile head displacement, $y_N/y_1$, as a function of the number of loading cycles. The results indicate that higher values of the cyclic load symmetry parameter $\zeta_c$ correspond to larger normalized displacements. The observed trends are well represented by both the logarithmic and power-law formulations. The fitted degradation parameters obtained from Figure 31 are plotted in Figure 32 as a function of the cyclic load amplitude ratio, where a linear relationship appears to reasonably describe the influence of the load cycle amplitude on these coefficients.

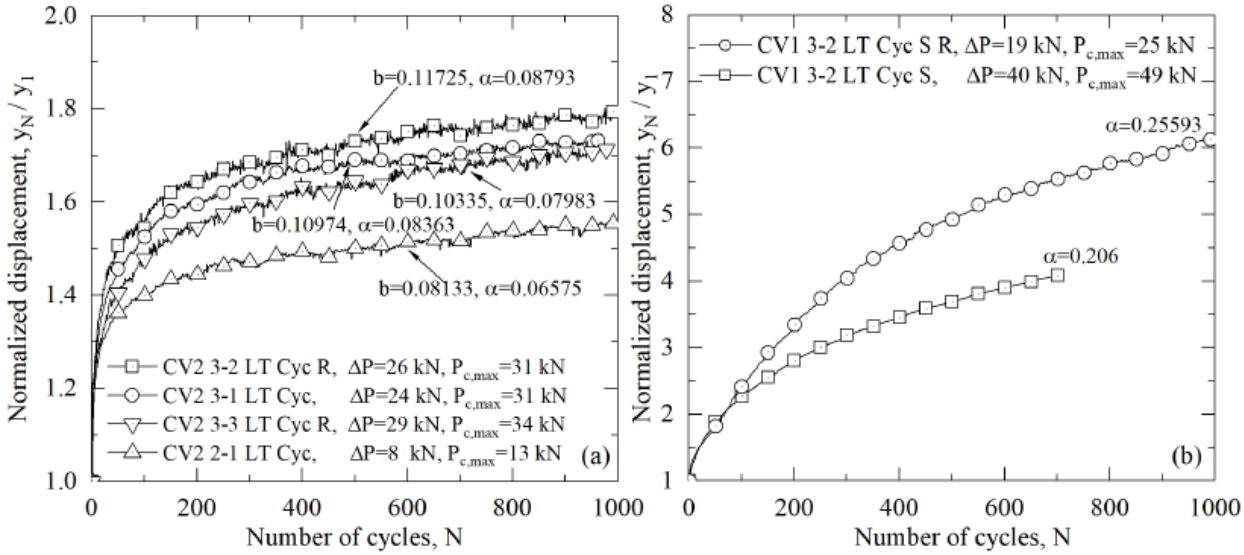


*Figure 31. Normalized pile head displacement for different CVs versus the number of cycles, N in: a.) cohesive soil and b.) granular soil.*

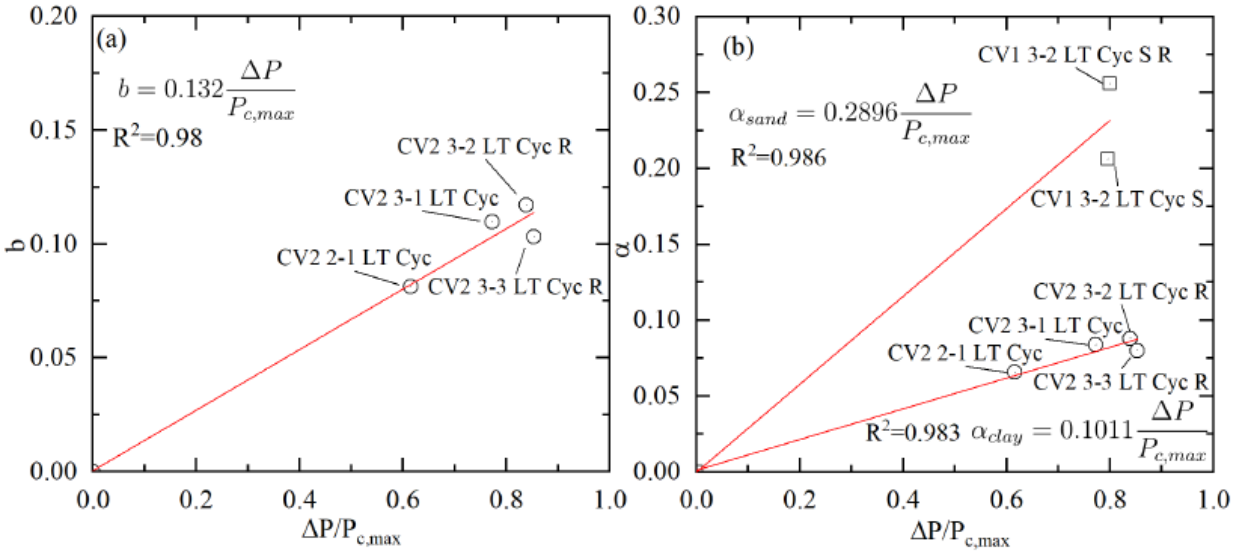


*Figure 32. a.) b coefficient for cohesive soil and b.) cyclic $\alpha$-coefficients for cohesive and granular soil. Coefficients are plotted versus cyclic load ratio $\Delta P/P_{c,max}$.*

Based on the limited cyclic test results available, the pile head horizontal displacement at the maximum cyclic load, $P_{c,\max}$, can be expressed using the following empirical relationships. For cohesive soils, the accumulated displacement after $N$ cycles may be represented by either a logarithmic,

$$y_N = y_1[1 + 0.132\frac{\Delta P}{P_{c,\max}}\ln(N)] \quad (15)$$

or power-law formulation,

$$y_N = y_1 N^{0.1011\,\Delta P/P_{c,\max}} \tag{16}$$

For granular soils, the accumulated displacement is represented by a power-law relationship,

$$y_N = y_1 N^{0.2896\,\Delta P/P_{c,\max}} \tag{17}$$

where $\Delta P$ is the cyclic load amplitude and $N$ is the number of loading cycles.

Relationships of this form may be used to estimate accumulated pile head displacement under cyclic loading anticipated during a single loading event or over the service life of a structure. The required initial displacement, $y_1$, can be readily obtained from conventional $p$–$y$ curves used in pile design or, as in this study, from monotonic load test results. It is emphasized, however, that the empirical coefficients are dependent on collar vane geometry, soil properties, and the cyclic load symmetry parameter $\zeta_c$. These relationships were developed from a limited set of tests and soil conditions in which an HP–CV system was subjected to $\zeta_c \geq 0.7$ and exhibited measurable displacement accumulation. Additional data at lower cyclic load amplitudes are required to confirm the applicability of these formulations for low values of $\Delta P/P_{c,\max}$, soil conditions, and CV configurations.

The maximum bending moment is commonly regarded as the governing parameter in the design of laterally loaded piles. Figure 33 presents bending moment profiles for various CV geometries subjected to cyclic lateral loading. The results indicate that the maximum bending moment generally increases with the number of loading cycles, with the most pronounced changes in the moment distribution occurring within the first 100 cycles. This behavior is attributed to a progressive reduction in lateral resistance at shallow soil depths, which shifts load demand deeper along the pile shaft as cyclic loading progresses.

The influence of cyclic loading on bending moment response can be quantified by examining the ratio $M_{\max,N}/M_{\max,1}$, where $M_{\max,N}$ is the maximum bending moment corresponding to the peak load in cycle $N$and $M_{\max,1}$ is the maximum bending moment measured during the first loading cycle. Figure 34 presents the normalized maximum bending moment as a function of cycle number. In general, all configurations exhibited a cumulative increase in relative bending moment with increasing cycles; however, this increase typically stabilized after a certain number of cycles (approximately 100 cycles for most cases). This stabilization generally coincided with the onset of ratcheting behavior observed in the lateral displacement response. Similar trends have been reported in prior studies of cyclically loaded piles (Garnier, 2013).

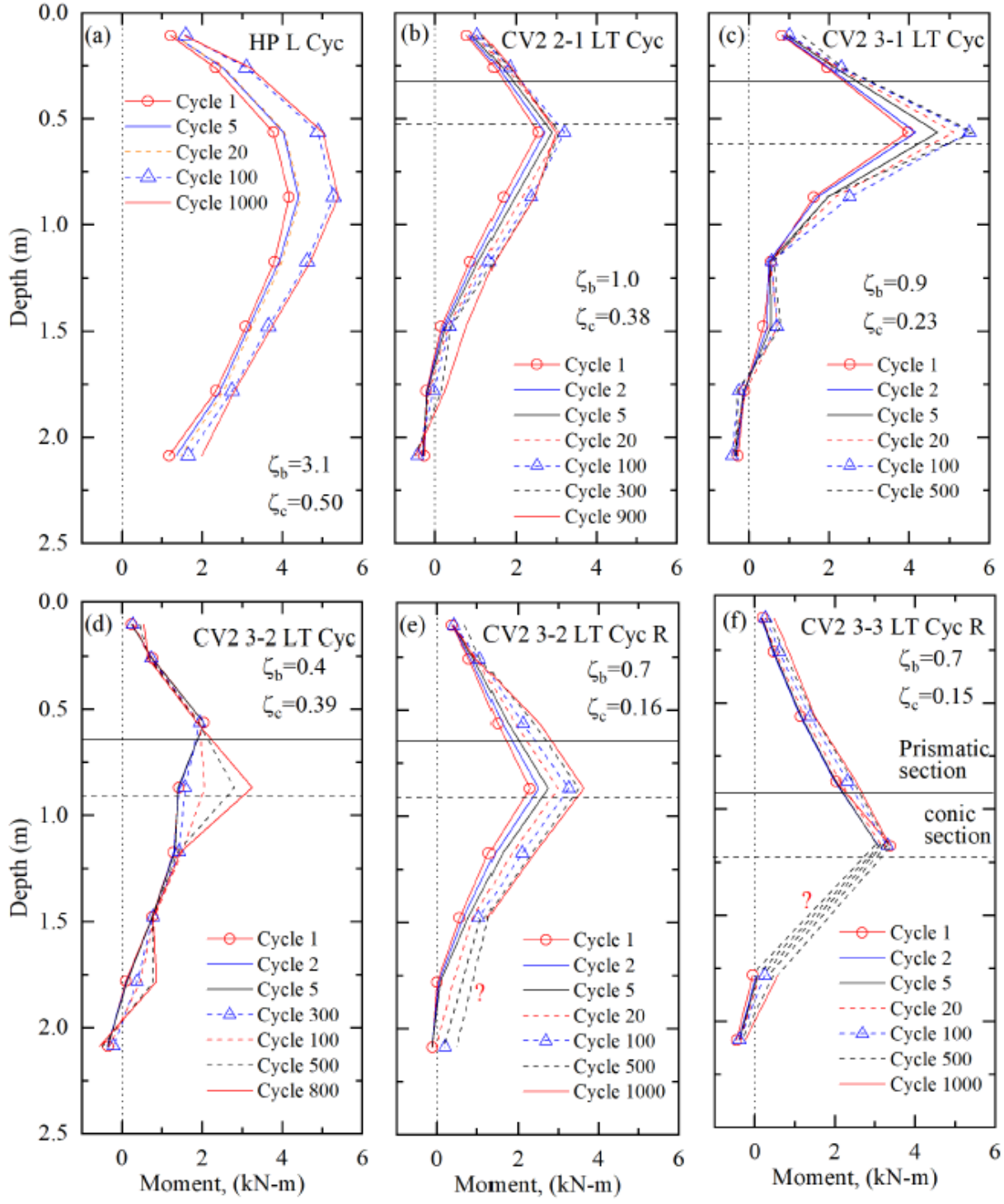


*Figure 33. Cyclic bending moment profiles at various load cycles: a.) without Collar Vane and b.-f.) with a Collar Vane*

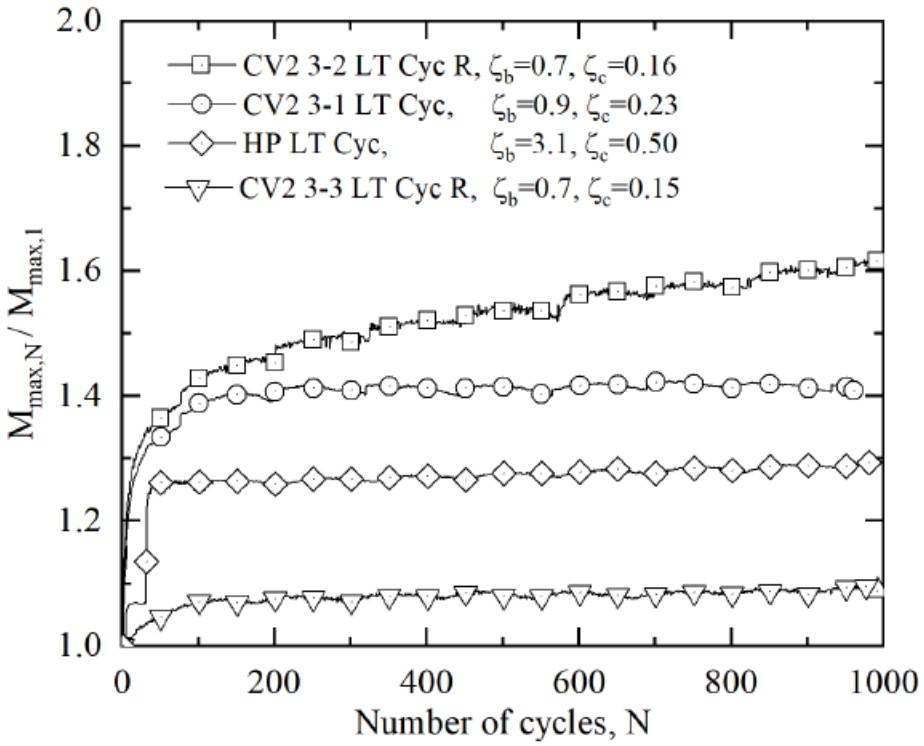


*Figure 34. Normalized maximum moment vs loading cycles.*

## Torsion Load Tests

Table 6 summarizes the collar vane (CV) configurations tested under different cyclic loading combinations. For all cases, torsional load tests were conducted after completion of the lateral cyclic loading phase (i.e. LT sequence). The characteristic cyclic torsional loading parameters are defined as $\zeta_b = T_{c,\max}/T_{\theta=4^\circ}$ and $\zeta_c = T_{c,\min}/T_{c,\max}$, where $T_{\theta=4^\circ}$ is the reference torque corresponding to a CV rotation of 4°. The Florida Department of Transportation (FDOT) serviceability-based failure criterion for traffic signs specifies a limiting rotation of 15° (Hu et al., 2006). However, the smaller reference rotation adopted in this study was selected based on monotonic test results, which showed that the CVs included in the cyclic testing program—particularly the larger CV configurations reached their peak $T$–$\theta$ response at approximately 4°.

Figure 35 and Figure 36 present the torsional response results for tests conducted in cohesive soil. In these figures, the measured torque–rotation responses include the contribution of the helical pile (HP), as it was not possible to isolate the HP torsional resistance from the CV under cyclic loading conditions. This differs from the monotonic torsional tests, in which the contribution of the HP alone was subtracted from the overall HP–CV system response.

Figure 35 shows the torque–rotation curves for CV configurations with a diameter of $D = 0.61$ m. For the two-piece CV, different levels of accumulated rotation were observed for each piece (i.e. one- vs. three blade sides). The blade attached to the single-fin collar section where the connection flange was also not welded to the blade accumulated rotation, consistent with monotonic tests. The one-piece CV exhibited a more uniform torsional response, with all blades rotating in a uniform

(i.e. rigid) manner. The torsional response for diameter of $D = 0.91$ m (Figure 36) was similar was generally similar to the smaller diameter vanes. For the two-piece CV, different levels of accumulated rotation were observed on opposing blade sides, whereas the one-piece CV exhibited a more uniform ratcheting rotation response, like the 0.61 m diameter CVs. However, notably, when similar cyclic load levels were applied, the maximum rotations associated with two-piece CVs did not differ substantially from one-piece vanes in cohesive soil.

*Table 6. Summary of cyclic loading conditions applied for torsional tests.*

| Collar Vane | $T_{\theta=4^\circ}$ (kN-m) | $T_{c,max}$ (kN-m) | $\Delta T$ (kN-m) | $\zeta_b$ | $\zeta_c$ | N |
|---|---|---|---|---|---|---|
| | Cohesive Soil | | | | | |
| CV2 2-1 LT Cyc | 7.8 | 13.7 | 7.3 | 1.8 | 0.47 | 950 |
| CV1 2-2 T Cyc | 15 | 26 | 18 | 1.7 | 0.31 | 1000 |
| CV2 3-1 LT Cyc | 23 | 24 | 15 | 1.0 | 0.38 | 1000 |
| CV2 3-2 LT Cyc | 24 | 18 | 8 | 0.8 | 0.56 | 1000 |
| CV2 3-2 LT Cyc R | 24 | 18 | 12 | 0.8 | 0.33 | 1000 |
| CV1 3-2 LT Cyc | 41 | 43 | 33 | 1.0 | 0.23 | 1000 |
| CV2 3-3 LT Cyc | 24 | 23 | 14 | 1.0 | 0.39 | 850 |
| CV2 3-3 LT Cyc R | 24 | 26 | 16 | 1.1 | 0.38 | 930 |
| | Granular Soil | | | | | |
| CV1 3-2 LT Cyc S | 45 | 44 | 34 | 1.0 | 0.22 | 85 |
| CV1 3-2 LT Cyc S R | 45 | 32 | 24 | 0.7 | 0.25 | 800 |

**Note:** R stands for 'repeated' test with a different $\zeta_b$ or $\zeta_c$.

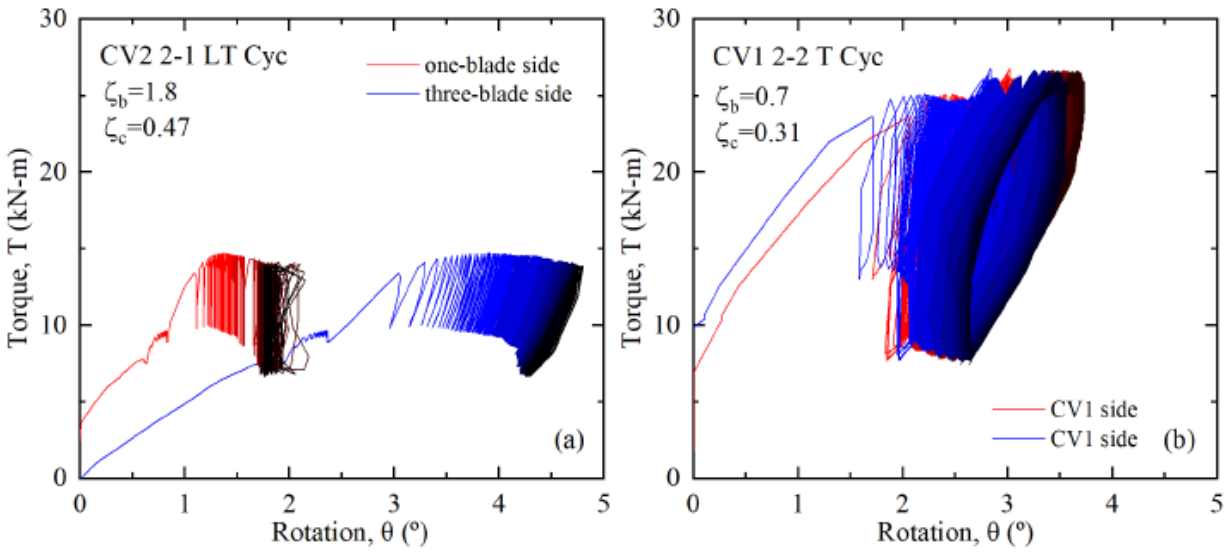


*Figure 35. Cyclic torque-rotation curves in cohesive soil illustrating the difference in rotation associated with the one- and three-blade sides of the two-piece Collar Vane with a one-piece collar vane for: a.) CV2 2-1 and b.) CV1 2-2.*

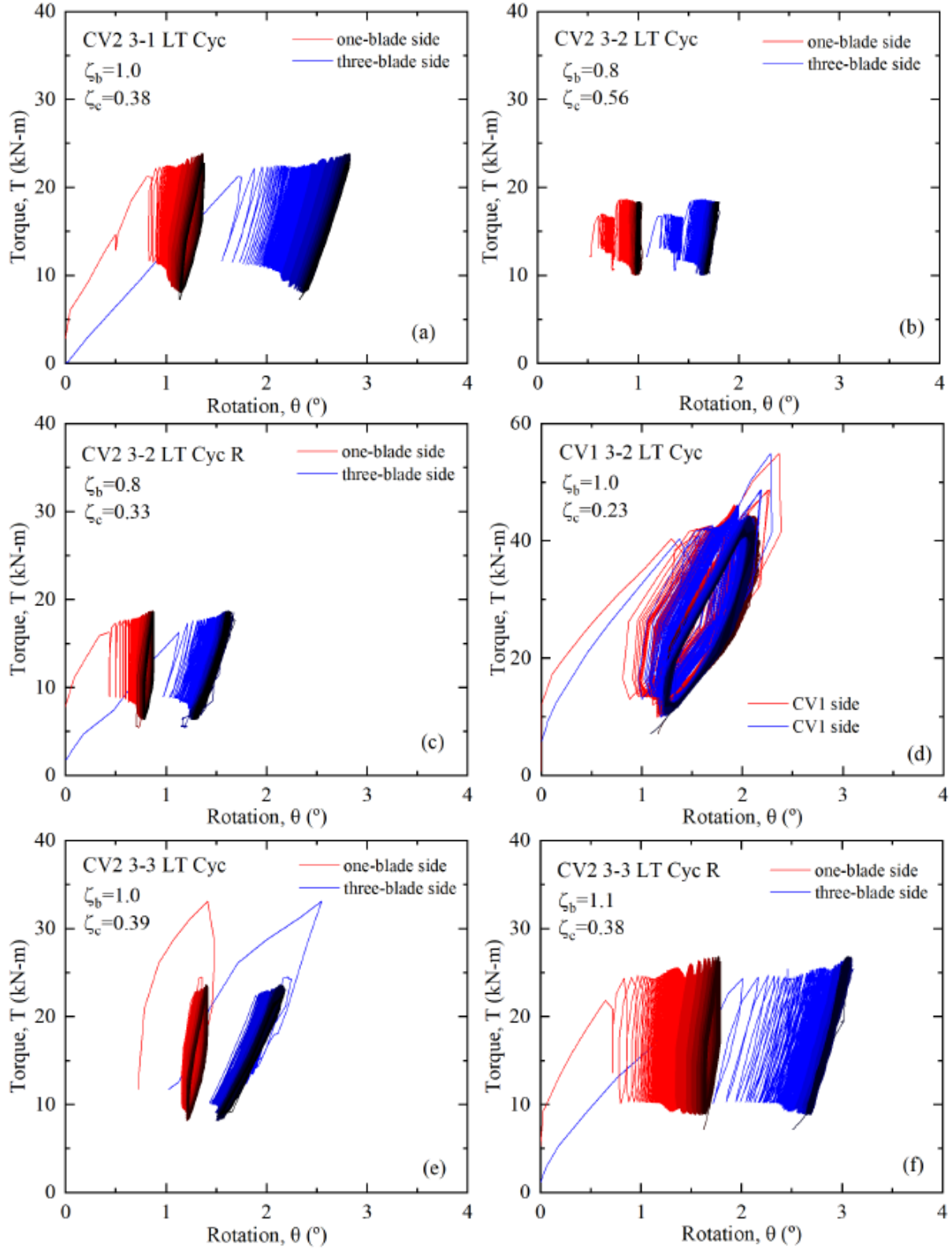


*Figure 36. Cyclic torque-rotation curves in cohesive soil for: a.) CV2 3-1; b.) CV2 3-2; c.) CV2 3-2; d.) CV1 3-2; e. CV2 3-3; f.) CV2 3-3.*

Figure 37 presents the cyclic torsional response of collar vanes tested in sand. The same CV configuration (CV1 3-2) was used for both tests, with different cyclic load ratios, $\zeta_b$. In the first test with $\zeta_b = 1$, the CV reached its ultimate torsional capacity after only 85 loading cycles (Figure 37a). For the case where $\zeta_b = 0.7$, the same amount of rotation was not achieved until after approximately 800 cycles of loading (Figure 37b).

Figure 38 and Figure 39 present field photographs from the cyclic torsional tests conducted in sand. The test shown in Figure 38 was associated with the high-amplitude cyclic torsional loading ($\zeta_b = 1$), which led to 20-25 degrees of rotation after only 85 cycles. The photograph clearly shows the development of a cylindrical failure surface that developed around the perimeter of the collar vane fin blades. In contrast, the test shown in Figure 39 was associated with lower-amplitude cyclic lateral loading ($\zeta_b = 0.7$), where soil subsidence was observed around the CV during torsional loading.

Though the number of cycles required to achieve the same amount of rotation at $\zeta_b = 0.7$ was substantially greater, it's notable that not ratcheting effect was observed. In fact it appears that te amount of rotation associated with each 100 cycles is approximately the same—or even marginally increases. Thus, a load level of $\zeta_b = 0.7$ was ultimately significant enough such that deformations never stabilized. It's likely that as a cylindrical failure surface progressively developed, so did a residual shear resistance (i.e. lower than a

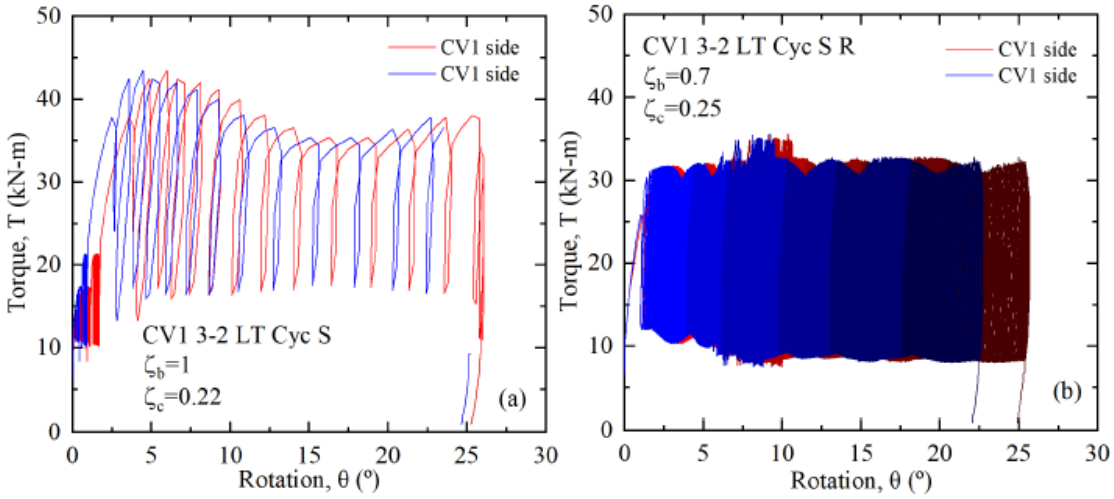


*Figure 37. Cyclic torque-rotation curves in granular soil for: a.) CV1 3-2 with $\zeta_b$ = 1.0 (N=90) and b.) CV1 3-2 with $\zeta_b$ = 0.7 (N=800).*

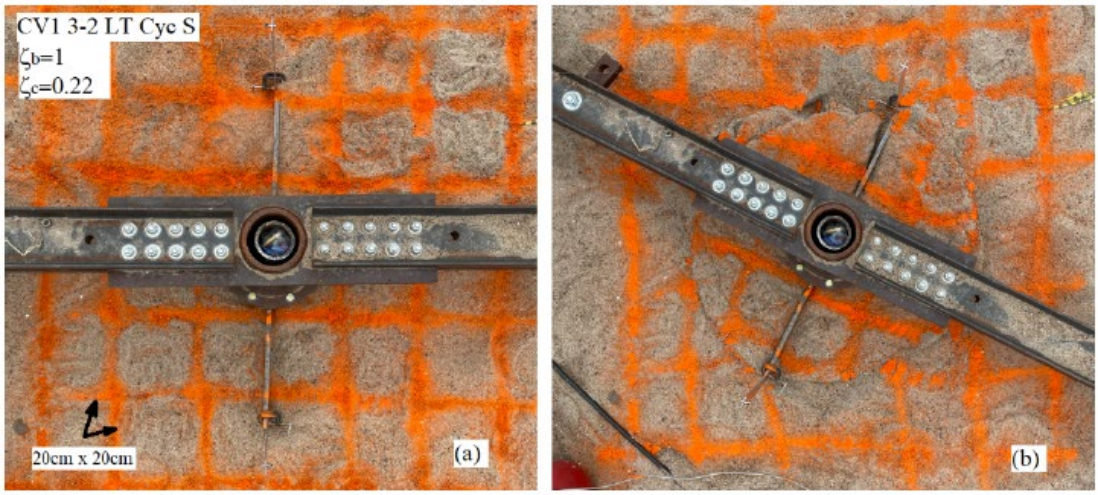


*Figure 38. Photograph illustrating a.) pre-test conditions that's compared with ground deformations and a cylindrical failure surface that developed b.) after cyclic testing when $\zeta_b = 1.0$.*

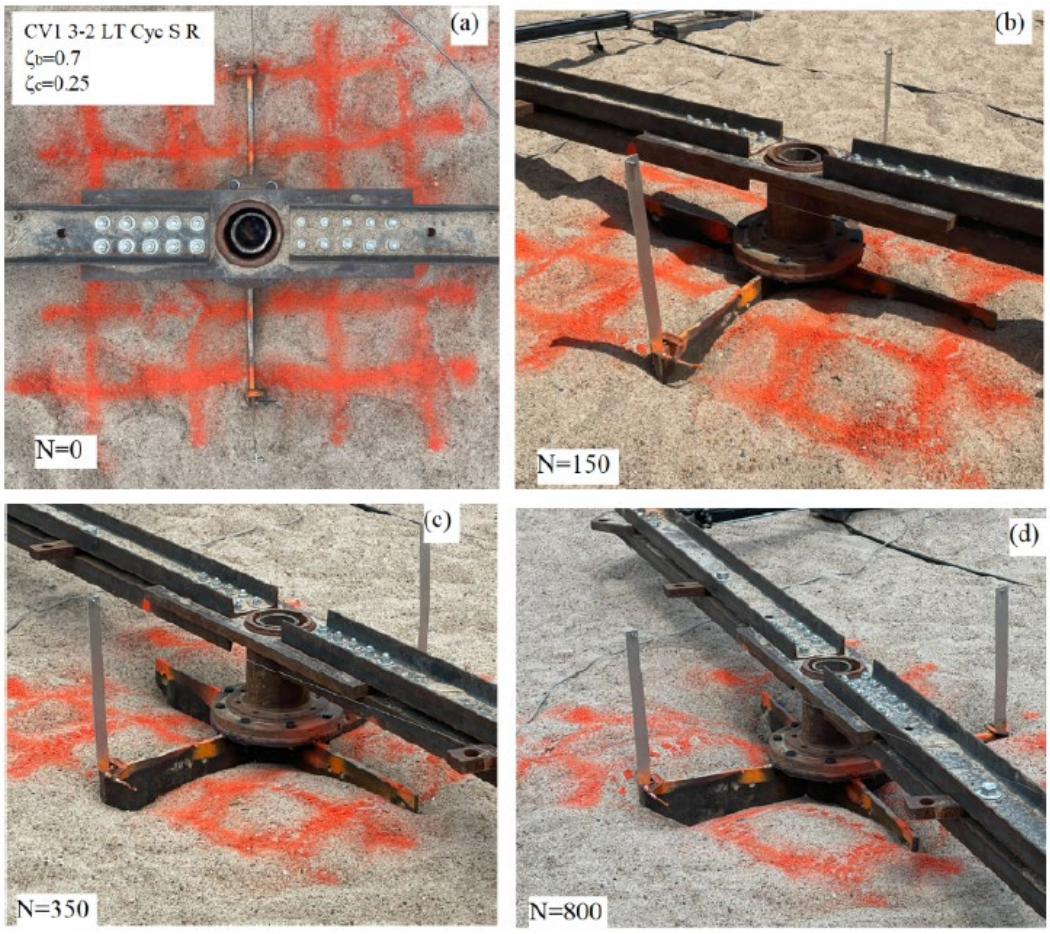


*Figure 39. Soil subsidence adjacent to Collar Vane fins for CV1 3-2 during the cyclic test after a.) 0 cycles; b.) 150 cycles; c.) 350 cycles; d.) 800 cycles.*

# Chapter 5: Full-Scale Testing: Overturning Resistance

The results presented in the preceding chapter demonstrate that collar vane (CV) technology can substantially enhance the lateral and torsional resistance of helical pile (HP) foundations by mobilizing shallow soil resistance and reducing demands on the slender pile shaft. While these loading modes are critical for many foundation applications, several practical infrastructure systems—most notably roadside sign, lighting, and signal structures—are governed by wind-induced overturning loads. In such cases, foundation performance is controlled by the combined action of lateral shear, torsion, and overturning-induced rotation at the pile head, not lateral and/or torsion only.

To address this design condition, a dedicated overturning load test program was conducted to evaluate the performance of HP–CV systems under combined loading representative of wind-induced overturning demands. This chapter describes the experimental setup, testing rationale, and measured system response under realistic service conditions, and compares the observed performance with that of conventional sign foundation types.

## 5.1 Load Test Details

### Background: Sign Loading

Traffic signs may be mounted on a variety of support structures, including poles, cantilevered arms, bridges, and span wires. Pole-mounted sign structures can be further categorized as roadside signs, overhead bridge-mounted signs, and overhead cantilever signs, as illustrated in Figure 40. Wind loading is the primary source of demand for these structures. In the United States, the AASHTO *Standard Specifications for Structural Supports for Highway Signs, Luminaires, and Traffic Signals* (AASHTO LTS; AASHTO, 2022) establishes the minimum design requirements for sign support structures.

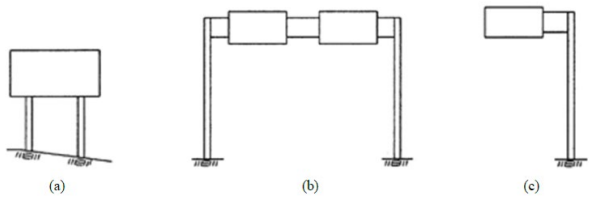


*Figure 40. Schematic of different pole-mounted sign structures: a.) Roadside sign; b.) Overhead bridge; and c.) Overhead cantilevers. Modified from AASHTO (2022).*

Wind loads on sign structures are determined by calculating the wind pressure acting on the sign panel(s), supporting structural elements, and associated attachments. Wind pressure is primarily a function of wind speed, which is selected based on the importance of the structure, geographic location, and the potential consequences of failure. Design wind speeds are obtained from ASCE 7 (ASCE, 2021), which provides wind speed maps for different structural categories across the United States. For example, the design wind speed for roadside signs in the state of Maine is 34 m/s (76 mph), whereas design wind speeds in other states may be as high as 51 m/s (113 mph). In addition to wind speed, wind pressure is influenced by parameters accounting for wind exposure, directionality, and the aerodynamic characteristics of the sign structure components.

The horizontal wind pressure generated by air flow induces forces on the sign panels and supporting structure, which must be transferred through the foundation system and ultimately resisted by the surrounding soil. For foundation design, these wind-induced demands are typically resolved into axial and lateral forces, as well as overturning and torsional moments. In most cases, the governing demand for the foundation and supporting members is the overturning moment produced by the eccentricity of the resultant lateral load.

Carvajal Muñoz (2023) evaluated wind-induced foundation loads for a range of sign sizes and two representative support configurations—a centered single-post system and a cantilevered system—as shown in Figure 41. Results from the lateral and torsional testing of the collar vane presented in the preceding sections indicate that HP–CV systems can resist lateral (shear) loads on the order of approximately 20 to greater than 50 kN, as well as torsional loads ranging from approximately 20 to greater than 50 kN·m. Comparison of these measured resistance capacities with the torsional and shear demands imposed on foundations for typical sign structures (e.g., Figure 41a, c, d) demonstrates that the collar vane can effectively augment helical pile foundations, enabling them to accommodate the loading demands associated with many common sign sizes and support configurations. However, performance of HP-CV systems subjected to overturning loads (Figure 41b) were not directly evaluated via the load testing program presented in the preceding section.

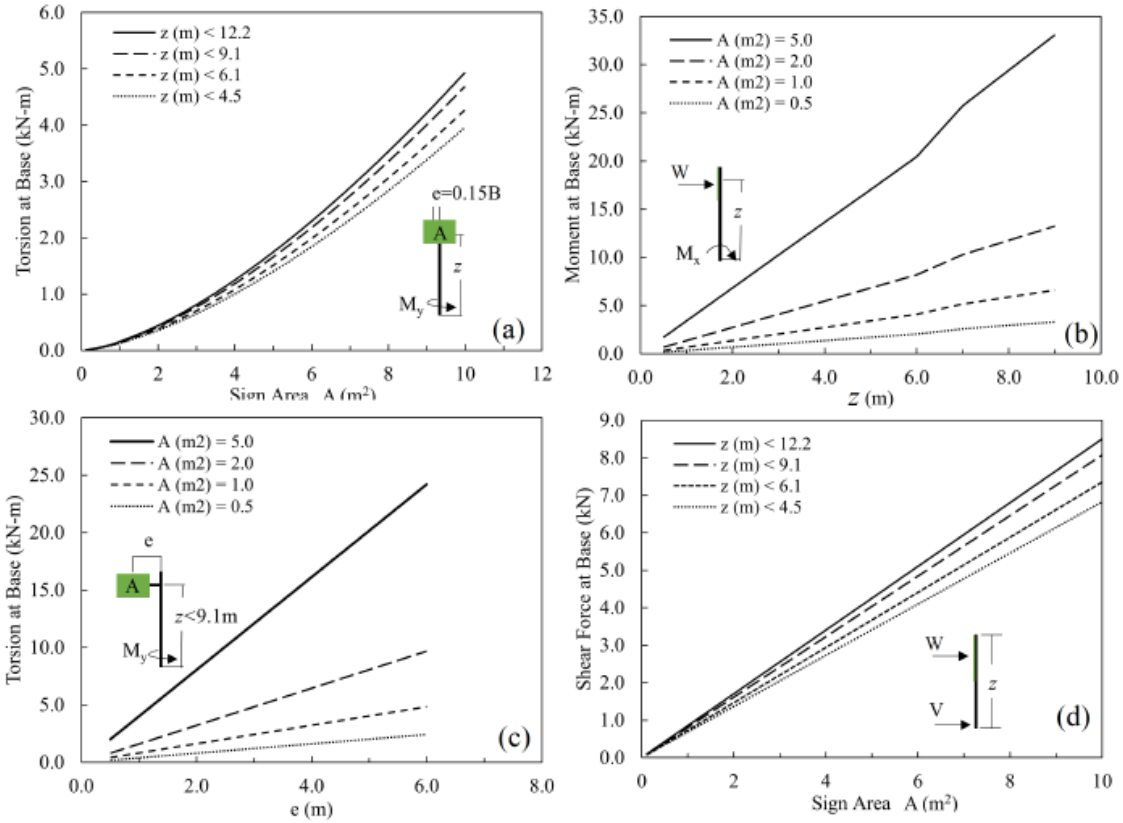


*Figure 41. Computed loads at the foundation base for different sign structure configurations for state of Maine design wind speeds assuming a 1.5W:1H dimensioned road sign; a.) torsion for a single post sign; b.) bending moment for a single post sign; c.) torsion for a cantilevered sign; d.) shear for a single supported sign.*

For the overturning load test program, design loading was selected to represent a common roadside sign configuration used by state DOTs, with performance evaluated relative to conventional foundation systems typically specified for these structures. As expected, foundation details recommended by state DOTs are generally similar and most often consist of reinforced concrete elements with diameters ranging from 0.46 m (18 in.) to 0.91 m (36 in.) and embedment depths between 1.5 m (5 ft) and 2.4 m (8 ft).

To constrain the scope of the experimental program, specific design guidance provided by the Maine Department of Transportation (MaineDOT) for single-post-mounted roadside sign structures was adopted. Table 7 summarizes the conventional reinforced concrete foundation geometries and their corresponding sign sizes and heights, which were used to define overturning load demands applied to HP–CV systems that had previously been evaluated under lateral and torsional loading.

*Table 7. Recommended drilled shaft sizes for single-post mounted roadside sign structures (MaineDOT, 2020).*

| Diameter (m) | Length (m) | Sign area, A ($m^2$) | Max. mounting height |
|---|---|---|---|
| 0.46 | 1.7 | $0.93 < A \leq 1.48$ | 3.66 m to the center of |
| 0.61 | 2.13 | $1.48 < A \leq 3.90$ | sign panel |

Figure 42 summarizes foundation design shear forces ($P_h$) and overturning moments ($M_{z0}$) for a single-post-mounted roadside sign with the largest area (3.90 $m^2$) from Table 7, following the procedures outlined in AASHTO (2022). For single-post sign installations, U.S. Departments of Transportation (DOTs) typically limit the sign panel area to a maximum of 3.9 $m^2$ (42 $ft^2$). Accordingly, the analysis was performed by varying wind speed ($V_w$) and sign height ($z$) while maintaining this maximum sign panel area.

As shown Figure 42b and Figure 42c, both $P_h$and $M_{z0}$ increase with increasing wind speed. However, the shear force $P_h$ is independent of sign height for a given wind speed, whereas the overturning moment $M_{z0}$ increases linearly with increasing sign height. For a max wind speed of 52 m/s (115 mph), the design shear force is approximately 6 kN (1.35 kips), while the corresponding overturning moment ranges from approximately 15 kN·m (11 kips-ft) to 22 kN·m (22.2 kips-ft), depending on sign height. Moments ultimately applied during the testing program correspond to the largest sign size and moments associated with the different wind speeds shown in Figure 42.

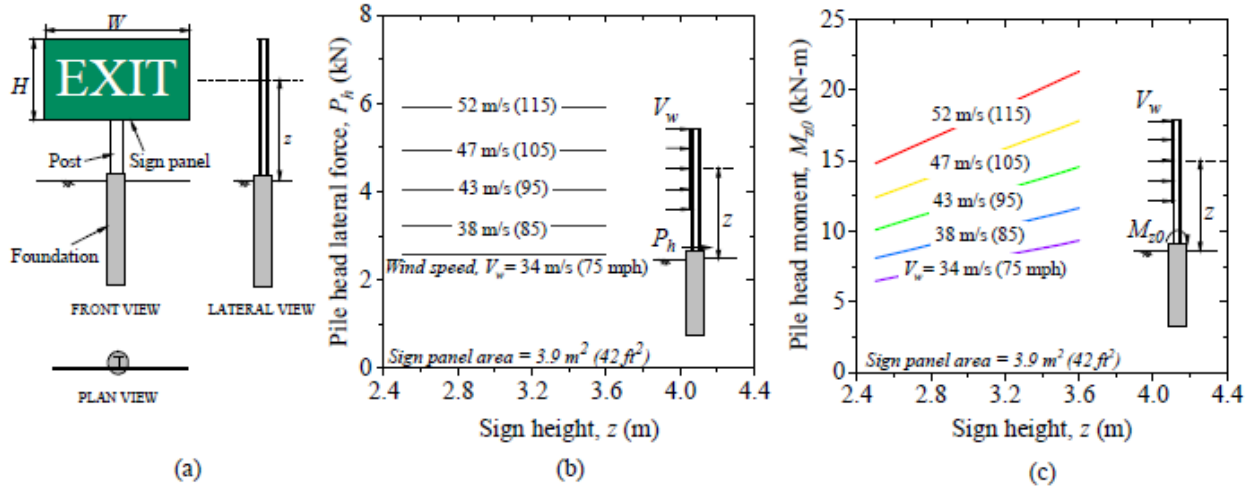


*Figure 42. Design loads for roadside sign foundations: a.) schematic of a single-post mounted roadside sign to compute wind-induced design loads of a single-post mounted roadside sign with the largest sign area (3.90 $m^2$) associated with conventional foundation type; b.) lateral shear force associated with different wind speeds; and c.) overturning moment for different wind speed ($V_w$) and sign heights (z).*

## Load Frame Design

Figure 43a illustrates the experimental setup and primary components used for the overturning load tests conducted in this study. A purpose-built load frame was developed to allow combined lateral load and overturning moment to be applied independently at the pile head of the foundation element being tested. The load frame consisted of a triangular truss assembly connected to a base plate that was bolted to the HP–CV system; details of this connection are shown in Figure 43b.

Inclined and vertical anchors were used to provide reaction forces for the applied horizontal ($P_h$) and vertical ($P_v$) loads, respectively. As shown in Figure 43c, basic static equilibrium indicates that the horizontal load component primarily controls the resultant shear force ($V$), while the vertical load applied at the end of the triangular frame governs the applied overturning moment ($M$) at the head of the HP-CV system. These loads were applied using two independent hydraulic actuators. A hand-operated hydraulic pump supplied fluid pressure to the vertical actuator connected at node C, while the horizontal actuator, connected at node F, was powered by a gasoline-driven hydraulic pump equipped with a Tescom ER5K hydraulic pressure controller to supply and maintain near-constant fluid pressure. Because the lateral component of force $F_{AC}$ near the pile head must be equal and opposite of $F_{BC}$, applied higher up on the load frame, the force imposed by the vertical actuator imposed no shear on the foundation; shear was controlled independently with the actuator orientated horizontally (Figure 43).

Instrumentation used to measure applied loads and foundation response included: (1) two calibrated S-type load cells with a maximum capacity of 50 kN, positioned adjacent to the hydraulic actuators; (2) three string potentiometers and two dual-axis analog tilt sensors used to measure pile head lateral displacement ($\delta$) and rotation ($\theta$), respectively; and (3) six pairs of strain gauges installed along the pile shaft, as shown in Figure 43d. The strain gauges were installed using two different configurations: a half-bridge configuration was employed for the second and

lowest gauge pairs (counting from the pile head), while a quarter-bridge configuration was used for the remaining four gauge pairs to provide redundancy at locations more susceptible to damage during installation and testing.

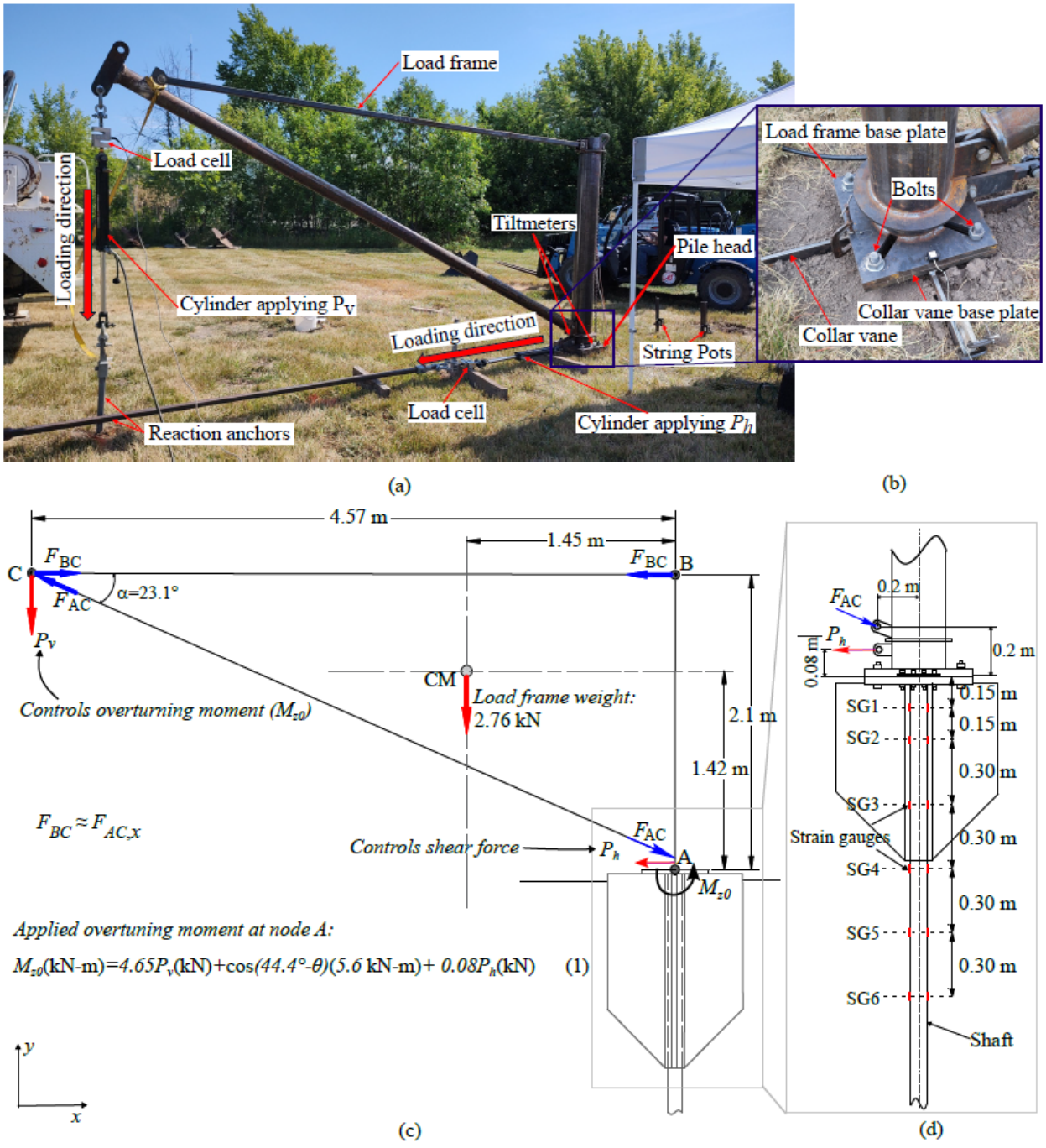


*Figure 43. Load test frame for overturning; a.) photo illustrating load frame configuration and components; b.) photo illustrating the connection of the collar vane and base plate of the load frame; c.) free body diagram illustrating forces and dimensions of the load frame; d.) details of test pile connections and strain gauge location on the helical pile shaft.*

A truck-mounted crane was used to lift the load frame and position it onto the CV base plate. The strain gauges were zeroed prior to placing the load frame, as its self-weight induces an overturning moment due to eccentricity of its center of mass (see Figure 43c). The string potentiometers, tilt sensors, and load cells were installed and zeroed after the load frame was secured to the CV base plate. As a result, pile head deformations caused by the self-weight of the load frame were not explicitly measured. However, these deformations are expected to be minimal, particularly for larger CV configurations or under stiff soil conditions such as the clayey field site used in this study.

Validation of the applied overturning moment was performed using an instrumented helical pile installed in the clay field *without* a collar vane. The objective of this validation exercise was to confirm that the applied overturning moment corresponded to the bending moment interpreted at the strain gauge located nearest to the pile head.

The theoretically applied overturning moment was calculated using an analytical expression derived from static equilibrium (i.e. using FBD illustrated in Figure 43), accounting for the load frame geometry, self-weight, base plate rotation (i.e., pile head rotation), and the applied horizontal and vertical loads. Figure 44 compares the theoretically applied overturning moment with the bending moment interpreted from the uppermost pair of strain gauges at various stages of loading. When the load frame was not installed, strain gauge readings indicated negligible bending moment. Upon installation of the load frame and transfer of its self-weight to the pile head, the interpreted bending moment increased and showed good agreement with the computed overturning moment due to self-weight. As horizontal and vertical loads were subsequently applied, excellent agreement between the computed and measured moments was maintained. These results confirmed the validity of the overturning load test methodology adopted in this study.

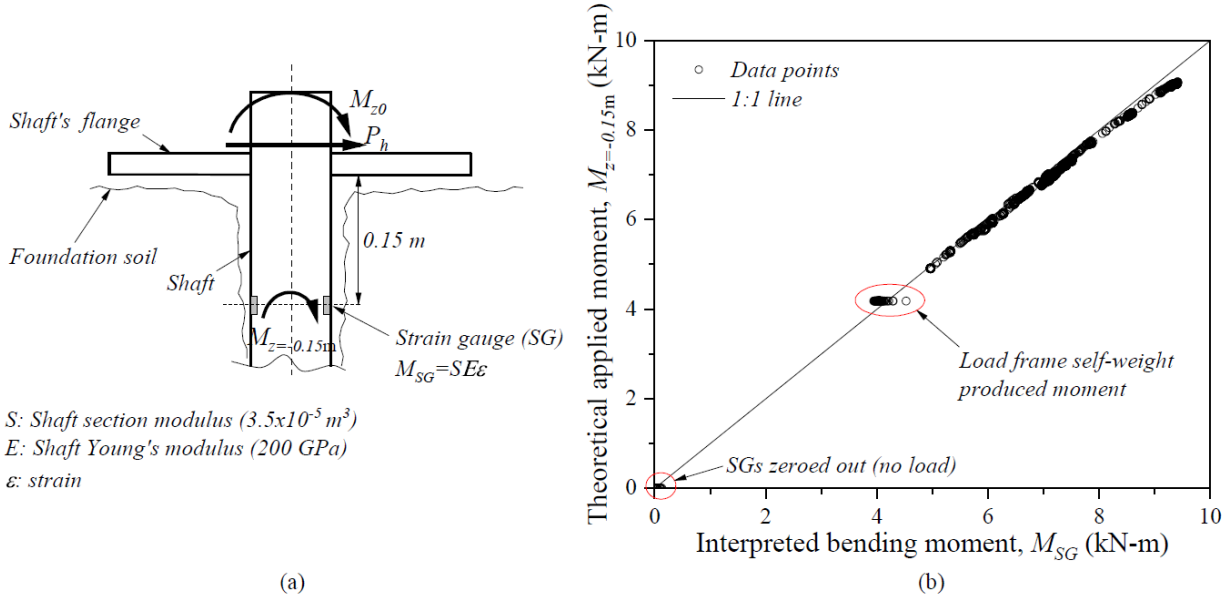


*Figure 44. Validation of load test frame: a.) schematic of applied forces to a helical pile using the test frame and measured bending moment at the shallowest strain gauge; b.) comparison of the theoretical applied overturning moment ($Mz$ at $z = 0.15m$) and measured bending moment with strain gauges ($M_{SG}$).*

Validation was performed without a collar vane (CV) because the CV alters the lateral load transfer mechanism by concentrating mobilized soil resistance near the pile head, which significantly affects the bending moments measured at the uppermost strain gauge. This behavior was discussed previously and is revisited later in the context of overturning response. In contrast, for a helical pile (HP) installed without a CV, a small gap typically forms between the pile shaft and the surrounding soil during installation, resulting in negligible soil resistance at shallow depths. Consequently, bending moments measured at the uppermost strain gauge primarily reflect the applied loading, which is consistent with the theoretical assumptions used in the validation analysis.

## Load Test Procedure

A loading procedure was developed to simulate wind-induced loads acting on a single-post-mounted roadside sign structure with a sign panel area of 3.9 m² and varying sign heights ($z$). The applied loads were selected assuming a constant design wind speed of 52 m/s (115 mph). Under these conditions, the lateral load (i.e., shear) remains constant, while the overturning moment increases with increasing sign height, as illustrated in Figure 42.

Accordingly, pile head loading was applied in two stages. First, a lateral load of 6 kN was applied and maintained at an approximately constant level throughout the test. The overturning moment was then applied monotonically by increasing the vertical load ($P_v$). All tests were conducted in general accordance with ASTM D3966 (ASTM, 2022), although this standard does not provide explicit guidance for pile testing under relatively large overturning moments.

## Testing Program Summary

The overturning load test program consisted of a total of 15 tests, including 11 tests conducted on different HP–CV configurations and 4 tests performed on drilled shaft foundations. Table 8 summarizes the HP–CV configurations tested in both clay and sand. The helical piles used in this study consisted of a 2.1 m long square-shaft (SS175) lead section equipped with three helices having diameters of 254, 304, and 355 mm; two 1.2 m long square-shaft (SS175) extension sections each with a 355 mm diameter helix; and a 2.14 m long hollow round shaft (RS3500.300) with an outer diameter of 88.9 mm and a wall thickness of 7.15 mm.

An efficient test layout was adopted to minimize the number of inclined reaction anchors required for the overturning tests. Figure 45a presents an aerial photograph of the test site, indicating the locations of the sand pit and clay field. The specific test layouts used in each area are shown in Figure 45b and Figure 45c for the sandy and clayey sites, respectively. A minimum center-to-center spacing of 3 m between test pile locations was maintained to limit interaction effects, except for the HP–CV systems and drilled shafts tested within the sand pit, where spacing was constrained by available area. The same minimum spacing criterion was also applied between test piles and the vertical and inclined reaction anchors.

*Table 8. Summary of overturning tests for HP-CV systems with different collar vane geometries.*

| Test pile | Site | Collar vane nomenclature | $D$ (m) | $H_p$ (m) | $t$ (mm) |
|---|---|---|---|---|---|
| TC1 | Clay | 2-2 | 0.61 | 0.61 | 9.52 |
| TC2 | Clay | 2-3 | 0.61 | 0.91 | 9.52 |
| TC3 | Clay | 3-2 | 0.91 | 0.61 | 12.7 |
| TC4 | Clay | 3-1 | 0.91 | 0.30 | 12.7 |
| TC5 | Clay | No CV | - | - | - |
| TC6 | Clay | 3-3 | 0.91 | 0.91 | 12.7 |
| TC7* | Clay | 2-2 | 0.61 | 0.61 | 9.52 |
| TS1 | Sand | 2-2 | 0.61 | 0.61 | 9.52 |
| TS2 | Sand | 2-3 | 0.61 | 0.91 | 9.52 |
| TS3 | Sand | No CV | - | 0 - | - |
| TS6 | Sand | 3-3 | 0.91 | 0.91 | 12.7 |

*Indicates a repeated test.

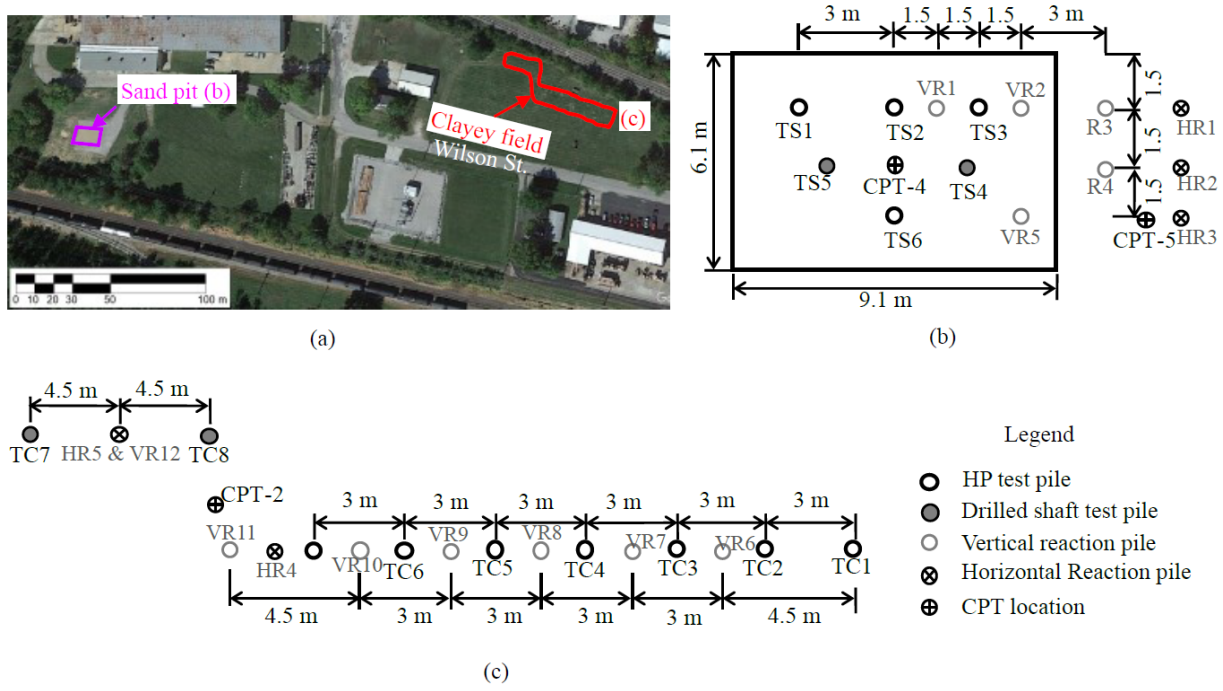


*Figure 45. a.) aerial photo of the testing site showing the sand pit and clay field. Test layout for the overturning load tests followed in the b.) sand pit and c.) clay field.*

To enable comparison between the performance of CV–augmented helical piles and conventionally recommended drilled shaft foundations for roadside sign support, a total of four drilled shaft test specimens were constructed—two in the sand test pit and two in the clay field. Two drilled shaft geometries were evaluated: (1) a 1.68 m long shaft with a diameter of 0.46 m, and (2) a 2.14 m long shaft with a diameter of 0.61 m. These dimensions were selected based on typical sign foundation details recommended by the state of Maine.

Figure 46 illustrates the construction process for the drilled shafts tested in this study. The shaft excavations were first advanced using a truck-mounted auger. In the sand test pit, cylindrical forms

were required to maintain the desired shaft geometry; accordingly, cardboard sondex tubes with diameters of 0.46 m and 0.61 m were installed. Following excavation and form placement, concrete with a compressive strength of 27.5 MPa was placed. In lieu of a rebar cage or other steel element, a modified lighting foundation *Instant Foundation* manufactured by Hubbell Power Systems, Inc. was installed at the center of the shaft to serve as reinforcement and provide a connection point for the load frame. From a geotechnical perspective, the presence of this steel casing reinforcement was not expected to significantly influence foundation performance, as the drilled shafts tested in this study behave as rigid or short foundations.

Table 9 summarizes the drilled foundation geometries for tests performed in clay and sand.

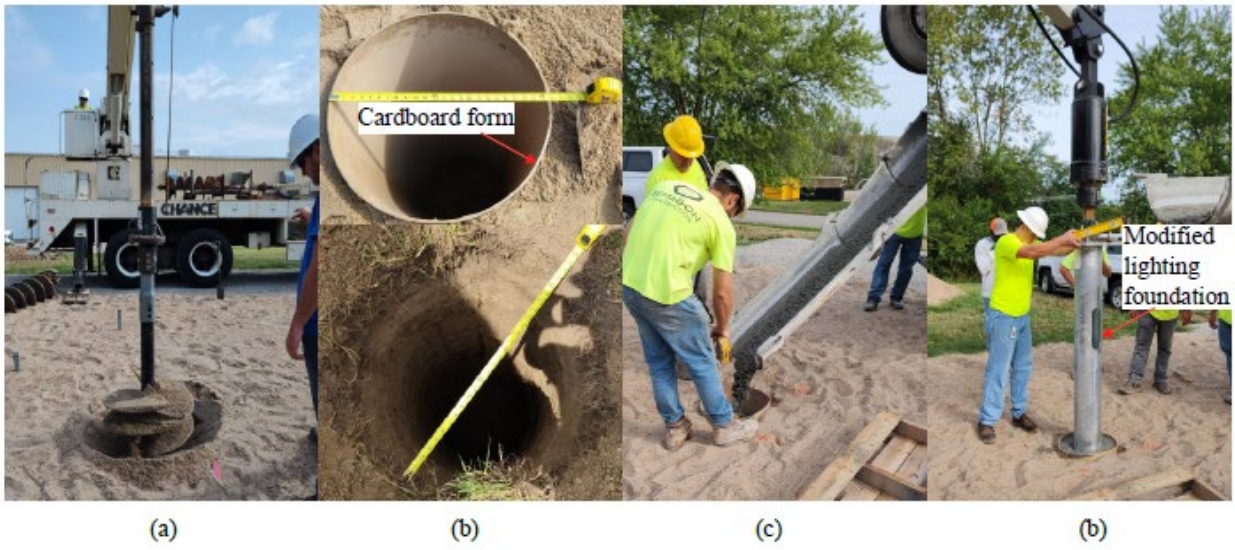


*Figure 46. Construction of concrete drilled shafts: a.) drilling hole; b.) drilled hole with and without casing; c.) concrete pour; and d.) steel casing reinforcement.*

*Table 9. Summary of drilled shafts tested in clay and sand.*

| Test pile | Site | Diameter (m) | Length (m) |
|---|---|---|---|
| TC7* | Clay | 0.46 | 1.68 |
| TS8 | Clay | 0.61 | 2.14 |
| TS4 | Sand | 0.46 | 1.68 |
| TS5 | Sand | 0.61 | 2.14 |

*The test could not be completed due to issues with the hydraulic controller.

## 5.2 Load Test Results

### Overturning Moment Capacities and Performance

Figure 47 presents the pile head lateral response of the tested foundation elements under applied overturning moments, including lateral deflections ($\delta$) and rotations ($\theta$), for tests conducted in clay (Figure 47a, c) and sand (Figure 47b, d). In these figures, the horizontal shaded bands denote the design overturning moments corresponding to different wind speeds, as presented earlier in Figure 42.

In general, lateral capacity increased with increasing foundation element size for both helical piles equipped with collar vanes (HP–CV systems) and drilled shafts. Larger foundation elements exhibited stiffer lateral responses and higher ultimate capacities. At a pile head lateral deflection of 8 mm, the increase in lateral capacity provided by the collar vane ranged from approximately 2.4 to 12.5 times that of a helical pile without a collar vane in clay, and from approximately 2.7 to 4.6 times in sand.

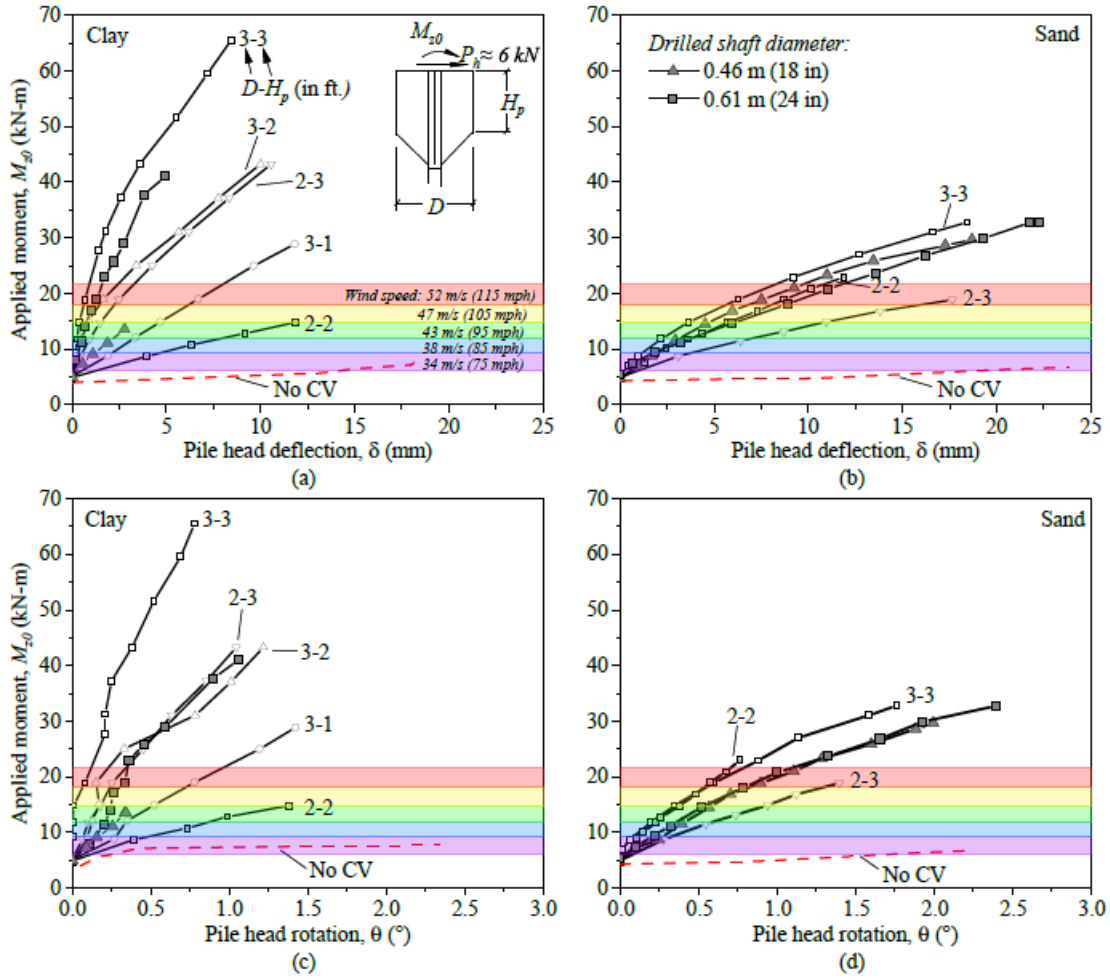


*Figure 47. Response of tested elements to overturning moment: a.) pile head deflection in clay; b.) pile head deflection in sand; c.) pile head rotation in clay; and d.) pile head rotation in sand.*

Comparison with conventional drilled shaft foundations indicates that only the helical pile equipped with a 3-3 collar vane marginally outperformed both the 0.46 m and 0.61 m diameter drilled shafts in clay. The CV 3-2 and 2-3 configurations exhibited performance comparable to the 0.61 m drilled shaft, particularly at mobilized resistances corresponding to loads representative of the highest design wind speeds. Helical piles with 3-2 and 2-3 collar vanes exceeded the performance of the 0.46 m drilled shaft in clay, while the 3-1 configuration exhibited comparable resistance. The 2-2 collar vane configuration was the only case that did not perform as well as the 0.46 m drilled shaft. Notably, all collar vane configurations tested in clay were capable of mobilizing resistance associated with the highest design wind speeds, with the exception of the CV 2-2 configuration.

In sand, the performance of all collar vane configurations and drilled shafts was generally similar. The CV 2-3 configuration was the only case that exhibited appreciably lower mobilized resistance at larger deflections; however, aside from this configuration, all HP–CV systems were able to mobilize resistance associated with the highest design wind speeds. Based on trends observed in clay and monotonic testing, the 2-3 configuration would be expected to perform at least as well as the 2-2 configuration. The unanticipated response of the CV 2-3 system in sand is attributed to variability in local soil conditions, including: (1) changes in moisture content due to rainfall during testing, which may have partially saturated the sand and induced suction, thereby increasing apparent soil strength; and/or (2) changes in relative density resulting from the shaft drilling process. In contrast, helical piles tested without collar vanes exhibited negligible lateral capacity in both clay and sand, indicating that they are unsuitable on their own for supporting large roadside sign structures.

Figure 48a–d summarizes pile head lateral deflections for helical piles equipped with collar vanes tested in clay, plotted as a function of the prismatic section height ($H_p$) for wind speeds of 34 m/s (75 mph), 38 m/s (85 mph), 43 m/s (95 mph), and 47 m/s (105 mph), respectively. The results indicate that lateral deflections decrease with increasing collar vane size, achieved through increases in either $H_p$or diameter ($D$). For collar vanes with a diameter of 0.91 m (3 ft), the marginal reduction in deflection diminishes as $H_p$ increases, suggesting decreasing returns in lateral resistance at greater embedment depths. In contrast, for configurations with $H_p = 0.61$ m, increasing the collar vane diameter is more effective in reducing lateral deflections than further increasing $H_p$.

Overall, the results indicate that CV–augmented helical pile systems can provide lateral and overturning performance comparable to, and in some cases exceeding, that of conventionally recommended drilled shaft foundations for roadside sign structures. These findings demonstrate that HP–CV systems represent a viable alternative foundation solution for this application, offering sufficient resistance to wind-induced demands while maintaining a relatively compact foundation footprint. As such, collar vane technology shows promise for use in roadside sign support applications where conventional drilled shafts are typically specified.

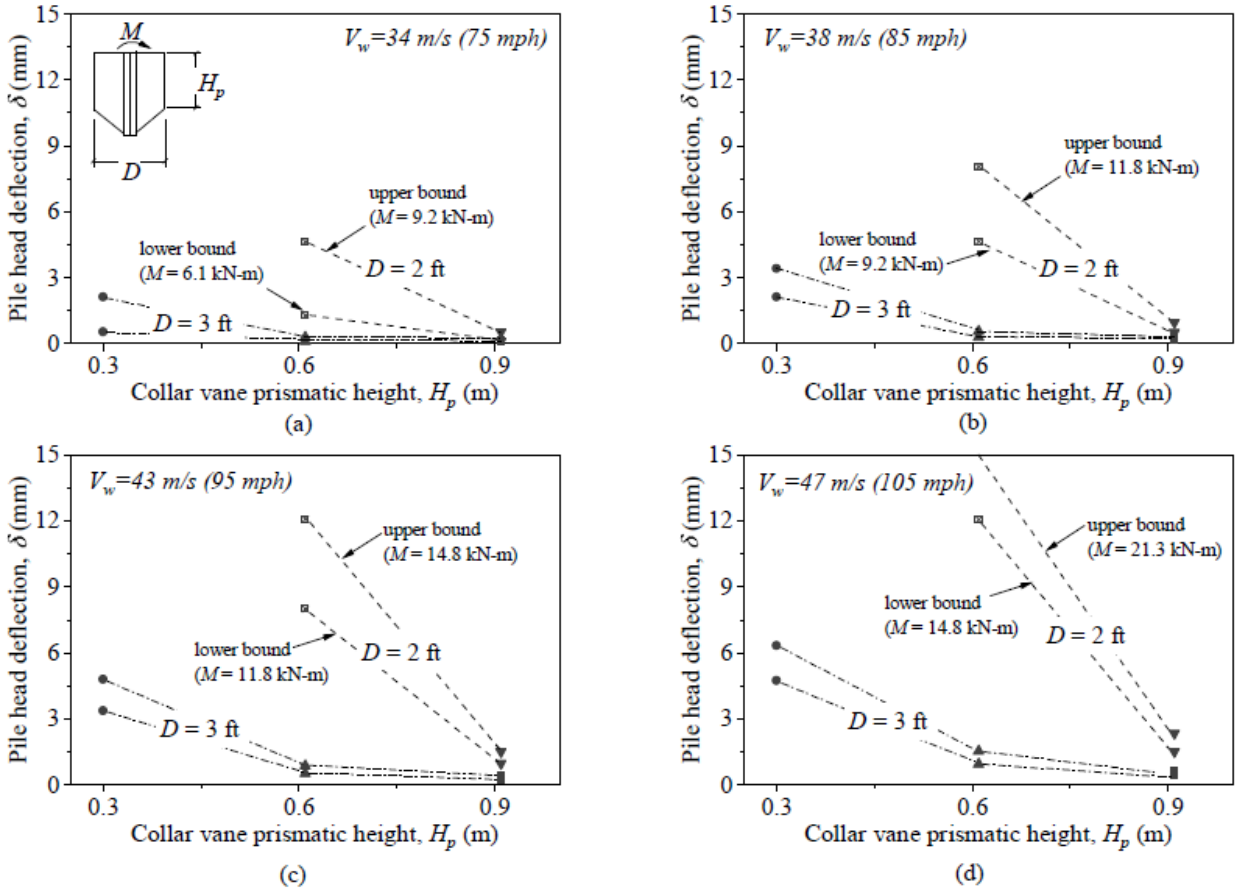


*Figure 48. Pile head deflections of different HP-CV systems tested in clay for simulated wind speeds of: a.) 34 m/s (75 mph); b.) 38 m/s (85 mph); c.) 43 m/s (95mph); d.) 47 m/s (105 mph).*

## Structural Bending Moments

Figure 49 compares bending moment distributions along the shaft of a helical pile tested in clay, both with and without a collar vane, under varying applied overturning moments ($M_{z0}$). Two distinct response patterns are observed. For a helical pile without a collar vane, the applied overturning moment is concentrated near the pile head, resulting in relatively large bending moments in the upper portion of the shaft, as shown in Figure 13a. In contrast, for a helical pile equipped with a collar vane, bending moments near the pile head are substantially reduced and increase approximately linearly with depth to the bottom of the collar vane (Figure 49b). Although the profiles shown correspond to a helical pile with a 2-3 collar vane, similar bending moment shapes were observed for all collar vane configurations tested in both clay and sand, with differences primarily reflected in the magnitude and depth of the peak bending moment.

The reduction in shaft bending moment near the pile head for helical piles with a collar vane reflects the redistribution of overturning resistance between the pile shaft and the collar vane, with the collar vane contributing a significant portion of the resisting moment due to its greater stiffness and ability to mobilize shallow soil resistance. The approximately linear variation of bending moment along the shaft segment encapsulated by the collar vane indicates that little to no

additional shear is transferred to the shaft over this region, consistent with a constant shear force distribution. This response suggests minimal interaction between the pile shaft and surrounding soil or collar along most of the collar length—which was the same behavior exhibited for lateral load tests.

Peak bending moments were generally observed near the bottom edge of the collar vane, where localized interaction may occur as soil partially fills the annular gap between the shaft and the collar. Such interaction can alter the local shear force distribution and lead to the development of a maximum bending moment at or near the base of the collar vane.

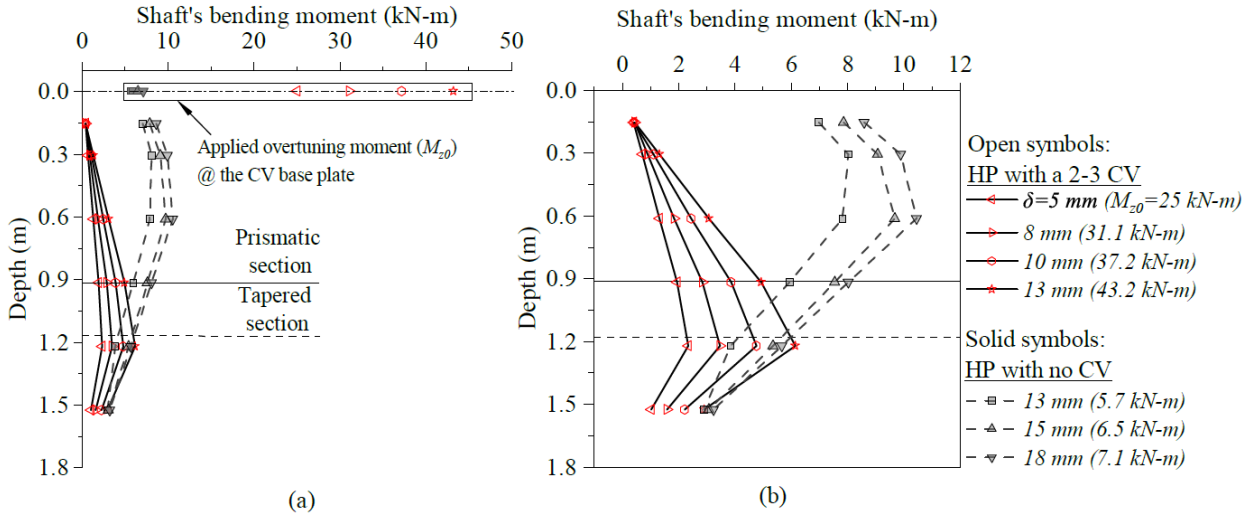


*Figure 49. Comparison of the nature of the bending moment profile of a Helical Pile with a 2-3 CV and with no CV.*

Figure 50 presents the evolution of the peak bending moment in the pile shaft ($M_{\max}$) as a function of the applied overturning moment ($M_{z0}$). For reference, the factored bending moment capacity of the shaft ($\phi M_n = 13$ kN·m) is indicated by the horizontal dashed line. In general, $M_{\max}$ increases with increasing $M_{z0}$ for all collar vane configurations tested in both clay and sand.

The rate at which $M_{\max}$ increases relative to $M_{z0}$, however, varies depending on the magnitude of the applied load, collar vane size, and soil conditions. At relatively small values of $M_{z0}$, $M_{\max}$ increases gradually, whereas at larger overturning moments the rate of increase becomes more pronounced. Smaller collar vane configurations exhibit steeper growth rates of peak shaft bending moment compared to larger configurations. Additionally, in sand—where pile head deflections were greater for the same overturning moments applied in clay—the rate of increase in $M_{\max}$ with $M_{z0}$ is greater than that observed in clay.

For nearly all collar vane configurations tested, the maximum factored bending moment capacity of the helical pile shaft was not exceeded, even under loading corresponding to the highest design wind speeds. These results demonstrate that the collar vane effectively limits bending demands in the shaft, enabling the use of relatively slender pile sections while maintaining adequate resistance to wind-induced overturning moments typical of roadside sign design.

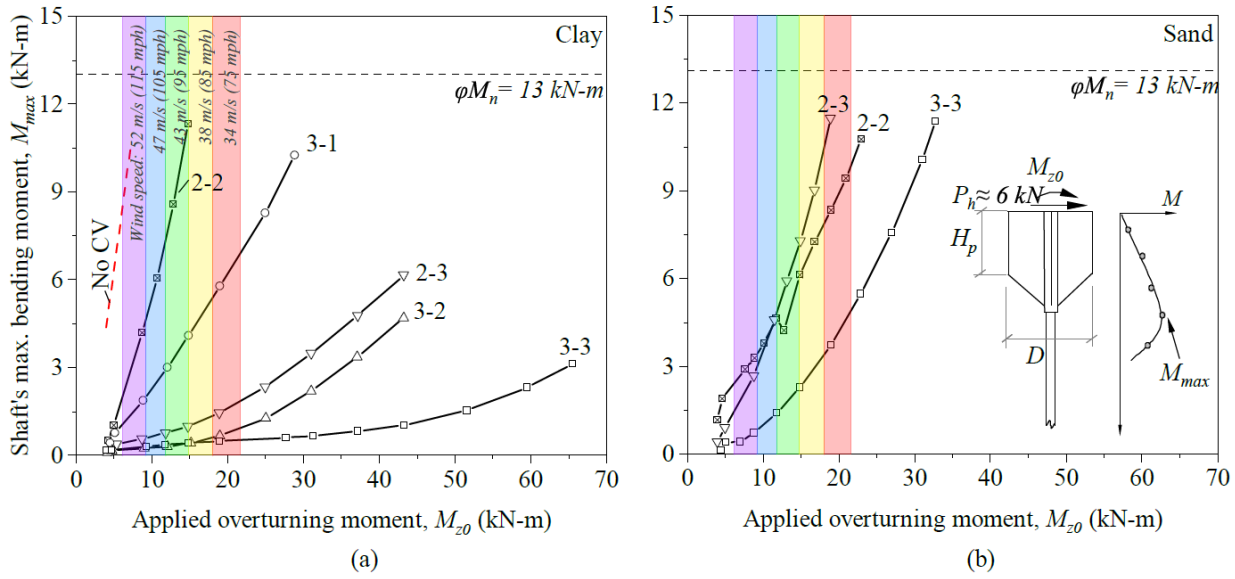


*Figure 50. Comparison of the HP shaft's maximum bending moment versus the applied overturning moment in a.) clay; and b.) sand.*

## 5.3 Load Transfer Mechanics

The load-transfer mechanism of a helical pile equipped with a collar vane (HP–CV system) differs fundamentally from that of conventional piles due to the separation of load resistance and load transfer functions between the collar vane and the pile shaft. Figure 51 illustrates the undeformed and deformed configurations of the HP–CV system and the associated load paths. The pile shaft is structurally connected to the collar vane at the pile head through a bolted flange, ensuring deformation compatibility at that location, while the collar's inner diameter exceeds the shaft outer diameter, creating an annular gap along the length of the collar (Figure 51a–b).

Under lateral and overturning loading, the collar vane behaves as a relatively rigid element due to its high bending stiffness, while the pile shaft bends within the collar (Figure 51c). Because the shaft segment enclosed by the collar is isolated from the surrounding soil, lateral soil resistance is not mobilized directly along that portion of the shaft. Instead, lateral soil resistance is mobilized primarily by the collar vane and transferred to the pile shaft at the pile head connection (Figure 51d). As a result, the internal shear force within the shaft is reduced and approximately constant where it is encapsulated by the collar, consistent with bending moment distributions observed in this study.

At larger deformations, localized contact between the pile shaft and collar may occur, most likely near the bottom of the collar where relative displacements are greatest (see Figure 51d). Such contact can introduce localized reaction forces that alter the internal shear distribution within the shaft below the collar; however, these forces do not constitute independent load paths. Instead, they contribute to reducing the bending moment demand in the helical pile shaft associated with the applied overturning moment at the pile head. In effect, contact between the shaft and the bottom

of the collar generates a counteracting moment within the HP–CV system that offsets a portion of the applied pile head moment, thereby reducing bending demands in the slender pile shaft.

Collectively, these mechanisms explain the reduced bending demands observed in the pile shaft and the ability of HP–CV systems to resist combined lateral and overturning loads efficiently. The collar vane effectively mobilizes shallow soil resistance and concentrates load transfer near the pile head, enabling slender pile shafts to perform adequately under overturning demands representative of wind-loaded roadside structures.

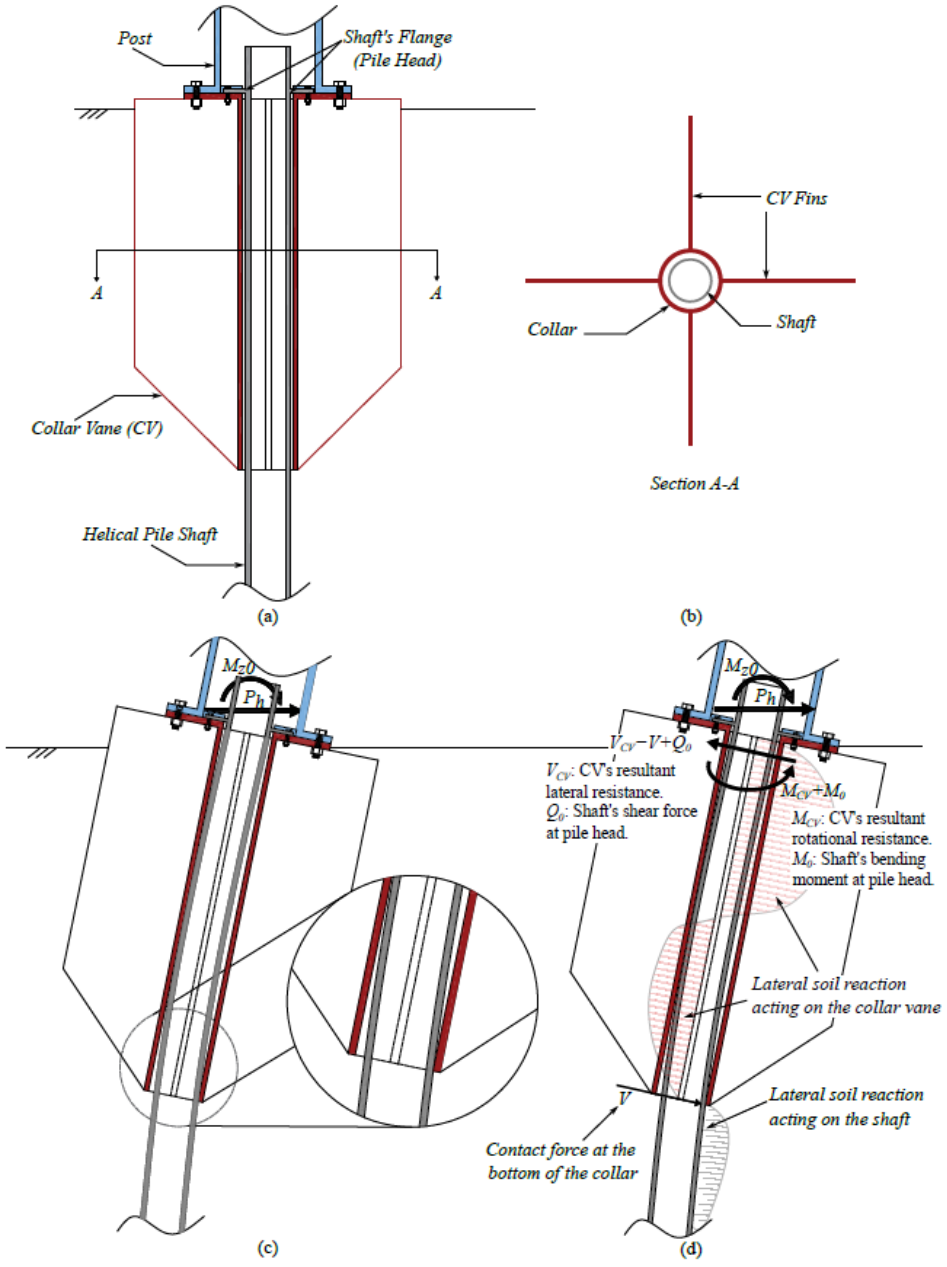


*Figure 51. Mechanics of a laterally loaded helical pile with a collar vane: a.) undeformed configuration; b.) plan view of section A-A; c.) exaggerated deformed configuration; d.) forces acting on a helical pile with a collar vane.*

# Chapter 6: Summary and Conclusions

This study investigated the effectiveness of collar vane (CV) technology for enhancing the lateral, torsional, cyclic, and overturning performance of helical pile (HP) foundations through an extensive full-scale field testing program conducted in cohesive and granular soils. The overarching objective was to evaluate whether shallow, finned collar elements attached near the pile head can fundamentally change load-transfer mechanisms in slender helical piles and enable their use in applications traditionally reserved for larger, more intrusive foundation systems.

## 6.1 Key Technical Findings

**Substantial increase in lateral resistance and stiffness:** The addition of a collar vane significantly increased lateral resistance and stiffness of helical piles relative to piles without a collar. Across all soil conditions and CV geometries tested, the majority of lateral resistance was mobilized by the collar vane at shallow depths, where lateral deformations are greatest. In many cases, more than 80% of the lateral resistance was provided by the CV, even at relatively large displacements. As a result, HP–CV systems exhibited load–deflection responses comparable to much larger foundation elements.

**Effective reduction of bending demands in slender shafts:** A defining outcome of this study is the demonstrated reduction in bending moments within the helical pile shaft when a collar vane is present. Strain-gauge measurements confirmed that lateral and overturning loads are largely resisted by the CV and transferred to the pile head connection, rather than being distributed along the shaft. This load-transfer mechanism results in nearly linear moment distributions through the collar region and substantially lower peak bending moments near the pile head, enabling the use of slender steel shafts without exceeding structural capacity.

**High torsional resistance governed by CV geometry and connection details:** Collar vanes were shown to mobilize large torsional resistances through cylindrical and conical shear surfaces analogous to field vane shear mechanisms. Torsional capacity increased systematically with CV diameter and embedment depth and was largely independent of the helical pile shaft configuration. One-piece collar vanes generally exhibited stiffer torque–rotation responses than two-piece systems due to improved rotational compatibility. For larger CV geometries, connection strength at the pile head was identified as the governing limit state rather than geotechnical failure.

**Stable cyclic performance under wind-type loading:** Under cyclic lateral and torsional loading representative of long-term wind effects, HP–CV systems demonstrated stable behavior for moderate cyclic load ratios. Displacement accumulation, stiffness degradation, and bending moment growth were most pronounced during early loading cycles and generally stabilized thereafter. The observed trends are consistent with established cyclic pile behavior and indicate that CV-augmented helical piles can perform reliably under repetitive service loading conditions relevant to transportation infrastructure.

**Strong performance under combined overturning loads:** Overturning load tests showed that HP–CV systems can effectively resist combined lateral shear and overturning moments representative of wind loading on roadside sign structures. In both clay and sand, multiple HP–CV

configurations performed comparably to, and in some cases marginally better than, conventional reinforced concrete drilled shafts commonly specified by state DOTs. Importantly, nearly all CV configurations tested resisted overturning demands associated with the highest design wind speeds without exceeding shaft bending capacity.

## 6.2 Design Implications

**Implications for Helical Pile Foundation Design:**
The results of this study demonstrate that collar vane technology fundamentally alters how lateral, torsional, and overturning loads are resisted by helical pile foundations. By mobilizing shallow soil resistance and concentrating load transfer near the pile head, HP–CV systems overcome long-standing limitations associated with slender pile shafts and installation-induced soil disturbance. This creates new opportunities to use helical piles in applications where lateral stiffness, torsional capacity, or overturning resistance has historically governed design.

**Relevance to DOT Sign Structure Foundations:**
For roadside sign, lighting, and signal structures—where wind-induced overturning typically controls foundation design—the findings indicate that HP–CV systems represent a viable alternative to conventional drilled shaft foundations. Compared to drilled shafts, HP–CV systems offer the potential advantages of reduced excavation, faster installation, minimal spoil generation, and adaptability to constrained sites, while still meeting or exceeding performance demands imposed by DOT design criteria. The experimental results support the consideration of HP–CV systems as a practical and efficient foundation solution for transportation infrastructure subject to combined wind-induced loading.

## 6.3 Concluding Remarks

Overall, this research confirms that collar vane technology can substantially expand the application envelope of helical pile foundations. Through improved load-transfer mechanisms and enhanced resistance at shallow depths, HP–CV systems provide a structurally efficient and constructible foundation option for infrastructure systems subjected to lateral, torsional, cyclic, and overturning loads. The findings establish a strong experimental basis for future design guidance, analytical modeling, and broader implementation of collar vane–augmented helical piles in transportation and civil infrastructure projects

## References


Adams, J. I., & Klym, T. W. (1972). *A study of anchors for transmission line structures*. Canadian Geotechnical Journal, 9(1), 89–104. https://doi.org/10.1139/t72-009

AASHTO. (2022). *Standard specifications for structural supports for highway signs, luminaires, and traffic signals* (8th ed.). American Association of State Highway and Transportation Officials.

Abd Elaziz, A. Y., & El Naggar, M. H. (2015). Performance of single helical piles under axial cyclic loading. *Canadian Geotechnical Journal*, 52(7), 927–940. https://doi.org/10.1139/cgj-2014-0203

ASCE. (2021). *Minimum design loads and associated criteria for buildings and other structures (ASCE/SEI 7-22)*. American Society of Civil Engineers.

Brown, D. A., Reese, L. C., & O'Neill, M. W. (1988). Cyclic lateral loading of pile groups. *Journal of Geotechnical Engineering*, 114(11), 1326–1343.

Carvajal-Muñoz, J. (2023). *Performance of helical piles augmented with collar vanes under lateral, torsional, and cyclic loading* (Master's thesis). University of Maine.

Cheang, L., & Matlock, H. (1983). Earth pressure due to cyclic lateral pile movement. *Journal of Geotechnical Engineering*, 109(6), 848–867.

Cuéllar, P., Baeßler, M., & Rücker, W. (2009). Ratcheting and soil densification effects on pile foundations under cyclic lateral loads. *Soil Dynamics and Earthquake Engineering*, 29(5), 698–706.

Elkasabgy, M., El Naggar, M. H., & Shehata, H. (2019). Lateral response of helical piles in sand. *Canadian Geotechnical Journal*, 56(1), 66–79. https://doi.org/10.1139/cgj-2017-0414

Fellenius, B. H. (2008). Effective stress analysis and shaft resistance of piles. *Canadian Geotechnical Journal*, 45(9), 1330–1337.

Garnier, J. (2013). Cyclic loading effects on pile foundations. *Proceedings of the Institution of Civil Engineers – Geotechnical Engineering*, 166(2), 109–122.

Ghaly, A., Hanna, A., & Hanna, M. (1991). Installation torque of screw anchors in sand. *Journal of Geotechnical Engineering*, 117(5), 773–793.

Hu, Y., Lin, J., & Wang, J. (2006). Serviceability-based design of sign structures subjected to wind loading. *Journal of Structural Engineering*, 132(10), 1594–1603.

Hubler, M. H., Gallagher, P. M., & Olson, S. M. (2023). Lateral resistance of finned pile foundations. *Journal of Geotechnical and Geoenvironmental Engineering*, 149(3), 04022172.

Jamiolkowski, M., Ladd, C. C., Germaine, J. T., & Lancellotta, R. (2003). New developments in field and laboratory testing of soils. *Proceedings of the 11th European Conference on Soil Mechanics and Foundation Engineering*, 1, 57–153.

Keefe, J. (2020). *Hydraulic control systems for cyclic loading applications*. Tescom Technical Report.

Kulhawy, F. H., & Mayne, P. W. (1990). *Manual on estimating soil properties for foundation design*. Electric Power Research Institute.

Li, C., Zhang, Z., & Yang, Y. (2021). Soil particle migration and settlement around piles under cyclic loading. *Soils and Foundations*, 61(3), 657–670.

Long, J. H., & Vanneste, G. (1994). Effects of cyclic lateral loads on piles in sand. *Journal of Geotechnical Engineering*, 120(1), 225–244.

Lu, J., & Zhang, J. (2019). Cyclic lateral response of pile–soil systems in sand. *Soil Dynamics and Earthquake Engineering*, 120, 148–160.

Maier, C., & Oskoorouchi, A. M. (2010). Lateral resistance of piles with attached fins. *Proceedings of GeoFlorida 2010*, ASCE, 2239–2248.

Merifield, R. S., Lyamin, A. V., & Sloan, S. W. (2001). Three-dimensional analysis of screw pile capacity. *International Journal for Numerical and Analytical Methods in Geomechanics*, 25(6), 573–603.

Merifield, R. S., Lyamin, A. V., & Sloan, S. W. (2003). The ultimate bearing capacity of screw piles in sand. *Geotechnique*, 53(8), 769–773.

Merifield, R. S., Lyamin, A. V., & Sloan, S. W. (2006). Limit analysis of helical piles in clay. *Canadian Geotechnical Journal*, 43(4), 427–438.

Mitsch, M. P., & Clemence, S. P. (1985). Uplift capacity of helically anchored foundations in sand. *Proceedings of the 11th International Conference on Soil Mechanics and Foundation Engineering*, 1, 273–276.

Mondal, S., & Disfani, M. M. (2022). Cyclic lateral behavior of piles in sand. *Soil Dynamics and Earthquake Engineering*, 154, 107085.

Nanda, S., Patra, N. R., & Roy, A. (2017). Cyclic loading response of piles in sand. *International Journal of Geotechnical Engineering*, 11(3), 274–287.

Nasr, A. M. (2014). Numerical study of fin pile behavior under lateral loads. *Computers and Geotechnics*, 55, 294–306.

Peng, J. (2006). *Lateral behavior of finned piles* (Doctoral dissertation). University of Houston.

Perko, H. A. (2003). *Helical piles: A practical guide to design and installation*. John Wiley & Sons.

Perko, H. A. (2009). Helical piles and anchors—Applications and design considerations. *Geotechnical Special Publication*, 188, 1–20.

Prasad, Y. V. S. N., & Rao, S. N. (1996). Lateral capacity of helical piles in clay. *Journal of Geotechnical Engineering*, 122(11), 938–941.

Qin, Y., Zhang, J., & Liu, H. (2024). Lateral performance of pile foundations with detachable fins. *Journal of Geotechnical and Geoenvironmental Engineering*, 150(2), 04023112.

Reinert, J., & Newman, J. (2002). Lateral capacity of fin piles. *Proceedings of the Deep Foundations Institute Conference*, 1–12.

Sakr, M. (2009). Performance of helical piles in oil sand. *Canadian Geotechnical Journal*, 46(9), 1046–1061.

Sakr, M., Elkasabgy, M., & El Naggar, M. H. (2020). Lateral performance of finned piles in sand. *Journal of Geotechnical and Geoenvironmental Engineering*, 146(4), 04020013.

Stone, K. J. L., White, D. J., & Gaudin, C. (2020). Shallow foundation alternatives for lateral loading. *Geotechnical Engineering*, 173(4), 300–313.

Whitfield, J. W. (1992). *Surficial geology of central Missouri*. Missouri Geological Survey.

Zhang, L., Tang, W., & Ng, C. W. W. (2011). Cyclic degradation of pile–soil stiffness. *Soils and Foundations*, 51(4), 705–717.


Transportation Infrastructure Durability Center
AT THE UNIVERSITY OF MAINE

35 Flagstaff Road
Orono, Maine 04469
tidc@maine.edu
207.581.4376

**www.tidc-utc.org**